**NTNU – Trondheim**
Norwegian University of
Science and Technology

# Distributed and Concentrated Inelasticity Beam-Column Elements used in Earthquake Engineering

Armin Gharakhanloo

Civil and Environmental Engineering
Submission date: June 2014
Supervisor: Amir Kaynia, KT

Norwegian University of Science and Technology
Department of Structural Engineering

# Preface

This masters thesis has been written at the Department of Structural Engineering at the Norwegian University of Science and Technology (NTNU). It is the result of 20 weeks work in the spring semester of 2014, and finalizes my study in Civil Engineering with an emphasis on Computational Mechanics. My supervisor for the thesis has been Professor Amir M. Kaynia (NTNU).

## Acknowledgements

I would like to express deep gratitude to my supervisor Professor Amir M. Kaynia for inspiring me to seek out and study state-of-art structural engineering theory, as well as sharing his insight into nonlinear and earthquake analysis. His frequent counseling and advice throughout the semester has been very helpful and instructive, and has been of great significance for the final outcome of the thesis. I would also like to thank several others for contributions to my research:

- Doctor Georgios Tsionis at the European Labratory of Structural Assessment (ELSA), Joint Research Centre, Italy for providing experimental data and guidance on the pseudo-dynamic testing of a reinforced concrete frame.
- Gabriel Sabay at the European Labratory of Structural Assessment (ELSA), Joint Research Centre, Italy for giving advice on the modeling of material properties.
- Professor Filip C. Filippou at the University of California, Berkeley for providing assistance with OpenSees, as well as introducing me to the field of nonlinear structural analysis due to seismic loading at my exchange year at UC Berkeley in 2012 - 2013.
- Doctor Frank McKenna at the University of California, Berkeley for advice and troubleshooting of OpenSees scripts.

# Abstract

A suite of beam-column element formulations have been developed for assessment of the nonlinear response of structures under earthquake loading. They range from simple concentrated inelasticity elements, to the more advanced distributed inelasticity fiber elements. Research and development of new sophisticated models have been, and still are, of great interest, as rising computational power and technology has allowed even faster numerical calculations. Despite the increase of new and improved formulations, the elements in commonly used finite element software are prone to produce significant inaccuracies in their approximations of nonlinear structural response. This happens particularly for beam-column members experiencing strain-softening behaviour, which is common for columns with large vertical loading. The phenomena is called localization, and is due to inelastic deformations localizing in concentrated parts of a structural member. It brings with it the numerical disadvantage of non-objectivity, which means that the structural response differs depending on the discretization of elements and integration points.

This thesis makes a review of the commonly known inelastic beam-column element formulations with a focus on their advantages and disadvantages. These include the displacement-based and force-based distributed inelasticity formulations, concentrated inelasticity elements with springs at member ends, as well as the more sophisticated concentrated inelasticity elements with fiber discretization. Localization issues are presented; first the physical definition, which is observed on testing specimen of concrete columns, and second the numerical definition. Different regularization procedures to prevent numerical localization have been assessed, and a comprehensive verifying analysis has been performed with the use of OpenSees.

Finally, the beam-column element formulations are applied in the modelling of a one-story frame, which has been pseudo-dynamically tested in a laboratory. This is done in SeismoStruct, where the element discretization properties have been determined based on the results from the OpenSees analysis. Then, a numerical comparison between experimental and analysis results have been made. Conclusions on the application of the different elements have been drawn based on these results. The analysis of the one-story frame succeded in portraying the characteristics of the discussed element formulations, thus verifying their capabilities of modeling structures subjected to strong lateral forces.

# Sammendrag

En rekke elementformuleringer har blitt utviklet for vurdering av bjelke-søyler i ikke-lineær analyse av bygninger påkjent jordskjelvlaster. Disse omfatter alt fra enkle elementer med konsentrert plastisitet, til mer avanserte fiberelementer med plastisitet fordelt over hele dets lengde. Forskning og utvikling av nye elementmodeller er fortsatt av stor interesse, ettersom økningen i datakraft og tilgjengelig teknologi muliggjør enda raskere numeriske beregninger enn tidligere. Til tross for nye og forbedrete formuleringer, så er elementene benyttet i dagens elementprogrammer utsatt for å produsere betydelige unøyaktigheter i beregningene av ikke-lineær respons. Dette er spesielt tilfelle for bjelke-søyler som opplever negativ stivhet, noe som er vanlig for søyler med stor vertikal belastning. Dette fenomenet kalles lokalisering, og skyldes at de plastiske deformasjonene lokaliserer seg i en avgrenset del av elementet. En konsekvens av dette er at den numeriske analysen av bjelke-søylene blir utsatt for ikke-objektivitet, som vil si at responsberegningene avhenger av diskretiseringen av elementer og integrasjonspunkter.

Denne masteroppgaven går gjennom kjente bjelke-søyle elementformuleringer med fokus på deres fordeler og ulemper. Disse inkluderer forskyvningsbaserte og kraftbaserte elementer med fordelt plastisitet, konsentrerte plastisitet-elementer med fjærer på endene, i tillegg til mer avanserte konsentrerte plastisitet-elementer med fiberdiskretisering. Problemene med lokalisering blir presentert, og er delt inn i den fysiske definisjonen, som blir observert ved testing av betongsøyler, og den numeriske definisjonen. Ulike prosedyrer for å rette opp i numeriske feil, såkalt regularisering, har blitt vurdert, og en omfattende verifiseringsanalyse har blitt utført ved hjelp av OpenSees.

Til slutt har elementformuleringene blitt anvendt i modelleringen av en en-etasjes betongramme, som har blitt pseudodynamisk testet i et labratorium. Modelleringen har blitt utført i SeismoStruct, hvor diskretiseringen av elementene har blitt gjort basert på resultatene fra analysene i OpenSees. En numerisk sammenligning mellom resultater fra eksperiment og analyse har blitt utført. Konklusjoner knyttet til anvendelsen av de ulike elementene har så blitt trukket basert på disse resultatene. Analysen av betongrammen lyktes i å fremstille egenskapene til elementformuleringene, og dermed verifisere evnene de har til å modellere konstruksjoner utsatt for store horisontale krefter.

# Contents

# 1. Introduction

Structural design in earthquake prone regions is heavily dependent on accurate and reliable analysis procedures prior to construction. The ground accelerations experienced can create large lateral forces on the structures, which often will produce inelastic material behaviour. Before the arrival of the finite element method these analyses were done by simple static methods, commonly referred to as equivalent force method, similar to what is now found and is in use in building codes of countries with low seismic activity. These methods are however not sufficient for analysis of the stronger earthquakes, as change of structural properties due to inelasticity will affect the overall response. Because of this fact it is a rather cumbersome task to predict the behaviour of a building, especially since there is no known way to foresee what earthquake is next. The last decades improvement of computational power and technology has enabled more sophisticated analysis methods. To obtain more realistic approximations on structural response nonlinear time-history analysis is used. Many buildings codes now require the use of multiple time-histories so that several possible response outcomes are predicted, as they are very much dependent on the structures fundamental periods. Common output from these analyses is peak forces and displacements, as well as damage due to fatigue. This is called performance-based design, and is by many viewed on as the antithesis of code-based design, which has prescribed requirements for structures. The concept is that instead of fulfilling such requirements, the designer can from his own analysis prove that the desired performance goals are met. Performance-based earthquake engineering is the practice in several countries with seismic activity, such as the Unites States (ATC, 1997). An example is the earthquake prone city of San Francisco in California, where the building codes state a maximum number of storys being allowed for new buildings based on code-based design. This restriction can however be neglected if performance-based design is used, and the engineer can demonstrate that the building can withstand the prescriptive seismic ground motions (Moehle, 2012).

The main focus of this thesis, which is currently also of great research interest, is the element formulations used for the beam-columns in structural earthquake analysis. They are primarily divided into two categories; distributed inelasticity, where plasticity can form anywhere along the member length, and concentrated inelasticity, where the formation of plastic hinges is restrained to the member ends. The distributed inelasticity members are modelled with the fiber approach, which consists of discretizing the member section into several material fibers, in addition to discretization along the element length. Its two main formulations are the displacment-based (DB) method, which is the classical textbook finite element formulation, and the force-based (FB) method (Neuenhofer & Filippou, 1991). The DB formulation is based on displacement shape functions, while the FB formulation is based on internal force shape functions. Due to the FB el-

ements not having restrains on their displacement fields they are able to approximate inelastic structural response with a greater accuracy than DB elements. While these are the most known finite element formulations, there has also been presented others that either improve or do not possess their disadvantages (Alemdar & White, 2005; Lee & Filippou, 2009).

Physical localization is defined as structural properties being dependentent on the member's size when experiencing strain-softening. Strains, deformations, and ductility will differ for constant concrete section depending on its length (Jansen & Shah, 1997). However, the prepeak strain-stress response will remain identical for all height-diamater ratios. Research on specimen has resulted in several proposals on how to model localization response (Hillerborg, 1990; Markeset & Hillerborg, 1995). Another localization issue arises for the numerical analysis of softening behaviour, due to strains concentrating at section integration points with highest bending moment values. This yields non-objective response, which means that the calculated response differs based on finer mesh discretization and does not converge into one single solution (Zeris & Mahin, 1988; Coleman & Spacone; 2001; Calabrese, Almeida & Pinho, 2010). Regularization procedures have been developed to correct these issues, and thus obtain objective response. Some of these methods are adjusting extremity element length of DB members (Zeris & Mahin, 1988), adding a damage variable to the constitutive relation (Adessi & Ciampi, 2007), and the fracture energy criterion and post-processing of local response (Coleman & Spacone, 2001).

Concentrated inelasticity elements are designed to lump plasticity at their member ends, which is expected to occur for beam-columns subject to strong lateral forces. These elements range from simple one- or two-component models, often with nonlinear springs at member ends (Filippou, 2013), to more sophisticated elements with FB fiber modelling at predetermined plastic hinge lengths (Scott & Fenves, 2006; Scott & Ryan, 2013). The recent proposals for concentrated inelasticity elements are able to prevent the localization issues experienced in regular DB and FB formulations. Thus, a comprehensive analysis is performed to illustrate the fundamental differences between the discussed elements, comparing response, regularization procedures and necessary level of discretization.

To fully investigate the strength and accuracy of the element formulations, a comparison to experimental data is performed. This data is taken from the pseudo-dynamic testing of a one-story reinforced concrete structure in Italy (Ferrara & Negro, 2004). The comparison with the numerical analysis is done for both global force-displacement and local moment-rotation response. Finally, the conclusions drawn is that the element formulations yield satisfactory predictions of the response. However, the FB elements give better base shear values than DB elements, since their force field is enforced, in addition to having less computational demand due to requiring fewer elements for each structural member.

# 2. Distributed plasticity elements

## 2.1 Model assumptions

The following beam-column elements presented have been based on the Euler-Bernoulli beam theory. Although the majority of the numerical examples have been performed in a two-dimensional plane, the assumptions will be presented in three dimensions. In addition, as the torsional response is considered uncoupled from both the axial and flexural responses, it will be left out from the models for simplicity.

The variables of the element displacement field are described by

$$\boldsymbol{u}(x) = \begin{pmatrix} u(x) \\ w(x) \\ v(x) \end{pmatrix} \tag{2.1}$$

where $u(x)$ is the axial displacement, and $w(x)$ and $v(x)$ are the transverse displacements in respectively the z- and y-direction. The section deformation vector, which contains the axial strain and curvatures, is given by

$$\boldsymbol{e}(x) = \begin{pmatrix} \varepsilon_a(x) \\ \kappa_z(x) \\ \kappa_y(x) \end{pmatrix} = \begin{pmatrix} \dfrac{\partial u(x)}{\partial x} + \dfrac{1}{2}\left(\dfrac{\partial^2 w(x)}{\partial x^2}\right)^2 + \dfrac{1}{2}\left(\dfrac{\partial^2 v(x)}{\partial x^2}\right)^2 \\ -\dfrac{\partial^2 w(x)}{\partial x^2} \\ \dfrac{\partial^2 v(x)}{\partial x^2} \end{pmatrix} \tag{2.2}$$

where the geometric nonlinearity is included in the expression for $\varepsilon_a(x)$. The normal strain $\epsilon_m$ at the point $m$ shown in figure (2.1), is given as

$$\epsilon_m(x, y, z) = \varepsilon_a(x) + y\kappa_z(x) + z\kappa_y(x) \tag{2.3}$$

where $\epsilon_a$ is the strain at the origin $a$, and $\kappa_z$ and $\kappa_y$ are the curvatures about the z- and y-axis. By defining the section kinematic matrix as

$$\boldsymbol{a}_s(y, z) = \begin{pmatrix} 1, & y, & z \end{pmatrix} \tag{2.4}$$

it is possible to write equation (2.3) as

$$\epsilon_m(x, y, z) = \boldsymbol{a}_s(y, z)\boldsymbol{e}(x) \tag{2.5}$$

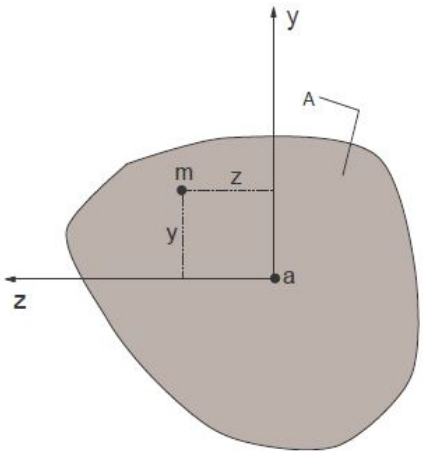


Figure 2.1: Section kinematics (Filippou, 2013).

The internal section forces, which are the axial force and bending moments, are defined as the vector

$$\boldsymbol{s}(x) = \begin{pmatrix} N(x) \\ M_z(x) \\ M_y(x) \end{pmatrix} \tag{2.6}$$

A constitutive relation is known for the section, and is described by

$$\boldsymbol{s}_{n+1}(x) = \boldsymbol{C}[\boldsymbol{s}_n(x),\ \boldsymbol{e}_n(x),\ \boldsymbol{e}_{n+1}(x)] \tag{2.7}$$

where $n$ denotes the analysis step. The internal section forces $\boldsymbol{s}_{n+1}(x)$ are thus calculated from the previous section forces $\boldsymbol{s}_n(x)$, and the current and previous section deformation vectors. The relation is linearized and incrementally given as

$$\Delta\boldsymbol{s}(x) = \boldsymbol{k}_s(x)\Delta\boldsymbol{e}(x) \tag{2.8}$$

where the section stiffness matrix is given by

$$\boldsymbol{k}_S = \frac{\partial \boldsymbol{S}}{\partial \boldsymbol{e}} = \begin{bmatrix} \frac{\partial N}{\partial \varepsilon} & \frac{\partial N}{\partial \kappa_y} & \frac{\partial N}{\partial \kappa_z} \\ \frac{\partial M_y}{\partial \varepsilon} & \frac{\partial M_y}{\partial \kappa_y} & \frac{\partial M_y}{\partial \kappa_z} \\ \frac{\partial M_z}{\partial \varepsilon} & \frac{\partial M_z}{\partial \kappa_y} & \frac{\partial M_z}{\partial \kappa_z} \end{bmatrix} \tag{2.9}$$

For simplicity the coordinate $x$ is left out from the expression for the section stiffness matrix. The equations stated above define the force-deformation relations of a material section, and the next step will be to assemble these relations to the element level.

## 2.2 Fiber model

Distributed plasticity models have the advantage that there is no predetermined length that concentrates the inelastic behaviour. Thus, inelasticity can form at any section point along the element length; where the points are determined by the numerical integration method used. The drawback of this property is that the computational effort is greatly increased compared to concentrated inelasticity models, as the interior span of the elements is not assumed linear elastic. Naturally the distributed inelasticity models will give a closer to exact solution, and thus give an improved approximation of the experimental response.

Structural members of reinforced concrete do not consist of homogenous material sections. A similar case applies for steel sections with initial stresses at the welding points, which will affect the overall response. This renders it impossible to model the exact element behaviour without discretizing the sections, and thus taking into account the different properties of the materials. This approach is called the fiber model, and is the commonly used distributed inelasticity element model. A fiber model of a reinforced concrete beam is illustrated in figure (2.2), where it can be seen that different fibers are made for the unconfined cover concrete, the confined core concrete, and the steel reinforcement bars. Thus, the element model will need to include three different material stress-strain relationships to render the correct response quantities. Computational effort can however be reduced by adjusting the level of the section discretization. For instance, the number of fibers in the z-direction of a beam can often be far less than in the y-direction. This is because the bending moment about the z-axis usually is significantly larger than about the y-axis, which will result in increased inelasticity and need for discretization. Although the fiber element is considered more "exact" than other element formulations, it has its numerical difficulties. One of the most significant is the interaction between the flexural and shear response, which still is under research.

The most common finite element formulations for the fiber element is the displacement-based stiffness method, and the force-based flexibility method (Neuenhofer and Filippou, 1997). Their advantages and disadvantages will be discussed in this paper. There exists several formulations that resolve some of the difficulties with these two methods. Examples are the mixed formulation, that combines properties from both stiffness and flexibility methods (Alemdar and White, 2005), and improved flexilibity-based elements like the Spreading Inelastic Zone Element (Lee and Filippou, 2009). These elements will however not be discussed further, instead the fundamental differences of the two methods first mentioned will be presented.

## 2.3 Displacement-based element formulation

The displacement-based (DB) stiffness method is based on interpolation functions for the axial and transverse displacements of the element. The commonly used functions for beam-column elements are linear Lagrangian shape functions for the axial displacements, and cubic Hermitian polynomials for the transverse displacements. These yield

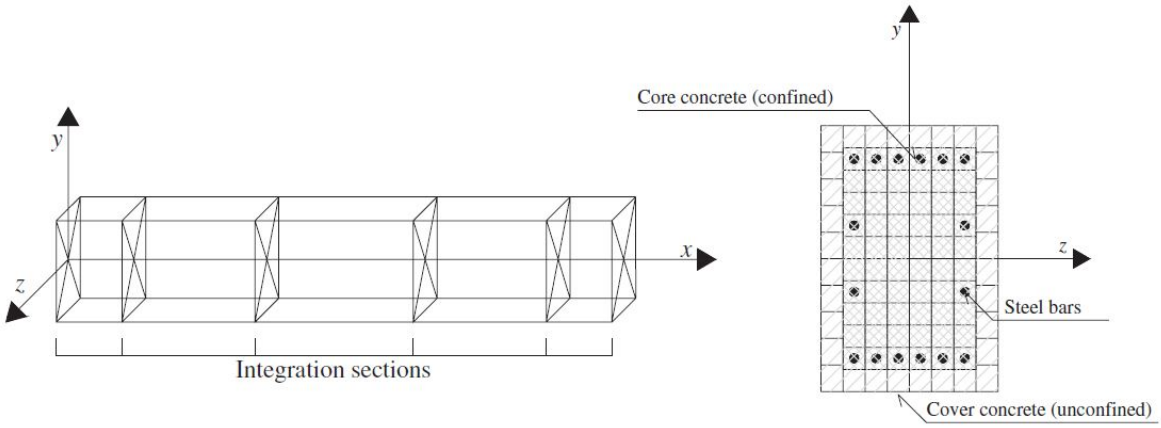


Figure 2.2: Fibre model of a reinforced concrete beam (Calabrese, Almeida & Pinho, 2010).

the exact response for a linear elastic, prismatic member (Neuenhofer and Filippou, 1997).

The displacement field $\boldsymbol{u}(x)$ is related to the nodal displacments $\boldsymbol{v}$ through the equation

$$\boldsymbol{u}(x) = \boldsymbol{N}(x)\boldsymbol{v} \tag{2.10}$$

where $\boldsymbol{N}(x)$ is a matrix containing the interpolation functions of the axial and transverse displacements. The section deformation vector $\boldsymbol{e}(x)$ (Eq. 2.2), is related to the nodal displacements by

$$\boldsymbol{e}(x) = \boldsymbol{B}(x)\boldsymbol{v} \tag{2.11}$$

The matrix $\boldsymbol{B}(x)$ contains the first derivative of the axial displacement shape function, and the second derivatives of the transverse displacement shape functions. By combining the linearized constitutive relation (2.8) with an incremental version of (2.11), the following expression is obtained for the section force increment

$$\boldsymbol{\Delta s}(x) = \boldsymbol{k}_s(x)\boldsymbol{\Delta e}(x) = \boldsymbol{k}_s(x)\boldsymbol{B}(x)\boldsymbol{\Delta v} \tag{2.12}$$

The equilibrium condition between the nodal forces $\boldsymbol{q}$ and the section forces $\boldsymbol{s}(x)$ is derived from the principle of virtual displacements, and is given by

$$\boldsymbol{q} = \int_L \boldsymbol{B}^T(x)\boldsymbol{s}(x)dx \tag{2.13}$$

while the element stiffness matrix is derived from its derivative with respect to the nodal displacements. This can easily be done by inserting the expression for $\boldsymbol{\Delta s}(x)$ (2.12) into (2.13). The resulting equation is thus

$$\boldsymbol{k} = \frac{\partial \boldsymbol{q}}{\partial \boldsymbol{v}} = \int_L \boldsymbol{B}^T(x)\boldsymbol{k}_s(x)\boldsymbol{B}(x)dx \tag{2.14}$$

Beam-column material sections very often have irregular and discontinous distribution of stresses. This is either due to different stiffnesses in the section, like what is the case for reinforced concrete, or large inelasticity that can result in a nonlinear curvature. The use of classical integration techniques to solve equations (2.13) and (2.14) are therefore very inconvenient. Rather numerical integration should be used, which makes it possible to rewrite the equations mentioned in a discrete form instead of continuous. The equilibrium condition is thus written as

$$\boldsymbol{q} = \int_L \boldsymbol{B}^T(x)\boldsymbol{s}(x)dx \approx L\sum_{i=1}^{N_p} \boldsymbol{B}_i^T \boldsymbol{s}_i \omega_i \tag{2.15}$$

and the element stiffness matrix as

$$\boldsymbol{k} = \int_L \boldsymbol{B}^T(x)\boldsymbol{k}_s(x)\boldsymbol{B}(x)dx \approx L\sum_{i=1}^{N_p} \boldsymbol{B}_i^T \boldsymbol{k}_{s,i} \boldsymbol{B}_i \omega_i \tag{2.16}$$

where $N_p$ is the number of integration points and $\omega_i$ is the weight of each point $i$.

## 2.4 Force-based element formulation

The force-based (FB) flexibility method is based on interpolation functions for the internal forces, and not displacements which are the common textbook finite element formulation, as well as used in the DB formulation. These functions are chosen so that they repesent the exact solution of the forces in the elements, and are usually of a lower deegre of polynomial than the displacement shape functions.

The section forces $\boldsymbol{s}(x)$, also called the force field, are related to the nodal forces $\boldsymbol{q}$ through the equation

$$\boldsymbol{s}(x) = \boldsymbol{b}(x)\boldsymbol{q} \tag{2.17}$$

where $\boldsymbol{b}(x)$ is a matrix containing the force interpolation functions mentioned. For instance, a column subject to horizontal nodal load will have a constant axial force and and a linearly distributed bending moment in one direction, which makes the choice of interpolation functions a simple task. The force interpolation matrix for such a case will be

$$\boldsymbol{b}(x) = \begin{bmatrix} 1 & 0 & 0 & 0 & 0 \\ 0 & \xi - 1 & \xi & 0 & 0 \\ 0 & 0 & 0 & \xi - 1 & \xi \end{bmatrix} \tag{2.18}$$

where the normalized coordinate $\xi = x/L$ is used. The section flexibility matrix is defined as

$$\boldsymbol{f}_s(x) = \boldsymbol{k}_s^{-1}(x) \tag{2.19}$$

and a similar mathematical procedure as for the DB formulation is used here. By combining the inverse form of (2.11) with the incremental version of (2.17), an expression for

the incremental section deformation is made

$$\boldsymbol{\Delta e}(x) = \boldsymbol{k}_s^{-1}(x)\boldsymbol{\Delta s}(x) = \boldsymbol{f}_s(x)\boldsymbol{\Delta s}(x) = \boldsymbol{f}_s(x)\boldsymbol{b}(x)\boldsymbol{\Delta q} \tag{2.20}$$

The principle of virtual forces is then used to define the compatibility condition between the nodal displacements and section deformations, which is

$$\boldsymbol{v} = \int_L \boldsymbol{b}^T(x)\boldsymbol{e}(x)dx \tag{2.21}$$

Equations (2.20) and (2.21) are then combined to derive the element flexilibity matrix

$$\boldsymbol{f} = \frac{\partial \boldsymbol{v}}{\partial \boldsymbol{f}} = \int_L \boldsymbol{b}^T(x)\boldsymbol{f}_s(x)\boldsymbol{b}(x)dx \tag{2.22}$$

The discrete form of the two equations above are given as

$$\boldsymbol{v} = \int_L \boldsymbol{b}^T(x)\boldsymbol{e}(x)dx \approx L\sum_{i=1}^{N_p} \boldsymbol{b}_i^T\boldsymbol{e}_i\omega_i \tag{2.23}$$

and

$$\boldsymbol{f} = \int_L \boldsymbol{b}^T(x)\boldsymbol{f}_s(x)\boldsymbol{b}(x)dx \approx L\sum_{i=1}^{N_p} \boldsymbol{b}_i^T\boldsymbol{f}_{s,i}\boldsymbol{b}_i\omega_i \tag{2.24}$$

## 2.5 Numerical integration rules

In structural analysis the most common numerical integration schemes are the Gaussian quadrature rules. The Gauss-Legendre quadrature is the most known rule, and is preferred in classical DB finite element formulations. It is accurate for polynomials up to a deegre of $2n-1$, where $n$ is the number of integrations points used. Another highly used rule is the Gauss-Lobatto quadrature, which is accurate for polynomials up to deegre of $2n-3$. Despite its reduced accuracy, it is the commonly used rule for FB elements, as it unlike the Gauss-Legendre rule has integration points at the element ends (Scott, 2011). The integration points and corresponding weights of both these quadrature rules are reported in tables (2.1) and (2.2), for the isogeometric element length $[-1, 1]$.

Table 2.1: Gauss-Legendre quadrature.

| Number of integration points, $n$ | Points, $x_i$ | Weights, $w_i$ |
|---|---|---|
| 2 | $\pm\sqrt{\frac{1}{3}}$ | 1 |
| 3 | 0 | $\frac{8}{9}$ |
| | $\pm\sqrt{\frac{3}{5}}$ | $\frac{5}{9}$ |
| 4 | $\pm\sqrt{(3-2\sqrt{\frac{6}{5}})/7}$ | $\frac{18+\sqrt{30}}{36}$ |
| | $\pm\sqrt{(3+2\sqrt{\frac{6}{5}})/7}$ | $\frac{18-\sqrt{30}}{36}$ |
| 5 | 0 | $\frac{128}{225}$ |
| | $\pm\frac{1}{3}\sqrt{5-2\sqrt{\frac{10}{7}}}$ | $\frac{322+13\sqrt{70}}{900}$ |
| | $\pm\frac{1}{3}\sqrt{5+2\sqrt{\frac{10}{7}}}$ | $\frac{322-13\sqrt{70}}{900}$ |
| 6 | $\pm$0.2386191860831969 | 0.4679139345726910 |
| | $\pm$0.6612093864662645 | 0.3607615730481386 |
| | $\pm$0.9324695142031520 | 0.1713244923791703 |
| 7 | 0 | 0.4179591836734693 |
| | $\pm$0.4058451513773971 | 0.3818300505051189 |
| | $\pm$0.7415311855993944 | 0.2797053914892766 |
| | $\pm$0.9491079123427585 | 0.1294849661688696 |

Table 2.2: Gauss-Lobatto quadrature

| Number of integration points, $n$ | Points, $x_i$ | Weights, $w_i$ |
|---|---|---|
| 3 | 0 | $\frac{4}{3}$ |
| | $\pm 1$ | $\frac{1}{3}$ |
| 4 | $\pm\sqrt{\frac{1}{5}}$ | $\frac{5}{6}$ |
| | $\pm 1$ | $\frac{1}{6}$ |
| 5 | 0 | $\frac{32}{45}$ |
| | $\pm\sqrt{\frac{3}{7}}$ | $\frac{49}{90}$ |
| | $\pm 1$ | $\frac{1}{10}$ |
| 6 | $\pm 0.2852315164806451$ | 0.5548583770354863 |
| | $\pm 0.7650553239294647$ | 0.3784749562978470 |
| | $\pm 1$ | 0.0666666666666667 |
| 7 | 0 | 0.4876190476190476 |
| | $\pm 0.4688487934707142$ | 0.4317453812098626 |
| | $\pm 0.8302238962785669$ | 0.2768260473615659 |
| | $\pm 1$ | 0.0476190476190476 |

### 2.5.1 Basic comparison of DB and FB element formulations

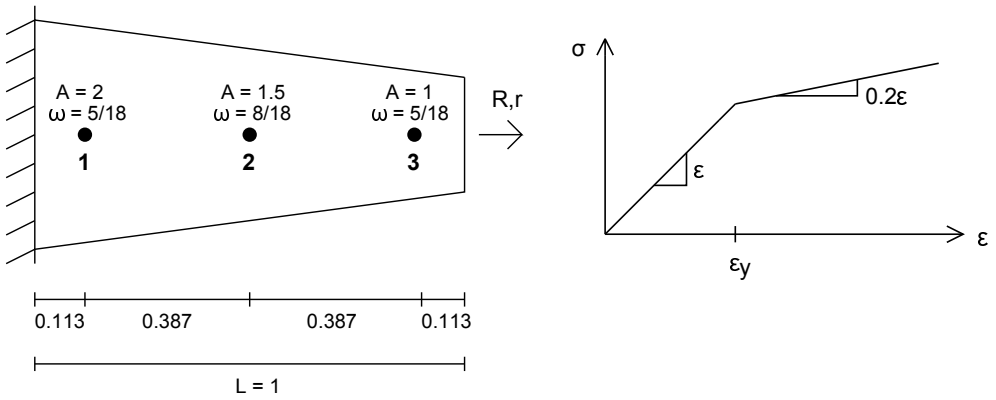


Figure 2.3: Cantilever beam with three Gauss-Legendre integration points, and corresponding stress-strain relationship.

The structure that has been analyzed is a cantilever beam with a linearly varying cross section, shown in figure (2.3). It consists of one element and is only loaded in its axial direction, which makes it necessary to consider one single deegre of freedom. Its simplicity will make it easier to illustrate the fundamental differences between the DB and FB methods. Three-point Gauss-Legendre integration have been used, and the stress-strain relationship is given by

$$\sigma = \begin{cases} \varepsilon & \text{for } \varepsilon \leq \varepsilon_y \\ \varepsilon_y + 0.2(\varepsilon - \varepsilon_y) & \text{for } \varepsilon > \varepsilon_y \end{cases} \tag{2.25}$$

where the yielding strain $\varepsilon_y$ is equal to 1.

#### FB element

Because the force-based flexibility method enforces the exact internal forces in the element, it is the the first method being used. A displacement of $v = 1$ is applied to beam end in the axial direction. The section flexibilities are derived from equation (2.9) and the stress-strain relationship (2.25), which gives

$$\boldsymbol{f}_s = \begin{cases} \dfrac{\partial \varepsilon}{\partial N} = \dfrac{1}{A}\dfrac{\partial \varepsilon}{\partial \sigma} = \dfrac{1}{A} & \text{for } \varepsilon \leq \varepsilon_y \\ \dfrac{\partial \varepsilon}{\partial N} = \dfrac{1}{0.5A}\dfrac{\partial \varepsilon}{\partial \sigma} = \dfrac{2}{A} & \text{for } \varepsilon > \varepsilon_y \end{cases} \tag{2.26}$$

Since there is only one deegre of freedom, which is in the axial direction, the force interpolation matrix will simply be the scalar

$$\boldsymbol{b} = 1 \tag{2.27}$$

The first step will be to apply to whole displacement $v = 1$, and calculate the strains at each integration point. Flexibilities at the sections are

$$\begin{pmatrix} f_{s,1} \\ f_{s,2} \\ f_{s,3} \end{pmatrix} = \begin{pmatrix} 1/2 \\ 2/3 \\ 1 \end{pmatrix} \tag{2.28}$$

which are then assembled to the element level with equation (2.24):

$$f = L \sum_{i=1}^{3} \boldsymbol{b}_i^T \boldsymbol{f}_{s,i} \boldsymbol{b}_i \omega_i = \left(1 \times \frac{1}{2} \times 1 \times \frac{5}{18}\right) + \left(1 \times \frac{2}{3} \times 1 \times \frac{8}{18}\right) + \left(1 \times 1 \times 1 \times \frac{5}{18}\right) = 0.713 \tag{2.29}$$

The nodal force is then calculated as

$$\boldsymbol{q} = \boldsymbol{f}^{-1} \boldsymbol{v} = \frac{1}{0.713} \times 1 = 1.403 \tag{2.30}$$

and by using equation (2.25), and the fact that the axial force is constant throughout the whole element, the following stresses and strains at each integration point are obtained

$$\begin{pmatrix} \sigma_1 \\ \sigma_2 \\ \sigma_3 \end{pmatrix} = \begin{pmatrix} 0.702 \\ 0.935 \\ 1.403 \end{pmatrix} \Rightarrow \begin{pmatrix} \varepsilon_1 \\ \varepsilon_2 \\ \varepsilon_3 \end{pmatrix} = \begin{pmatrix} 0.702 \\ 0.935 \\ 1.403 \end{pmatrix} \tag{2.31}$$

It can immediately be noticed that the yield strain $\varepsilon_y$ is exceeded at the third integration point. This makes it necessary to perform another step of calculations; basically an iteration. First the response values and load must be scaled to find the onset of inelasticity:

$$scale\ factor = \frac{1}{\boldsymbol{q}} = \frac{1}{1.403} = 0.713 \tag{2.32}$$

$$\begin{pmatrix} \sigma_1 \\ \sigma_2 \\ \sigma_3 \end{pmatrix}_{yield} = \begin{pmatrix} \varepsilon_1 \\ \varepsilon_2 \\ \varepsilon_3 \end{pmatrix}_{yield} = scale\ factor \times \begin{pmatrix} \varepsilon_1 \\ \varepsilon_2 \\ \varepsilon_3 \end{pmatrix} = 0.713 \times \begin{pmatrix} 0.702 \\ 0.935 \\ 1.403 \end{pmatrix} = \begin{pmatrix} 0.5 \\ 0.667 \\ 1 \end{pmatrix} \tag{2.33}$$

$$\Delta \boldsymbol{v} = (1 - scale\ factor)\boldsymbol{v} = (1 - 0.713) \times 1 = 0.287 \tag{2.34}$$

The section flexibilities for the next analysis step, assuming that the third integration point is yielding, will be

$$\begin{pmatrix} f_{s,1} \\ f_{s,2} \\ f_{s,3} \end{pmatrix} = \begin{pmatrix} 1/2 \\ 2/3 \\ 5 \end{pmatrix} \tag{2.35}$$

with the element flexibility

$$\boldsymbol{f} = L\sum_{i=1}^{3}\boldsymbol{b}_i^T\boldsymbol{f}_{s,i}\boldsymbol{b}_i\omega_i = \left(1\times\frac{1}{2}\times 1\times\frac{5}{18}\right)+\left(1\times\frac{2}{3}\times 1\times\frac{8}{18}\right)+\left(1\times 5\times 1\times\frac{5}{18}\right) = 1.824 \tag{2.36}$$

Finally, the nodal force increment, stresses, and strains are determined

$$\Delta\boldsymbol{q} = \boldsymbol{f}^{-1}\Delta\boldsymbol{v} = \frac{1}{1.824}\times 0.287 = 0.157 \tag{2.37}$$

$$\begin{pmatrix}\sigma_1\\ \sigma_2\\ \sigma_3\end{pmatrix} = \begin{pmatrix}\sigma_1\\ \sigma_2\\ \sigma_3\end{pmatrix}_{yield} + \begin{pmatrix}\Delta\sigma_1\\ \Delta\sigma_2\\ \Delta\sigma_3\end{pmatrix} = \begin{pmatrix}0.5\\ 0.667\\ 1\end{pmatrix} + \begin{pmatrix}0.079\\ 0.105\\ 0.157\end{pmatrix} = \begin{pmatrix}0.579\\ 0.772\\ 1.157\end{pmatrix} \tag{2.38}$$

$$\begin{pmatrix}\varepsilon_1\\ \varepsilon_2\\ \varepsilon_3\end{pmatrix} = \begin{pmatrix}\varepsilon_1\\ \varepsilon_2\\ \varepsilon_3\end{pmatrix}_{yield} + \begin{pmatrix}\Delta\varepsilon_1\\ \Delta\varepsilon_2\\ \Delta\varepsilon_3\end{pmatrix} = \begin{pmatrix}0.5\\ 0.667\\ 1\end{pmatrix} + \begin{pmatrix}0.079\\ 0.105\\ 0.785\end{pmatrix} = \begin{pmatrix}0.579\\ 0.772\\ 1.785\end{pmatrix} \tag{2.39}$$

A method to check if the obtained solution is correct is using the compatibility condition (2.23):

$$\boldsymbol{v} = L\sum_{i=1}^{N_p}\boldsymbol{b}_i^T\boldsymbol{e}_i\omega_i = \left(1\times 0.579\times\frac{5}{18}\right)+\left(1\times 0.772\times\frac{8}{18}\right)+\left(1\times 1.785\times\frac{5}{18}\right) = 1.000 \tag{2.40}$$

which gives the same nodal displacement as the one imposed.

**DB element**

The DB element will be subjected to the force that corresponds to the displacement in the FB element, which is the sum of the scaled value of (2.30) and the increment (2.37).

$$\boldsymbol{q} = scale\ factor\times\boldsymbol{q}_0 + \Delta\boldsymbol{q} = 0.713\times 1.403 + 0.290 = 1.290 \tag{2.41}$$

Section stiffnesses at each integration point are derived from (2.9) and (2.25) in a similar procedure as the flexibilites, but in the inverse form:

$$\boldsymbol{k}_s = \begin{cases}\dfrac{\partial N}{\partial\varepsilon} = A\dfrac{\partial\sigma}{\partial\varepsilon} = A & \text{for } \varepsilon\le\varepsilon_y\\[2ex] \dfrac{\partial N}{\partial\varepsilon} = \dfrac{A}{0.5}\dfrac{\partial\sigma}{\partial\varepsilon} = 2A & \text{for } \varepsilon>\varepsilon_y\end{cases} \tag{2.42}$$

Since there only is one free deegre of freedom in the cantilever, the shape function $\boldsymbol{N}(x)$ and its derivative $\boldsymbol{B}(x)$ are given as

$$\boldsymbol{N}(x) = \frac{x}{L} \;\Rightarrow\; \boldsymbol{B}(x) = \frac{1}{L} \tag{2.43}$$

The section stiffnesses are calulated as

$$\begin{pmatrix} \boldsymbol{k}_{s,1} \\ \boldsymbol{k}_{s,2} \\ \boldsymbol{k}_{s,3} \end{pmatrix} = \begin{pmatrix} 2 \\ 1.5 \\ 1 \end{pmatrix} \tag{2.44}$$

which gives the following element stiffness by using equation (2.16):

$$\boldsymbol{k} = L\sum_{i=1}^{N_p} \boldsymbol{B}_i^T \boldsymbol{k}_{s,i} \boldsymbol{B}_i \omega_i = \left(\frac{1}{1} \times 2 \times \frac{1}{1} \times \frac{5}{18}\right) + \left(\frac{1}{1} \times 1.5 \times \frac{1}{1} \times \frac{8}{18}\right) + \left(\frac{1}{1} \times 1 \times \frac{1}{1} \times \frac{5}{18}\right) = 1.5 \tag{2.45}$$

The nodal displacement is then

$$\boldsymbol{v} = \boldsymbol{k}^{-1}\boldsymbol{q} = \frac{1}{1.5} \times 1.290 = 0.860 \tag{2.46}$$

Equation (2.11) and the chosen shape functions (2.43) show that the axial strain $\varepsilon$ is constant through the element. This gives the following strain and stress

$$\varepsilon = \frac{v}{L} = \frac{0.860}{1} = 0.860 \Rightarrow \sigma = 0.860 \tag{2.47}$$

and the axial force distribution

$$\begin{pmatrix} N_1 \\ N_2 \\ N_3 \end{pmatrix} = \begin{pmatrix} 1.720 \\ 1.290 \\ 0.860 \end{pmatrix} \tag{2.48}$$

To check equilibrium, equation (2.15) is used:

$$\boldsymbol{q} = L\sum_{i=1}^{N_p} \boldsymbol{B}_i^T \boldsymbol{s}_i \omega_i = \left(\frac{1}{1} \times 1.720 \times \frac{5}{18}\right) + \left(\frac{1}{1} \times 1.290 \times \frac{8}{18}\right) + \left(\frac{1}{1} \times 0.860 \times \frac{5}{18}\right) = 1.290 \tag{2.49}$$

which is the same value as the imposed load.

**Observations**

The calculated axial forces and strains for both methods are presented in table (2.3). As previously mentioned, the FB formulation stricty enforces the exact force distribution through the element with the force interpolation function $\boldsymbol{b}(x)$. This can be seen from the results, where the axial force is constant and equal to 1.000 at every integration point. The same is however not the case for the DB formulation, where the axial force varies throughout the element. Force equilibrium is obviously obtained with the FB formulation, as the forces are exact. For the DB formulation equilibrium is achieved in a weighted sense, by averaging the values at each integration point based on their numerical rule. This means that it does not satisfy the force equilibrium at an arbitrary point in the element, but rather in a global sense. Basically, the FB method satisfies the strong form of equilibrium, while the DB method only satisfies the weak form.

Table 2.3: Axial forces and strains in cantilever beam.

| | Integration point | Axial force, $N$ | Strain, $\varepsilon$ |
|---|---|---|---|
| FB element | 1 | 1.000 | 0.579 |
| | 2 | 1.000 | 0.772 |
| | 3 | 1.000 | 1.785 |
| DB element | 1 | 1.720 | 0.860 |
| | 2 | 1.290 | 0.860 |
| | 3 | 0.860 | 0.860 |

Compared to differences in displacements and strains, differences in the axial force are not of a large concern, as global equilibrium are satisfied for both methods. A critical issue arises for the DB element, which can be seen from the results in table (2.3). Because the strains are assumed constant throughout the beam, the method does not detect that the third integration point should had begun yielding. This results in a stiffer element compared to the FB element, which has varying strains, and thus more accurately describes the response. Numerically this can be seen in the calculation of the nodal displacement (2.46). Although both elements are subjected to the same force of $\boldsymbol{q} = 1.290$, the stiffness method's displacement is calculated as $\boldsymbol{v} = 0.860$, compared to the flexibility method's $\boldsymbol{v} = 1.000$.

These observations show that the FB flexibility formulation is superior to the DB stiffness formulation in sake of accuracy. Both methods are vulnerable to numerical integration errors which are based on the number of integration points used. But, the DB formulation does also have an discretization error because of its interpolation functions. These displacements shape functions are not exact, and thus often result in errors like the one seen in the cantilever beam example, where the strain is assumed constant. The only way to increase the accuracy would therefore be to increase the number of DB elements for each structural member. However, the drawback of this is that number of nodes increase, and with it the computational effort.

## 2.6 Localization issues

### 2.6.1 Physical defintion

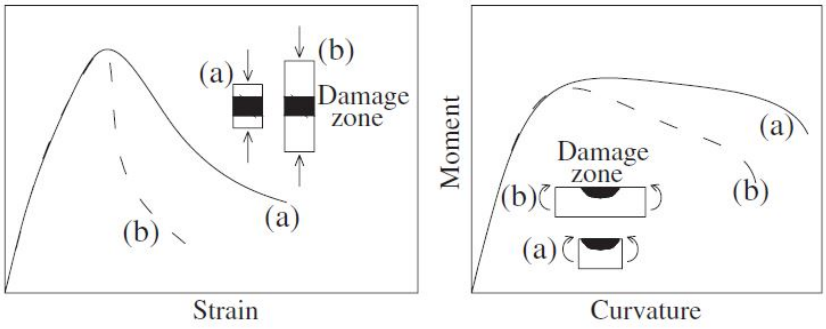


Figure 2.4: Size dependence due to localization (Calabrese, Almeida & Pinho, 2010).

Localization in structural members is defined as the structural properties being dependent on the member's size in the case of strain-softening. These properties include stress-strain relationships, peak strains and deformations, and ductility, among others. The localization phenomena occurs in concrete members for both tension, where it produces cracks, and for compression, where damage zones are made. Effects are well documented for the tensile case, and because the main focus of this thesis is on reinforced concrete where the steel bars handle the tensile forces, only localization due to compression is discussed further. Conceptual load-response diagrams are depicted in figure (2.4), which shows localization of structural members subjected to both uniaxial and flexural compression.

A concrete beam without reinforcement subjected to compressive stress is illustrated in figure (2.5). The concrete is divided into three sections, a failure zone with the length $L_Z$, and surrounding *bulk* concrete. As the member reaches its peak strength the damage begins concentrating in the failure zone, where the displacements increase as the load-carrying capacity decreases. To maintain equilibrium the bulk concrete experiences unloading, and thus a decrease in both stress and displacement. The mechanism is shown in the stress-strain relationships. In a) the bulk concrete carries the load up until the peak stress, and then unloads elastically as the failure zone softens and dissipates energy in b). Additonally, the preapeak energy is colored in a), while the postpeak energy is colored in b).

Several experiments have been performed that verify the localization issue, among the most cited are the ones by Jansen & Shah (1997). These were performed on both normal strength (45 MPa) and high strength (90 MPa) concrete, with height to diameter ratios from 2 to 5.5. Results from the experiments are shown in figure (2.6), with the normal strength concrete in a), and the high strength in b). From the stress-displacement curves it can be seen that the response is largely affected by localization, as the prepeak displacement is proportional to the member length. In addition, as the member length increases, the prepeak response becomes less steep while the postpeak response becomes steeper. However, the stress-strain curves show that the prepeak strain are identical for all the

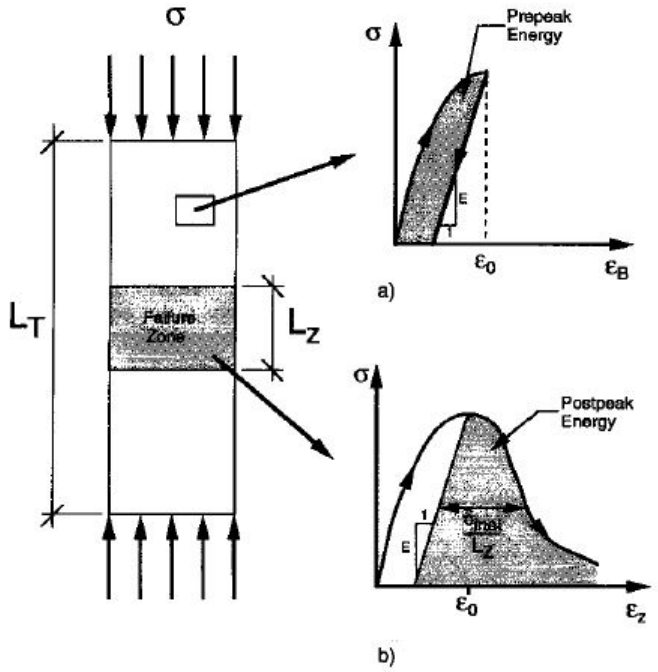


Figure 2.5: Localization behaviour in compression (Jansen & Shah, 1997).

different member lengths. The localization issue first takes place after the peak stress is reached, with steeper curves and lower ultimate strains as the length increases.

There have been several proposals on how to model the localization issue, particularly in fracture mechanics research. One of the earliest models presented is the one by Hillerborg (1990), which says that the stress-strain relation can be constructed by combining two different curves. The first curve, shown left in figure (2.7), describes the prepeak response, which is not affected by the member length. The second curve, shown in the middle, is the postpeak response, and is based on a function of the member length. Together these two curves combine into the stress-strain curve to the right in the figure.

The strain $\varepsilon'$ is calculated from the prepeak strain $\varepsilon$ from the strain-stress curve, and the post peak displacement $w$ from the strain-displacement curve. Hillerborg presented this in the given equation

$$\varepsilon' = \varepsilon + \frac{w}{l} \tag{2.50}$$

with

$$l = \beta \xi d \tag{2.51}$$

where $\xi d$ is the depth of the members compression zone, and $\beta$ is a proportionality factor commonly set to 0.8. An example of this model is illustrated in figure (2.8), where $x$ is set as the compression zone depth.

Later research showed that Hillerborg's formulation overestimated the effect of localization. Markeset and Hillerborg proposed the Compressive Damage Zone (CDZ) model in 1985, which takes into account the effect from longitudinal cracks, lateral strains and

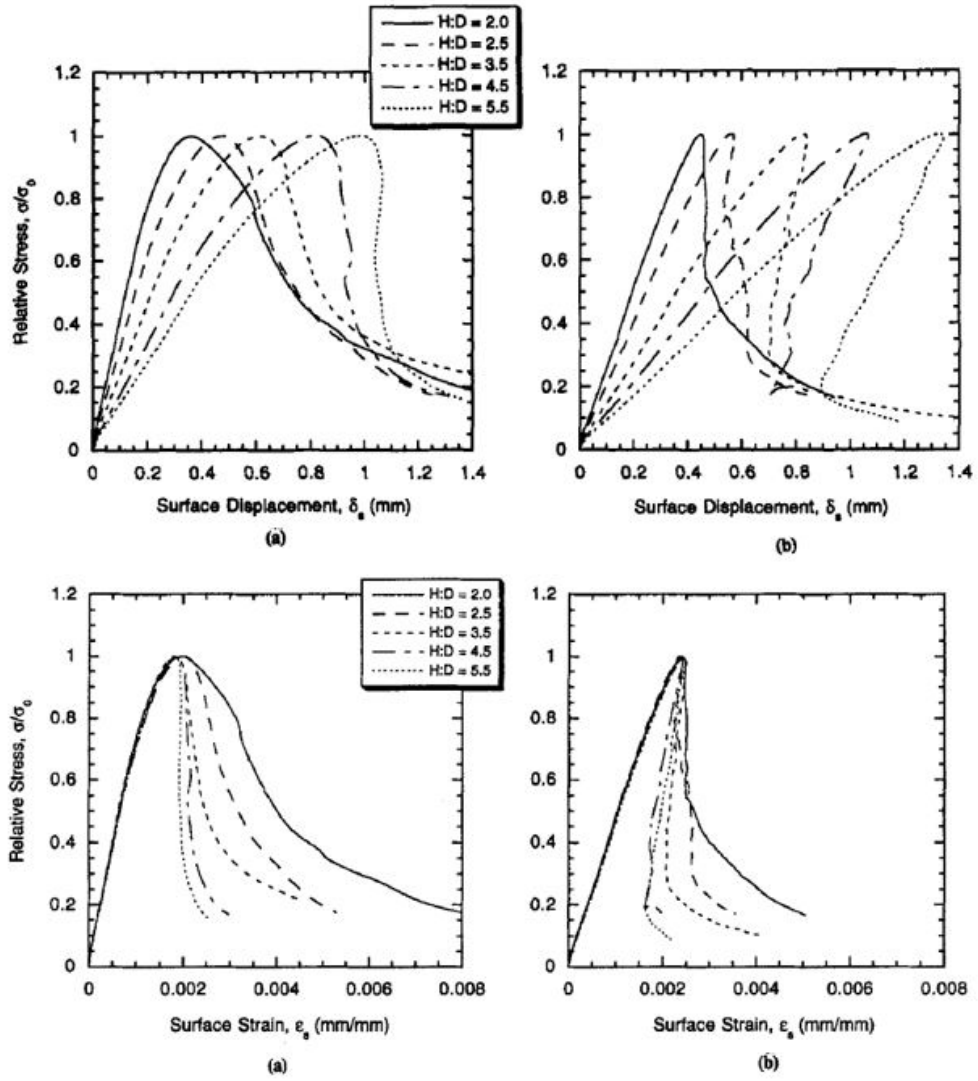


Figure 2.6: Behaviour of concrete columns in compression with different height-diameter ratios (Jansen & Shah, 1997).

shear deformations. An illustration of the CDZ model is shown in figure (2.9), which points out that it is based on three different load-response curves, instead of Hillerborg's original two. The first and third curve in the figure are similar to the curves used in Hillerborg's model, with the first describing the prepeak stress-strain relationship, and the third showing the stress-displacement curve of the postpeak response. The second curve shown in the figure is the new addition of the improved CDZ model. It describes the additional strain $\varepsilon_d$ caused by the formation of longitudinal cracks and additional lateral strains. In the fracture process, energy absorption per unit volume $W^s$ can also be calculated. Combining these three curves gives the complete stress-strain relationship illustrated in figure (2.10), and comparisons between experimental results and analyses done with the CDZ model are shown in figure (2.11). These results illustrate adequate approximations of the postpeak softening response of concrete.

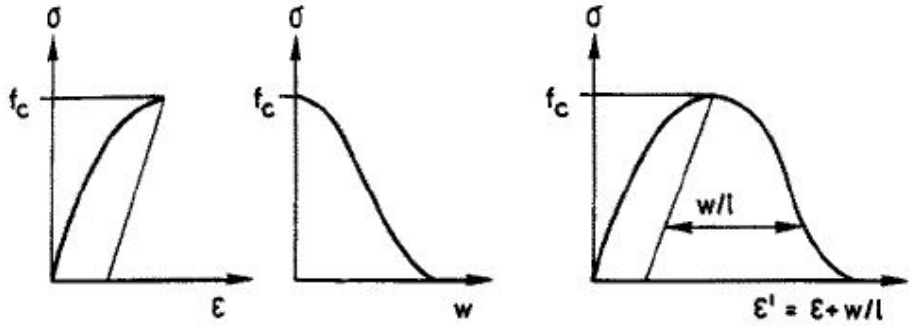


Figure 2.7: Stress-strain relationship adjusted for member length (Hillerborg, 1990).

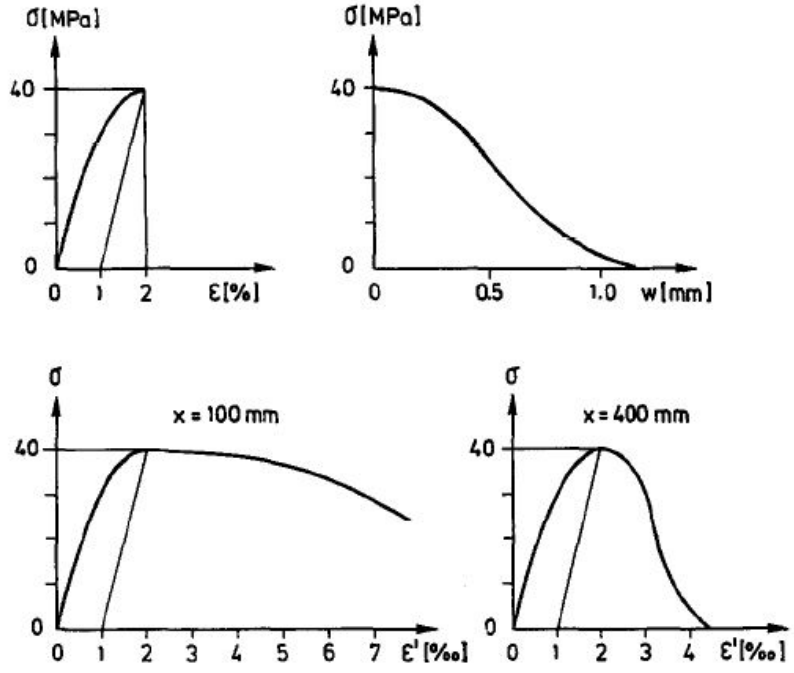


Figure 2.8: Numerical example of stress-strain curves based on Hillerborg's formulation (Hillerborg, 1990).

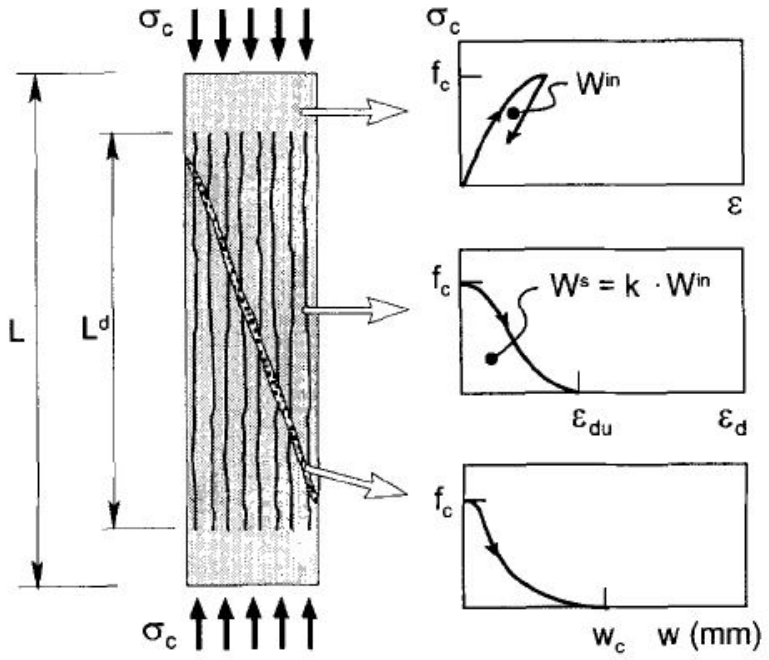


Figure 2.9: CDZ model subject to compression (Markeset & Hillerborg, 1995).

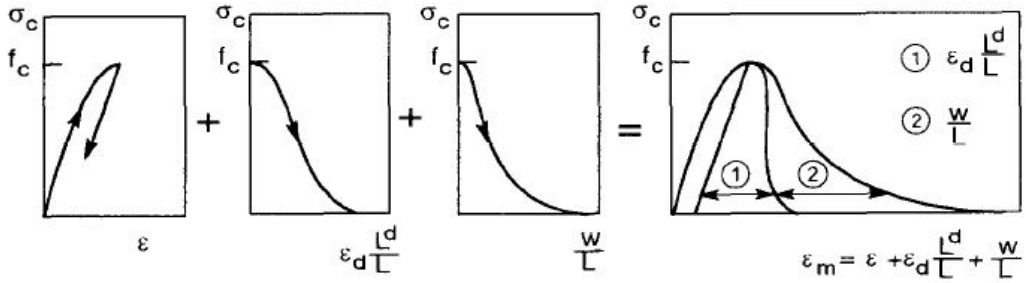


Figure 2.10: Complete stress-strain curve of the CDZ model (Markeset & Hillerborg, 1995).

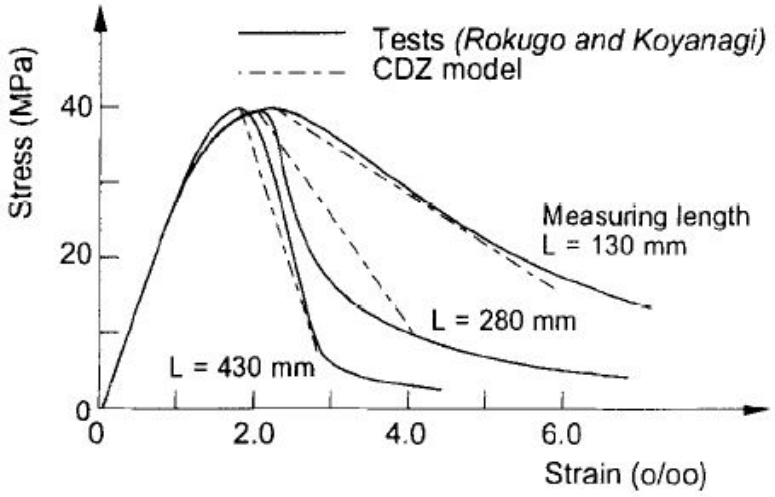


Figure 2.11: Comparison of experimental and numerical results with the CDZ model (Markeset & Hillerborg, 1995).

### 2.6.2 Numerical definition

**Objective and non-objective response**

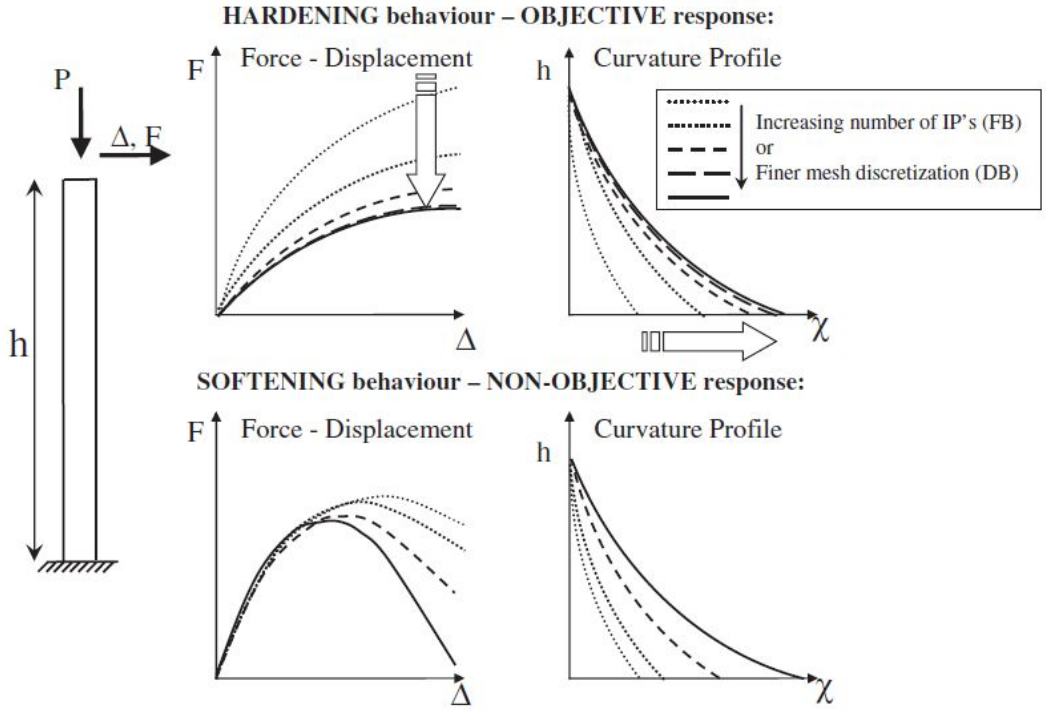


Figure 2.12: Objective and non-objective response of a cantilever column (Calabrese, Almeida & Pinho, 2010).

As discussed in the previous section, the physical definition of localization is that the material behaviour is dependent on the member length. This can be taken into account in the numerical analysis by altering the stress-strain relationships of the structural elements. However, another issue arises in the modelling of these structures. Both DB and FB elements experience numerical problems for strain-softening response. While hardening behaviour leads to stable solutions, which is called objective response, the elements do not convergence to a single solution for softening behaviour, called non-objective response. For the latter case this simply means the calculated response is dependent on the number of elements (DB formulation) or integration points (FB formulation) used, even though the external load and member properties are left unchanged. This applies for both global force-displacement response and the local moment-curvature response, and is due to a localization of the computed strains at the sections with the highest bending moments. A qualitative description of the problem is illustrated in figure (2.12). It should also be mentioned that unlike the physical localization issue, the numerical one is made entirely from the finite element assumptions, and is therefore not experienced in reality.

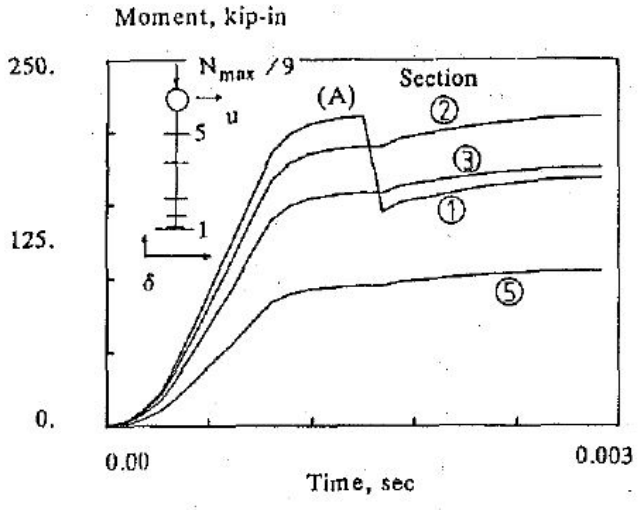


Figure 2.13: Displacement-based cantilever column under lateral dispacement (Zeris & Mahin, 1988).

**DB elements**

The main numerical localization issue in DB elements is explained by Zeris & Mahin (1988) for a simple cantilever column subjected to a lateral displacement at its tip. As the applied displacement increases, the sections near the column's base begin softening and lose their capacity. In order to maintain force equilibrium, the remaining sections have to unload elasticially, conceptually similar to the bulk concrete discussed in the previous section. The reason for the numerical failure is that while the base sections detects the softening behaviour through the defined constitutive relation, the rest of the column do not know that it should unload when assembling the element stiffness matrix (Eq. 2.16). This results in the unrealistic case where the base sections unload while the top sections continue to take more bending moment, which is illustrated in figure (2.13).

**FB elements**

Localization issues in FB elements have been under wide research, as it is gradually being accepted as having clear advantages over DB elements. Figures (2.14), (2.15) and (2.16) show three different response curves for a cantilever column subjected to a lateral displacment. Respectively strain-hardening, elastic-perfectly plastic, and strain-softening section response, all modelled with one single FB element. It should also be noted that unlike the DB elements, there is not an issue with force equilibrium in the FB elements after the onset of softening in a structural member; simply because equilibrium is strictly enforced in the formulation. Instead, other issues arise, and are discussed below.

In the strain-harderning case, both the global force-displacement and local moment-curvature responses are objective, and converge into a single solution as the number of integration points along the member is increased. The same is however not the case for

the elastic-perfectly plastic section, where the moment-curvature becomes non-objective. As the section and integration point reaches the plastic moment capacity of the member, the curvature increases with a constant bending moment. Due to the enforcement of equilibrium, the bending moment distribution is kept linear throughout the member, which forces the other sections to remain linear elastic. The number of integration points define the weight of the base section, which can be interpreted as the plastic hinge length. With the increase of integration points, this length will be shortened, and thus require higher curvatures to give the same global displacement. This can be understood from the calculation of the rotations of each integration point, which is

$$\theta_i = \phi_i \omega_i L \tag{2.52}$$

where $\phi_i$ is the curvature at each integration point, and $\omega_i$ is the weight, and $L$ is the length of the member. Next, the tip displacement of the column is determined from summing up and multiplying these rotations with their lengths from tip to integration point. This can be written as

$$\delta_i = \sum_{i=1}^{N_p} \theta_i L_i \tag{2.53}$$

where $N_p$ is the number of integration points, and $L_i$ is the distance from bottom of integration point length to top of column. The calculated global response remains objective since the displacement is prescribed and equilibrium is maintained. Naturally, the plastic hinge length would increase in a real member if the applied displacement were to be increased. The FB element would, however, not be able to detect it.

Strain-softening is often experienced in reinforced concrete columns that are subjected to large dead loads and lateral forces (Coleman & Spacone, 2001). In the numerical sense both the global and local response is non-objective, as seen in figure (2.16). Similarly to the elastic-perfectly plastic member section, the curvature localizes at the base section. But in contrast to the former case the base section begins softening, and is thus not able to carry the same loading as the section strains increase. Again, as the number of integration points increase and the plastic hinge region gets smaller, the resulting growing strains will inflict even lower material stiffness. This is observed in the local response plot, where increasing the number of integration points yields larger curvature and lower ultimate base shear. Even though the applied displacement is prescribed, the different amounts of material stiffness degradation affect the load-carrying capacity, and thus make the global response non-objective as well.

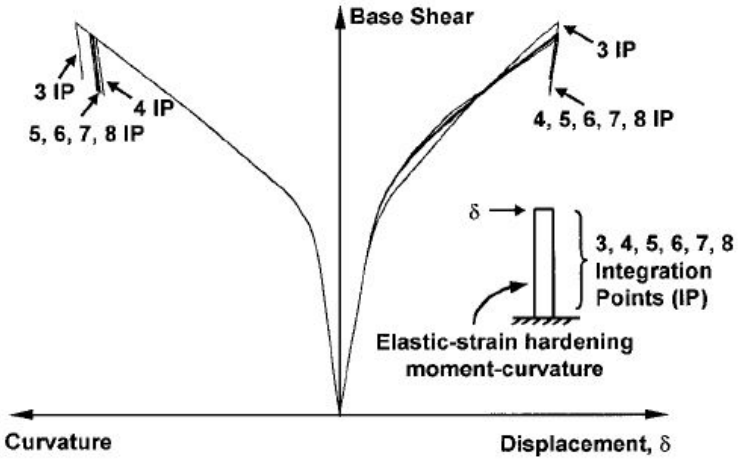


Figure 2.14: Cantilever column with strain-hardening response (Coleman & Spacone, 2001).

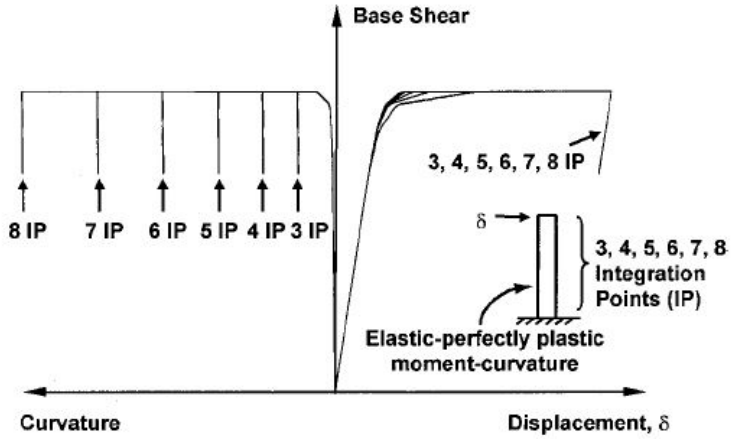


Figure 2.15: Cantilever column with elastic-perfectly plastic respons. (Coleman & Spacone, 2001).

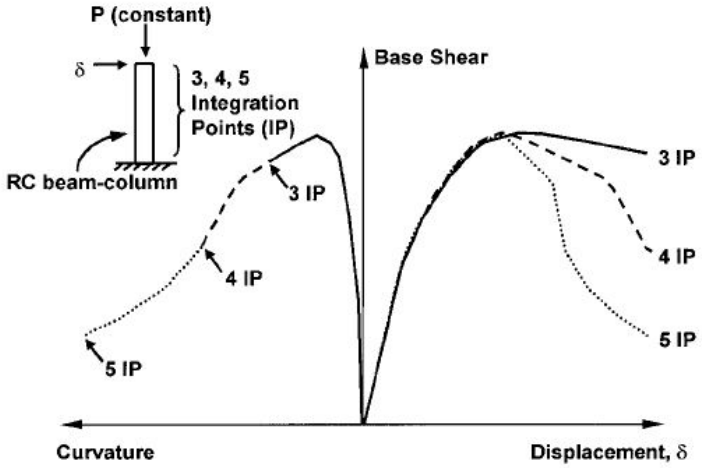


Figure 2.16: RC cantilever column with strain-softening response (Coleman & Spacone, 2001).

### 2.6.3 Regularization techniques

#### DB elements

The typical regularization procedure for DB beam-columns has been to adjust the elements lengths on a basis of the plastic hinge lengths of the member. Formerly it was common to define the size of the most strained element equal to the plastic hinge length, $L_p$. This was due to the belief that localization was forced within a single element, and not just one integration point. Later research showed that this was not true, and that localization occurs in one integration point, similar to FB element members (Zeris & Mahin, 1988). To ensure the correct regularization, the weight of the most strained integration point has to be equal to the predetermined $L_p$. In the case of an element with two Gauss-Legendre points, where each point have half the weight, it means that the most strained element should have the length $2L_p$. Table (2.4) depicts the necessary lengths of the extremity elements for different numbers of integration points.

A comparison between experimental data and analysis results can be seen in figure (2.17). The DB elements used have 2 integration points, which results in a regularized element length of $2L_p$. Apparently the increased element length gives a better approximation of the ultimate curvature of the member. However, neither of the regularized lengths render satisfactory bending moment values at the postpeak stage. This is due to the length of the extremity element being very large compared to the total column length. In the analysis shown, this element has the length 0.71 $m$ while the column is 1.65 $m$. The remaining elements are thus considerably smaller, which yield discrepancies in the analysis.

The plastic hinge length $L_p$ is, as previously mentioned, a predetermined modeling assumption. It is commonly estimated by a equation proposed by Paulay and Priestley

Table 2.4: Regularizaton of DB elements by size adjustment of extremity elements.

| Integration rule | Number of IPs | Weight of extremity IP, $\omega$ | Element length, $L_p$ |
|---|---|---|---|
| Gauss-Legendre | 2 | 1 | 2 |
| | 3 | 0.55556 | 3.6 |
| | 4 | 0.34785 | 5.74952 |
| | 5 | 0.23693 | 8.44142 |
| Gauss-Lobatto | 3 | 0.33333 | 6 |
| | 4 | 0.16667 | 12 |
| | 5 | 0.1 | 20 |

(1992), which is made from empirical observations:

$$L_p = 0.08L + 0.022 f_y d_B \tag{2.54}$$

where $L$ is the member length, $f_y$ is the yield stress of the steel reinforcement, and $d_b$ is the diameter of the longitudinal bars. Based on the information given in table (2.4), it is evident that a high number of integration points in the extremity element will cause it to have impractical lengths; often even longer than the member itself. This makes it obvious that only a low number of Gauss-Legendre integration points can be used for regularized DB element members.

A different regularization method is proposed by Adessi and Ciampi (2007), and is based on the integral definition of the associated variable governing the damaging evolution process. In others words, the constitutive relation is modified to have a damage variable that represents the irreversible degradation of the member strength and stiffness. This damage variable is given by the equation

$$D = \frac{Y - Y_0}{aY + R} \tag{2.55}$$

where $Y_0$, $a$ and $R$ are parameters adjusting the intitial conditions and damage rate. The variable $Y$ describes the flexural deformation state, and is given as

$$Y = \phi_e + \beta(\phi_p)\phi_p \tag{2.56}$$

where $\phi_e$ is the elastic curvature, and $\beta(\phi_p)$ is an increasing function of the plastic curvature $\phi_p$. Further it is assumed that the axial response is linear elastic, and that bending is only in one direction. By including the damage variable defined in equation (2.55), the section forces are written as

$$\boldsymbol{s}(x) = \begin{pmatrix} EA\varepsilon \\ (1-D)^2 EI(\phi - \phi_p) \end{pmatrix} \tag{2.57}$$

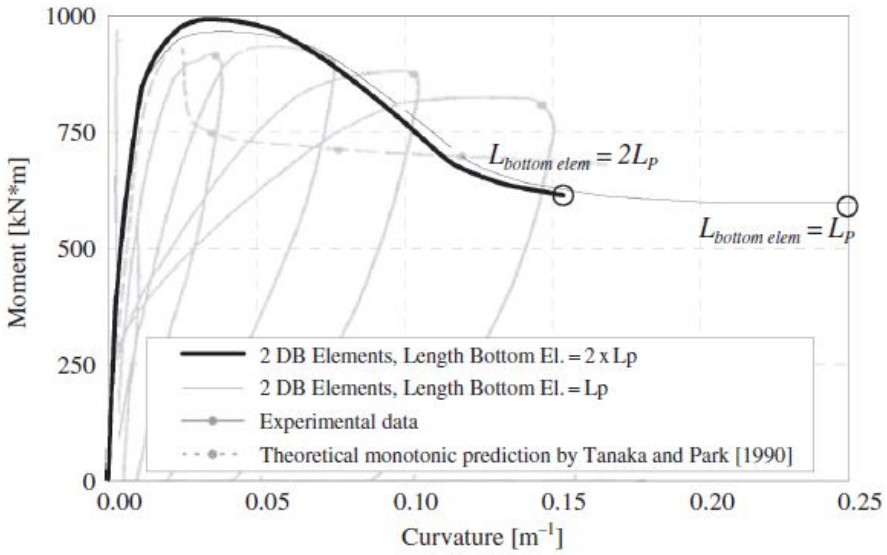


Figure 2.17: Local response of DB element member. (Calabrese, Almeida & Pinho, 2010)

where $\phi$ is the total curvature. The corresponding section stiffness is

$$\boldsymbol{k_s}(x) = \begin{bmatrix} EA & 0 \\ 0 & (1-D)^2 EI \end{bmatrix} \tag{2.58}$$

Adessi and Ciampi's approach has been shown to be effective, but only as long as the dimension of the extremity element are either smaller or the same size as the forming plastic hinge.

**FB elements**

Two recognized regularization techniques for members consisting of FB elements have been proposed by Coleman and Spacone (2001). The constant fracture energy criterion regularizes the global force-displacement response. It is based on including an additional material parameter, the fracture energy $G_f^c$, which is defined by

$$G_f^c = \int \sigma \, du_p = L_{IP} \int \sigma \, d\varepsilon_p \tag{2.59}$$

Here $u_i$ is the plastic displacement, $\varepsilon_p$ is the plastic strain, and $L_{IP}$ is the length of the integration point where the localization occur. The Kent and Park (1971) stress-strain relationship for concrete under compression is shown in figure (2.18). The shaded area describes the fracture energy divided by the length of the crack band, which is equal to $L_{IP}$ for FB elements. The postpeak response is linear softening untill it reaches 20 % of the compressive strength $f_c'$, where it is assumed to remain constant. This turning point

is predetermined by the strain value $\varepsilon_{20}$, while the fracture energy can be determined from experimental testing. From figure (2.18), the following equation is derived

$$\varepsilon_{20} = \frac{G_f^c}{0.6 f_c' L_{IP}} - \frac{0.8 f_c'}{E} + \varepsilon_0 \tag{2.60}$$

The quantities $G_f^c$, $f_c'$, Young's modulus $E$, and $\varepsilon_0$, which is the strain corresponding to the peak stress, are assumed constant. Because the length of the integration point $L_{IP}$ varies with the level of discretization, if follows that the value $\varepsilon_{20}$ has to be adjusted for a constant fracture energy to be preserved. By determining an unique value for $\varepsilon_{20}$ depending on the integration scheme used, constant stress-displacement is assumed instead of a constant stress-strain relation. This will ensure global objectivity for softening response, and thus yield better approximations of experimental results. The concept is similar to the physical localization theory in section (2.6.1), where the stress-strain relations where adjusted for the member lengths.

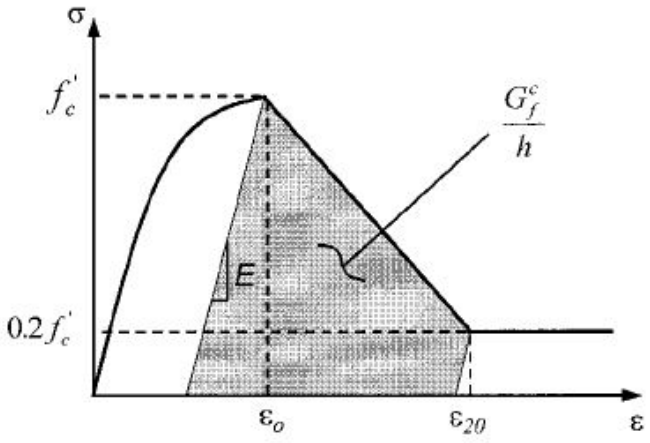


Figure 2.18: Kent-Park stress-strain law (Coleman & Spacone, 2001).

Because of the fact that the length of the first integration point does not always correspond to the length of physical plastic hinge, the constant fracture energy criterion is insufficient for regularization of local response. Thus Coleman & Spacone's second proposal is that the internal element forces and deformations have to be post-processed to obtain objectivity. A deformed beam is illustrated in figure (2.19), with the relevant moment and curvature distribution. The total curvatures of the plastic hinges consist of an elastic and an inelastic component. The inelastic curvature of the model is approximated as

$$\phi_i^{model} \approx \frac{\delta_i}{L_{IP}\left(\frac{L}{2} - \frac{L_{IP}}{2}\right)} \tag{2.61}$$

The inelastic hinge rotation is thus calulated as $\theta_i = \phi_i L_{IP}$. Alternatively, the actual

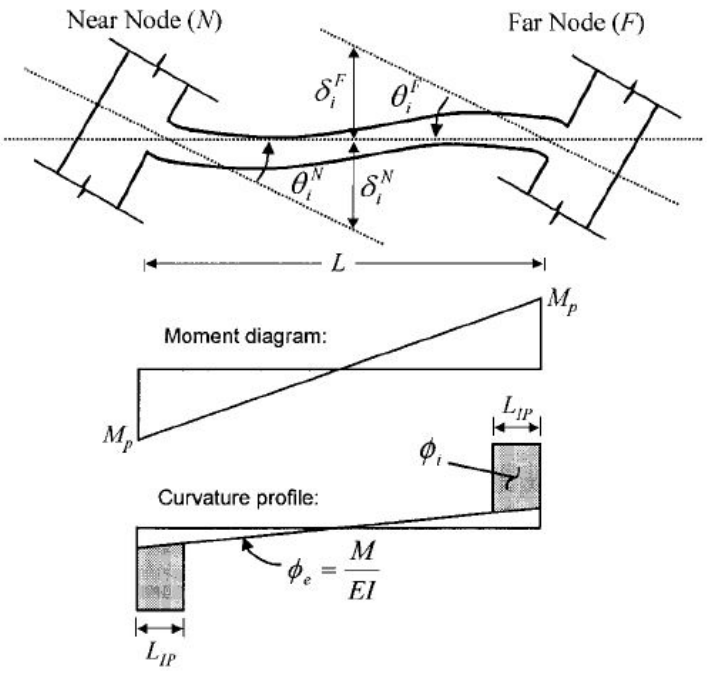


Figure 2.19: Deformed interior beam with plastic hinges. (Coleman & Spacone, 2001)

predicted length of the plastic hinge can be substituted in the equation (2.61), yielding

$$\phi_i^{predict} \approx \frac{\delta_i}{L_p\left(\frac{L}{2} - \frac{L_p}{2}\right)} \tag{2.62}$$

which is the true curvature of the deformed member. Calculation of the total curvature is done with the equation

$$\phi = \phi_e + (scale\ factor)\phi_i^{model} \tag{2.63}$$

where $\phi_e$ is the elastic curvature component. The scale factor is obtained by combining equations (2.61) and (2.62), and for a double-curvature member is given as

$$scale\ factor = \frac{\omega_{IP} L^2 (1 - \omega_{IP})}{L_p(L - L_p)} \tag{2.64}$$

where $\omega_{IP}$ is the weight of the extremal integration point. For members with single curvatures, like for instance cantilever columns, the expression is

$$scale\ factor = \frac{\omega_{IP} L^2 (2 - \omega_{IP})}{L_p(2L - L_p)} \tag{2.65}$$

Obviously, if the length of the first integration points $L_{IP}$ is equal to the length of the plastic hinge $L_p$, there is no need for a scaling factor, and thus no regularization is required to obtain objectivity. It is however problematic to ensure that these two lengths correspond to each other. Very often the length of the element has to be adjusted, with additional elements being necessary. Thus, the computational advantage of the FB formulation is lost. Alternatively the integration scheme can be changed. For short elements the number of integration points has to be decreased, which reduces accuracy, and for longer elements integration points have to be increased, which raises computational demand.

The damage variable regularization procedure by Adessi and Ciampi can also be used for FB elements. However, to fully be efficient it requires the structural members to be subdivided into several elements, which obviously eliminates one of the main benefits of the FB formulation.

## 2.7 Cantilever column subject to pushover analysis

### 2.7.1 OpenSees

The Open System for Earthquake Engineering Simulation, abbreviated as OpenSees, is used for the following analysis. It is developed by the Pacific Earthquake Engineering Research Center, which is located at the University of California, Berkeley. As it is primarily created for research purposes it lacks a graphical interface, and is rather based on input scripts written in a combination of the TCL programming language and integrated OpenSees commands. This makes it a tedious task to create large and complicated structural models. However, the fact that OpenSees is an open-source software has allowed developers from both academical and private institutions to contribute to improve the software. Because of this, OpenSees is one of the state-of-art structural engineering softwares available. The user interface is depicted in figure (2.20).

### 2.7.2 Model definition

The reinforced concrete cantilever column, shown in figure (2.21), has been used to show differences in response between DB and FB elements. Pushover analyses have been performed for both hardening and softening response. The column cross section shown has symmetric reinforcement about both section axes, and it is assumed that the hoop spacing is too large to provide any confinement effects for the concrete core. The steel reinforcement is described by a Giuffre-Menegotto-Pinto model with isotropic strain hardening, while the concrete is described by a Kent-Scott-Park model with zero tensile strength.

### 2.7.3 DB formulation

Based on the research done by Calabrese, Almeida and Pinho (2010), two Gauss-Legendre integration points has been used for the DB elements. Higher number of integration

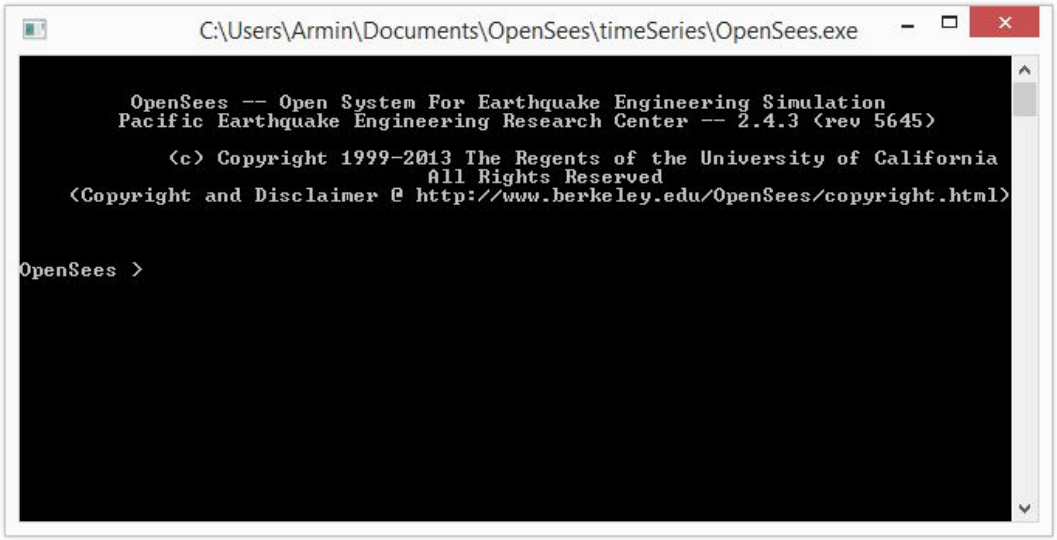


Figure 2.20: OpenSees user interface.

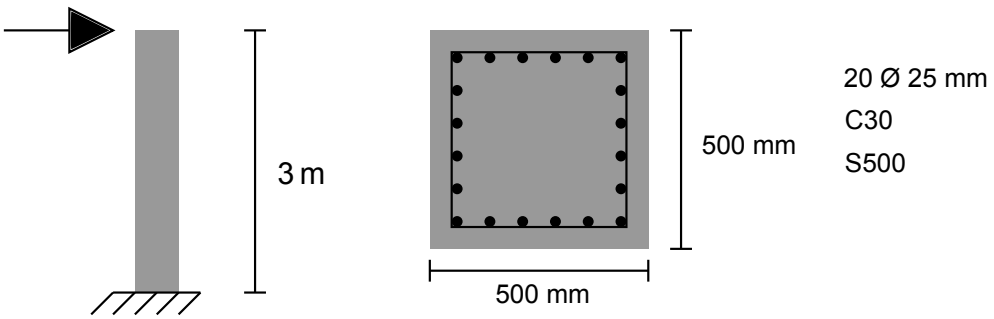


Figure 2.21: Reinforced concrete cantilever column-

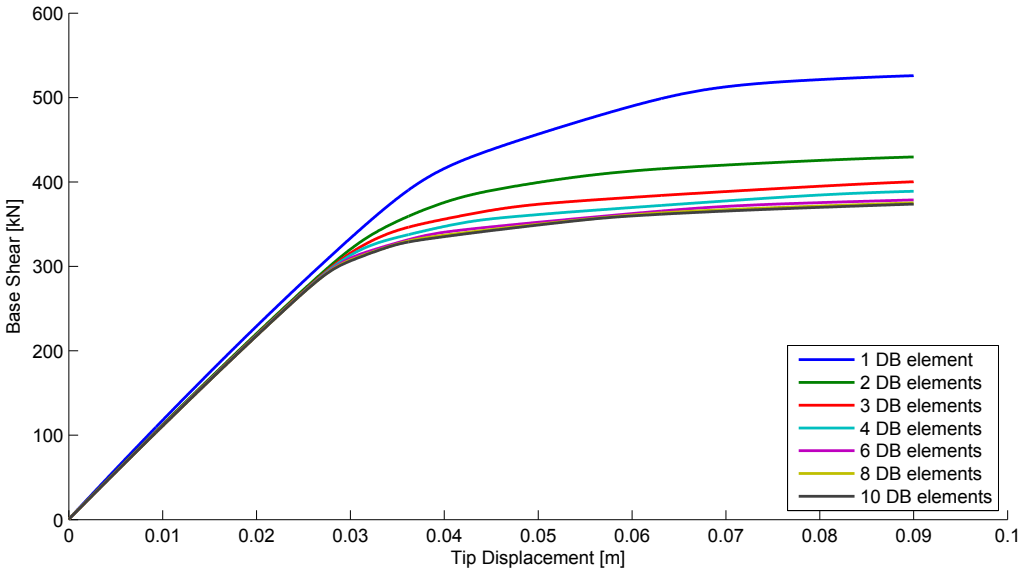


Figure 2.22: Global hardening response for DB formulation.

points do not give any significant improvement in accuracy, compared to increasing the number of elements. Also, all the elements have the same size within the different discretizations.

### Hardening response

The global force-displacement response illustrated in figure (2.22) shows hardening objetivity as the number of DB elements increase. Similar to what was experienced in the numerical example in section (2.5.1), using only a single DB element greatly overestimates the strength and post-yield stiffness of the beam-column member. The plots show that reasonable results are acquired with the use of six elements.

While objectivity is obtained for a relatively low number of elements for the global response, the same is not the case for the local moment-curvature response shown in figure (2.23). As can be seen, a similar response curve is achieved as the elements increase, but the ultimate curvature still differs with a large magnitude. This same issue with the DB elements has also been observed by Calabrese, Almeida and Pinho (2010). The reason for local non-objectivity is that the DB formulation only satisfies force equilibrium in an average sense.

### Softening response

To ensure a softening response, the column has been subjected to an additional axial compression load corresponding to 50 % of the axial yield limit. The global response is

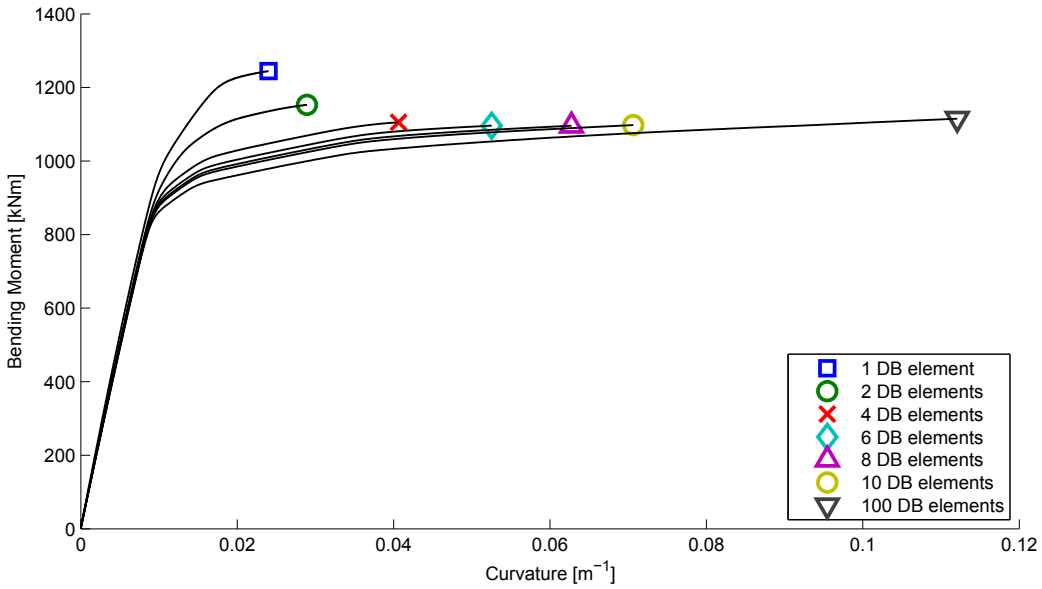


Figure 2.23: Local hardening response for DB formulation at 3 % drift.

shown in figure (2.24), where it is clearly non-objective compared to the hardening response. However, an important similarity is that for both response cases lower numbers of elements tend to overestimate the post-yield stiffness. Despite the large axial forces on the column, using only two DB elements nearly cancels out the expected softening response, and rather makes it close to perfectly plastic. The corresponding local response is illustrated in figure (2.25), where it like its hardening counterpart does not converge into a single solution as the number of elements increase.

### Regularization of softening response

The results obtained have been regularized by adjusting the length of the extremity element, so that the bottom integration point coincides with the plastic hinge length. The regularization procedure based on Adessi and Ciampi's damage variable is not implemented in OpenSees, and thus requires development and adjustment of already integrated commands. Because of this fact, it will not be used in this analysis. As shown in table (2.4), the necessary length for an element with two Gauss-Legendre integration points is $2L_p$. According to equation (2.54), the plastic hinge length of the column is equal to

$$L_p = 0.08L + 0.022 f_y d_B = 0.08 \times 3 + 0.022 \times 500 \times 0.025 = 0.515\ m \tag{2.66}$$

which means that the extremity base element has to have the length $1.030\ m$. The remaining elements have identical sizes, similar to the non-regularized discretization. Regularized softening responses are illustrated in figures (2.26) and (2.27), and show that

the procedure with adjusting extremity element lengths is highly effective. The global force-displacement response show nearly identical trends for all discretizations, while the local moment-curvature response follow a similar path untill an ultimate curvature of approximately 0.05 $m^{-1}$.

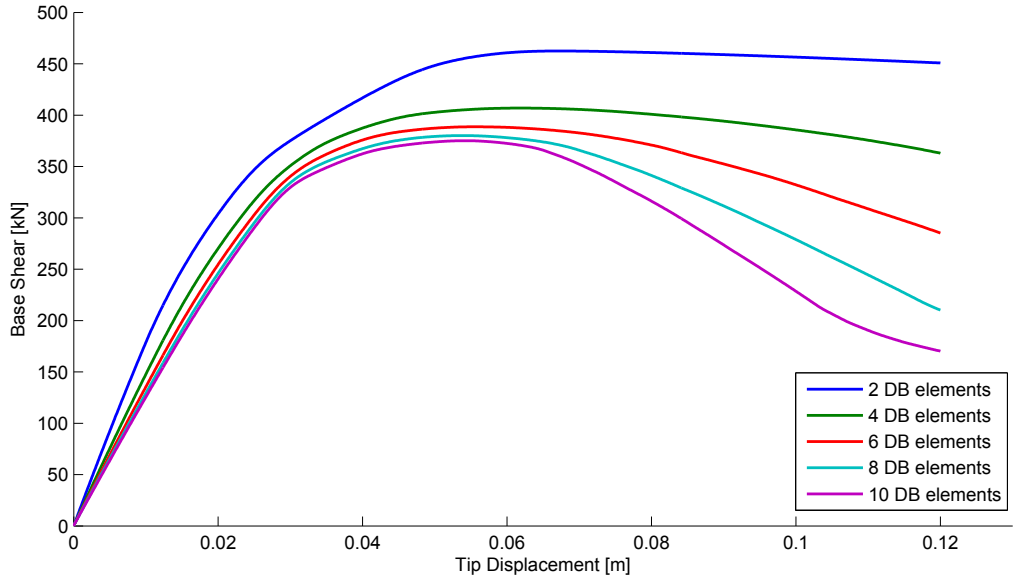


Figure 2.24: Global softening response for DB formulation

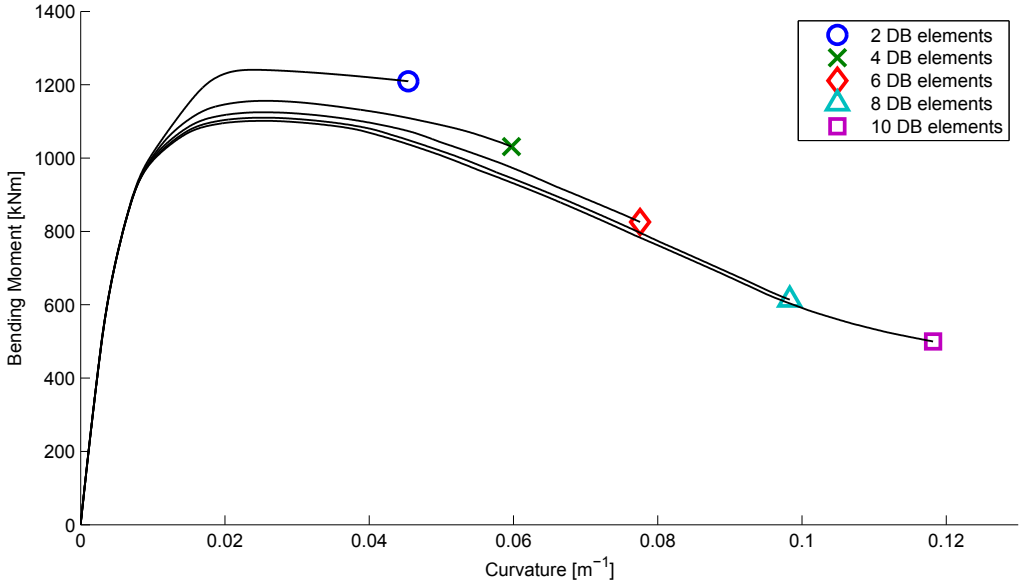


Figure 2.25: Local softening response for DB formulation at 4 % drift.

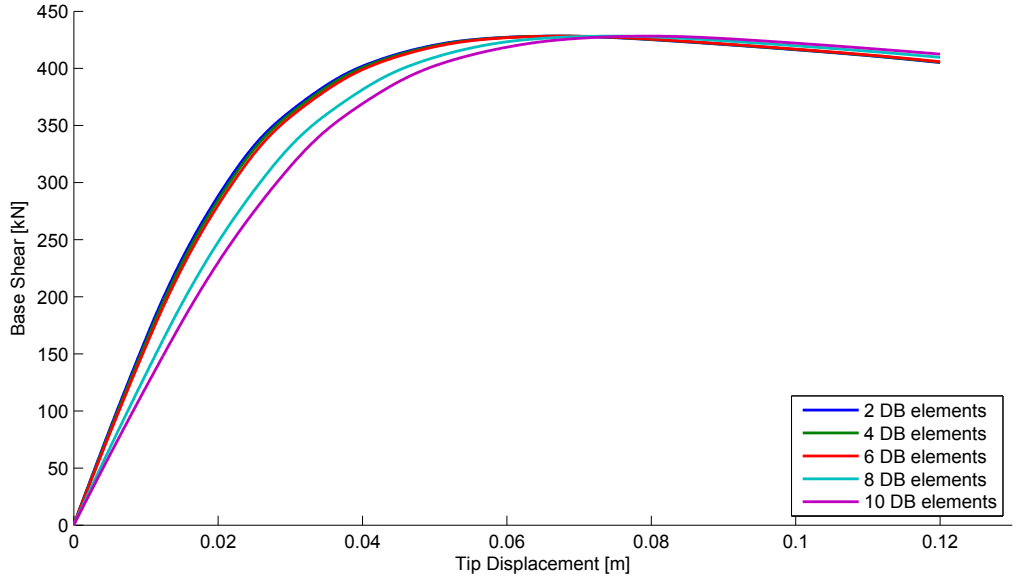


Figure 2.26: Regularized global softening response for DB formulation

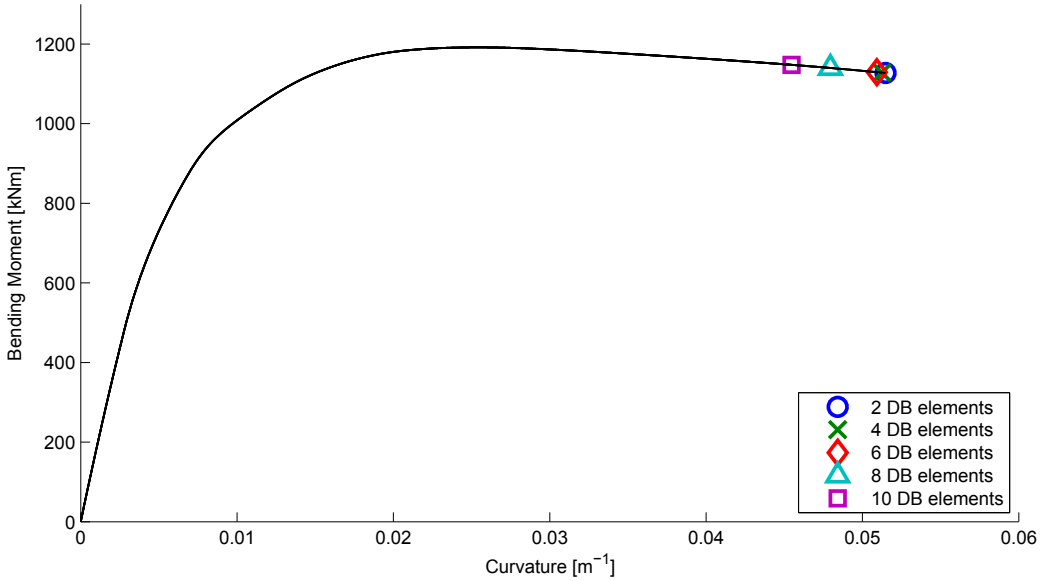


Figure 2.27: Regularized local softening response for DB formulation at 4 % drift.

### 2.7.4 FB formulation

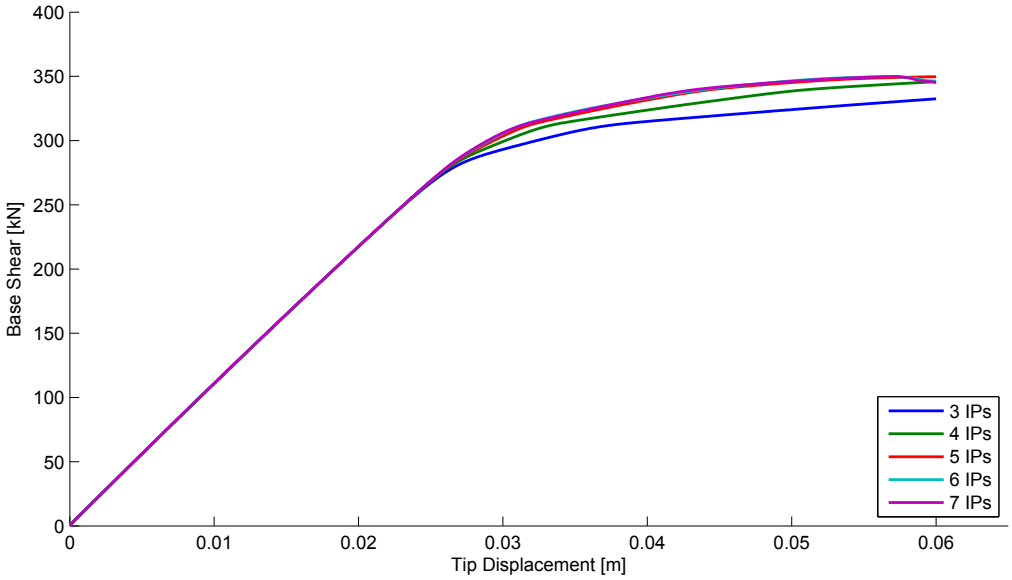


Figure 2.28: Global hardening response for FB formulation.

#### Hardening response

Global and local hardening for the FB formulation are depicted in figures (2.28) and (2.29). The results clearly show that both the global response lines and the local ultimate curvatures converge into single solutions as the number of integration points increase; a case of objectivity. Unlike the local hardening case of the DB formulation in figure (2.23) where the response was non-objective, the FB formulation achieves objectivity because it strictly enforces force equilibrium. This confirms that the FB elements not only have equilibrium on the element level, but also on section level.

#### Softening response

Similar to the softening case of the DB element column, there has been added an axial compression load corresponding to 50 % of the axial yield limit. Because of the fact that the FB formulation gives a more flexible solution, the softening response is clearly observed for all variants of section discretization. However, as expected, the global softening response illustrated in figure (2.30) in non-objective, and it can even be noticed that the member with six integration points show something similar to a snap-back behaviour. They do however show a nearly identical response untill the peak base shear is reached. The local response is depicted in figure (2.31), and also shows its expected non-objectivity.

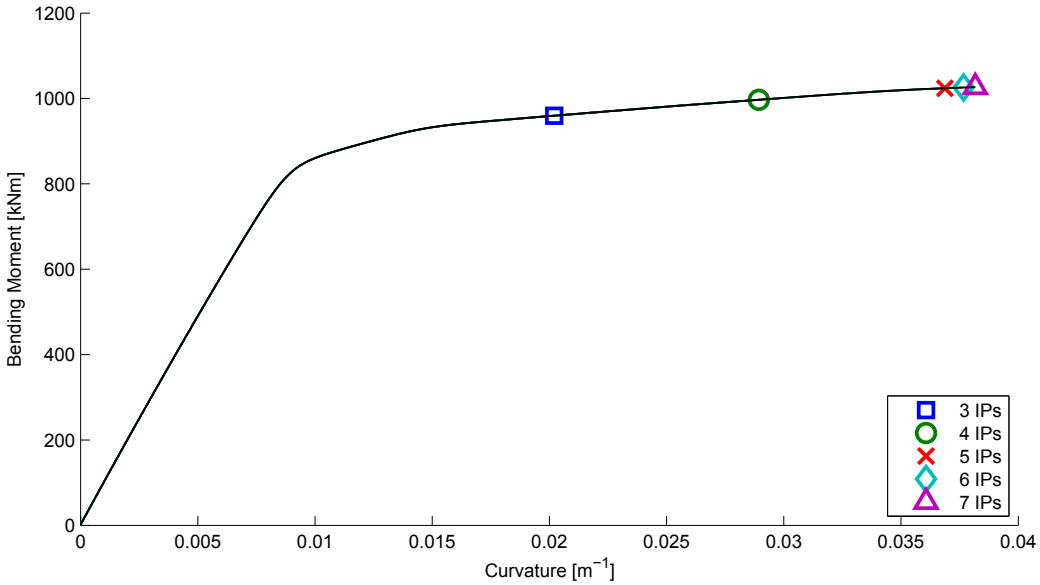


Figure 2.29: Local hardening response for FB formulation at 1.8 % drift.

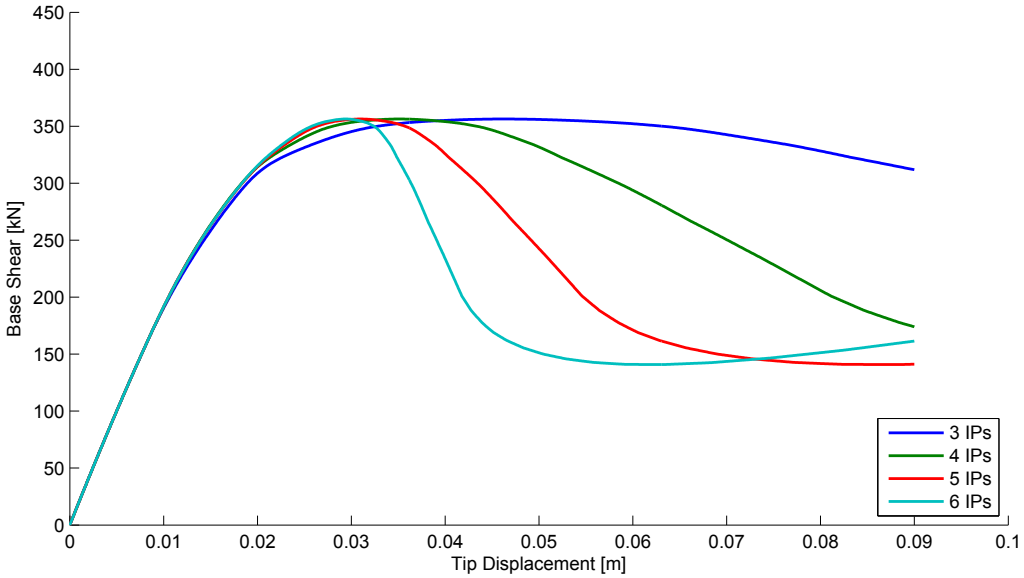


Figure 2.30: Global softening response for FB formulation.

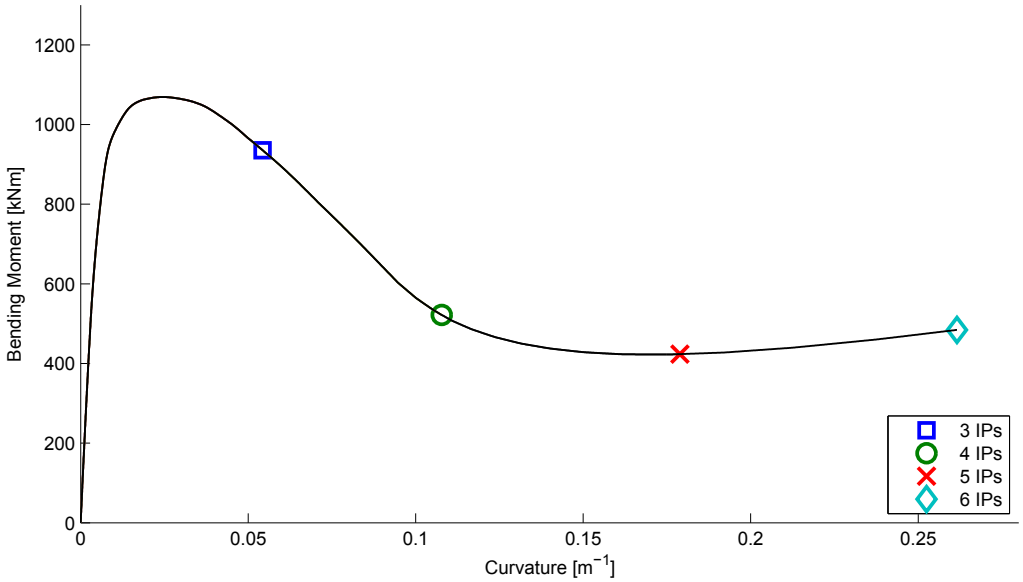


Figure 2.31: Local softening response for FB formulation at 3 % drift.

**Regularization of softening response**

The global softening response has been regularized using the constant fracture energy criterion. This means that instead of the commonly used ultimate strain of $\varepsilon_{20} = 20\ \varepsilon_0$, where $\varepsilon_0$ is the strain at the peak stress, separate ultimate strains are determined based on number of integration points used. The fracture energy $G_f^c$ is assumed to be 180 $MPa$, while the other material parameters are the previously used $f_c' = 30\ MPa$, $E_c = 30\ GPa$ and $\varepsilon_0 = 0.002$. Table (2.5) lists the different ultimate strains obtained for each specific plastic hinge length, based on equation (2.60).

Table 2.5: Ultimate strain values based on the constant fracture energy criterion.

| Number of IPs | Plastic hinge length, $m$ | Ultimate strain, $\varepsilon_{20}$ |
|---|---|---|
| 3 | 0.5 | 0.0212 |
| 4 | 0.25 | 0.0412 |
| 5 | 0.15 | 0.0679 |
| 6 | 0.10 | 0.1012 |

The regularized global response is depicted in figure (2.32), and shows a significant improvement compared to the non-regularized response in figure (2.30). All variations of section discretization have the same trend, but as the number of integration points increase higher force values are obtained in the post-yield response. This phenomena has

also been observed by Calabrese, Almeida and Pinho (2010). To enable the regularization of the local response according to the procedure presented in section (2.6.3), properties of the cracked concrete section have been determined. It is assumed that the reinforcing hoops have a diameter of 10 $mm$. Material moduluses are $E_s$ = 200 $GPa$ and $E_c$ = 30 $GPa$, while reinforcement yield strength is $f_s$ = 500 $MPa$. Based on linear elastic response of cracked sections (Moehle, 2012), the yield moment has been calculated:

$$b = 500\ mm \ \rightarrow\ d = (500 - 50 - 12.5 - 10)\ mm = 427.5\ mm \ \rightarrow\ d' = 72.5\ mm \tag{2.67a}$$

$$A_s = A'_s = (6 + 2/3 \times 2 + 1/3 \times 2) \times \pi \times (12.5\ mm)^2 = 3927\ mm^2 \tag{2.67b}$$

$$n = \frac{E_s}{E_c} = 6.667 \tag{2.67c}$$

$$\rho = \rho' = \frac{A_s}{bd} = 0.0184 \tag{2.67d}$$

$$k = \left[(\rho + \rho')^2 + 2\left(\rho + \rho'\frac{d'}{d}\right)n\right]^{1/2} - (\rho + \rho')n = 0.2916 \tag{2.67e}$$

$$k = 0.2916 \ \rightarrow\ kd = 124.7\ mm \tag{2.67f}$$

$$I_{cr} = \frac{b(kd)^3}{3} + (n-1)A'_s(kd - d')^2 + nA_s(d - kd)^2 = 2.7843 \times 10^9\ mm^4 \tag{2.67g}$$

$$M_{yield} = \frac{1}{n} \times \frac{f_s I_{cr}}{d - kd} = 689.6\ kNm \tag{2.67h}$$

The yield moment found was then used to find the corresponding yield curvature from the moment-curvature analysis results, which turned out to be equal to $\phi_{yield}$ = 0.00455 $m^{-1}$. Regularized local response, which is determined from post-processing the non-regularized analysis results, is illustrated in figure (2.33). It is clearly seen that the ultimate curvatures are now converging to similar values. However, the response paths do not coincide, which is due to the fact that only the curvature values are regularized. This simply means that the curvatures are adjusted to achieve objectivity by forcing the bending moments away from their original x-axis values.

The analysis performed shows that even though the FB formulation has its advantages, mainly not requiring an element discretization, it does not provide the same level of objectivity for the regularized softening response as the DB formulation.

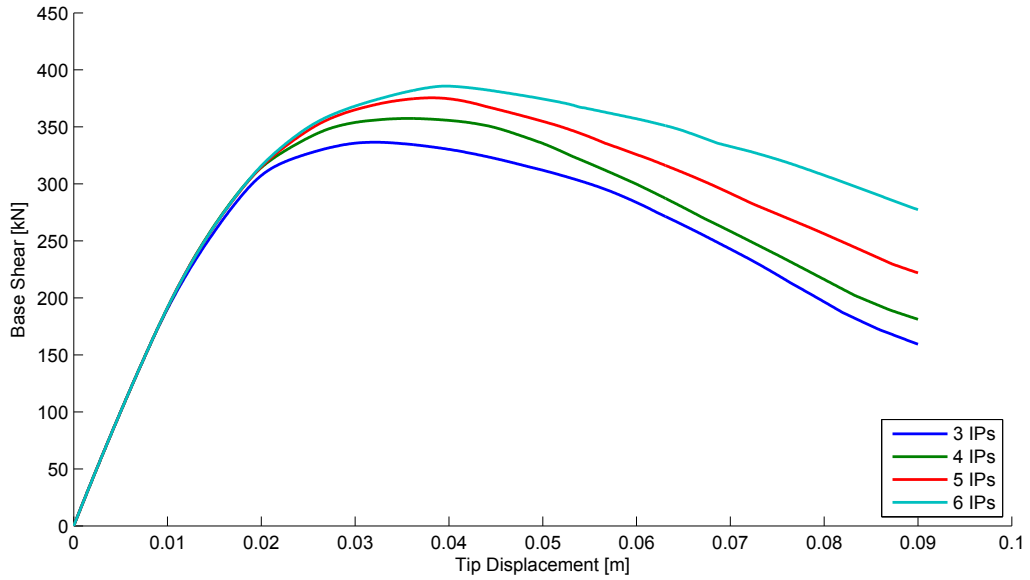


Figure 2.32: Regularized global softening response for FB formulation.

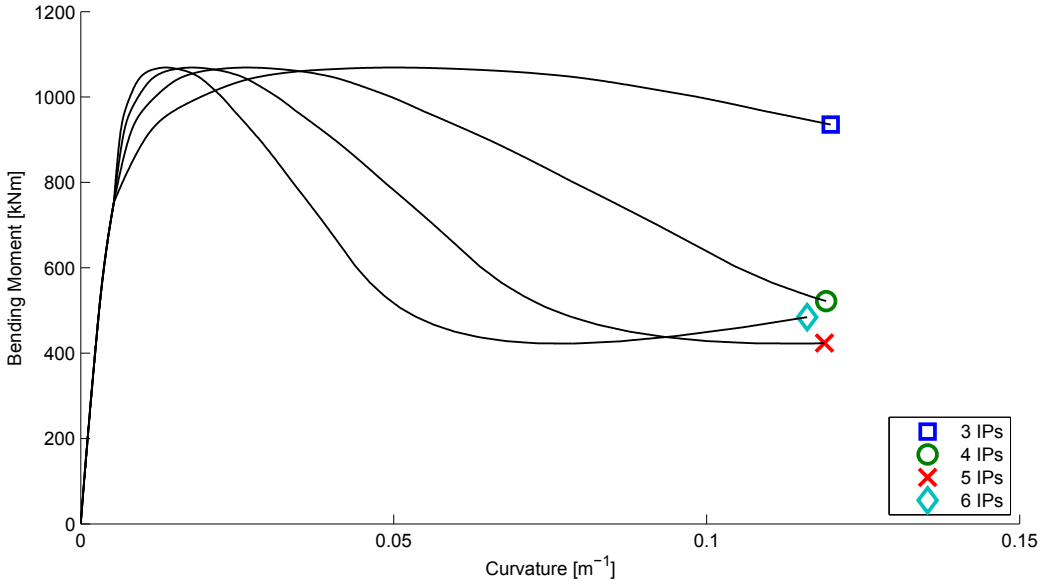


Figure 2.33: Regularized local softening response for FB formulation at 3 % drift.

## 2.8 Comparison and summary

Comparisons of response for both DB and FB element cantilever columns are depicted in figures (2.34) and (2.35). The discretizations used are considered to give reasonable accuracy for both element formulations. Global hardening response is shown to be close to identical for the DB and FB elements, with only the DB elements having a slightly stiffer inelastic response. The softening response, however, differs significantly, even though the responses have been regularized. This shows that the representation of strain softening behaviour is highly dependent on which element formulation is used to model the structural members. Obviously, this is making it difficult to predict which one to use without comparing analysis results versus experimental data. To sum it up, the characteristics of each element formulation discussed is listed in table (2.6).

Table 2.6: Properties of distributed inelasticity formulations.

| Displacement-based element (DB) | Force-based element (FB) |
|---|---|
| • Based on displacement shape functions. | • Based on internal force shape functions. |
| • Weak form of equilibrium is satisfied. | • Strong form of equilibrium is satisfied. |
| • Discrepancies from exact solution can arise from both numerical integration errors and inaccurate shape functions. | • Discrepancies from exact solution can only arise from numerical integration errors. |
| • Needs several elements to describe inelastic behaviour of a beam-column member accurately. | • Only one element per beam-column member is sufficient to represent inelastic behaviour. |
| • Gauss-Legendre is the commonly used integration method. | • Gauss-Lobatto is the commonly used integration method. |
| • Often gives a stiffer solution than the exact one. | |

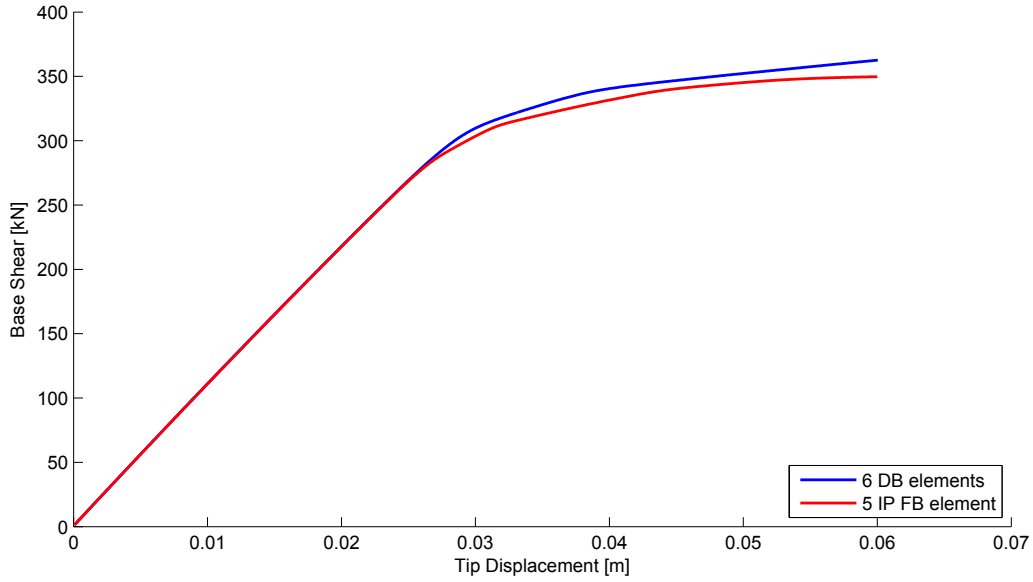


Figure 2.34: Global hardening response of 6 DB element member, and 5 integration point FB member.

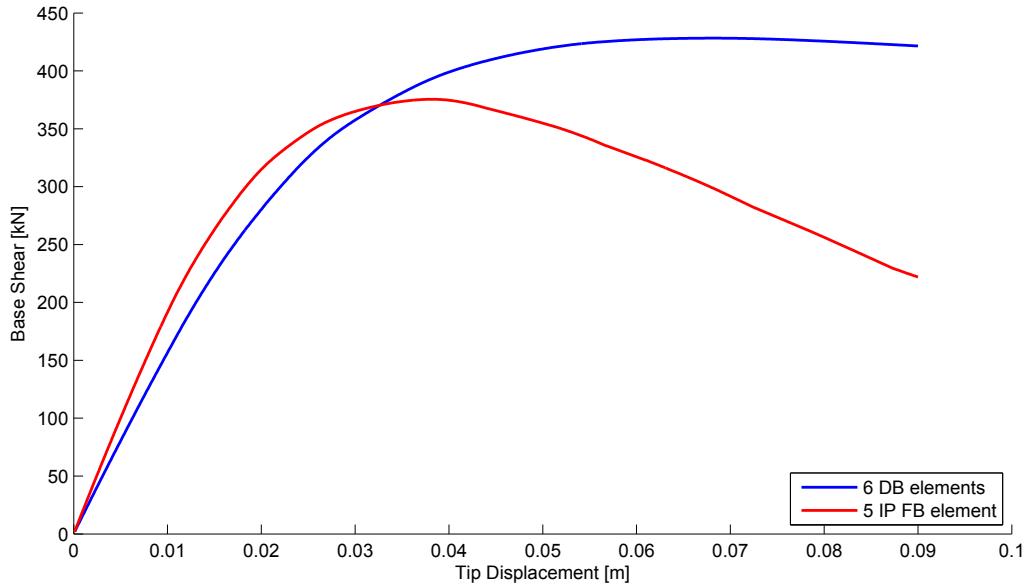


Figure 2.35: Global regularized softening response of 6 DB element member, and 5 integration point FB member.

# 3. Concentrated plasticity elements

## 3.1 Point-hinge models

Structures subject to strong lateral forces will have their most significant inelastic deformations at their member ends. The bending moments will experience larger values at these points, opposed to element dead and live loads that produce moments in the middle span of beam members. This knowledge was the basis for the earliest nonlinear beam-column member formulations. The first point-hinge model was introduced by Clough, Benuska and Wilson in 1965 (Filippou, 2013), and is named the two-component model. It consists of two structural beam components in a parallell series, as illustrated in figure (3.1). The lower component in the figure is elastic-perfectly plastic, while the upper one is elastic without any ultimate limit. The interaction between these two components enables the model to represent bilinear response.

As the formulation is based on a parallell model, the total beam stiffness is determined by directly summing up the stiffnesses of both components. The factor $\gamma$ represents the ratio between the elastic stiffness EI and the post-yield stiffness $(1-\gamma)EI$. Thus the elastic rotational stiffness will be the sum of both components

$$k_{elastic} = \gamma EI + (1-\gamma)EI = EI \tag{3.1}$$

while the post-yield stiffness will be the rotational stiffness of only the upper component, as the lower one has reached perfect plasticity, and therefore has zero stiffness. The moment-curvature relation of the two-component model is shown in figure (3.2), and illustrates the rotational response. Here the factor $\gamma$ is set to the stiffness ratio $(1-\beta)$ of an bilinear approximation, and $M_p$ is the yielding moment of the model. The red line describes the total response of the model, while the black line with slope $\beta EI$ represents the hardening stiffness contribution from the post-yield component.

Despite the two-component model's strength of simulating an exact bilinear response, it does not represent the cyclic loading of concrete members with sufficient accuracy. The model overestimaes the energy dissipation when members are subjected to inelastic load cycles. Therefore the model is only applicable for steel members with stable hysteresis loops, or non-cyclic inelastic deformations concrete members (Fardis, 2009).

To prevent the issues experienced with the two-component model, Giberson proposed the one-component model in 1967 (Filippou, 2013). As illustrated in figure (3.3), it consists of a series model of a linear elastic beam with nonlinear rotational springs at its member ends. These springs only contribute to the rotational stiffness when the plastic capacity of the beam is reached at a particular end. The force-displacement relation

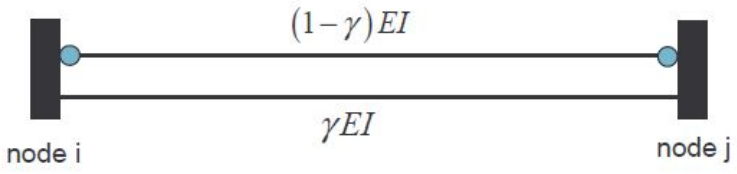


Figure 3.1: Two-component model (Filippou, 2013).

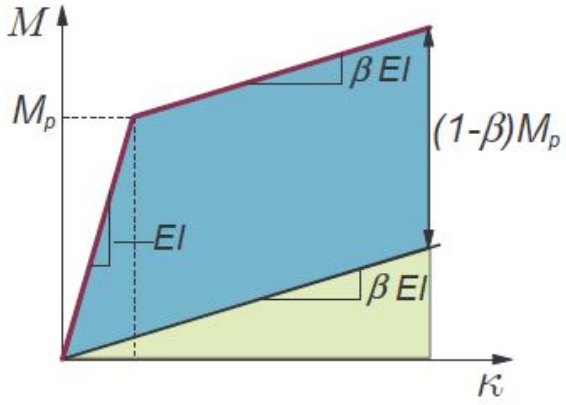


Figure 3.2: Moment-curvature relation of a two-component model (Filippou, 2013).

in figure (3.3) shows the linear hardening response of each spring under antisymmetric bending, where $\eta$ is the hardening stiffness ratio. Since it is a series model, the total beam stiffness is found by inverting the sum of the component flexibilities. The flexibility matrix of the elastic beam component is

$$\boldsymbol{f}_{elastic} = \frac{L}{6EI}\begin{bmatrix} 2 & 1 \\ 1 & 2 \end{bmatrix} \tag{3.2}$$

while the flexibilities of the nonlinear springs are

$$\boldsymbol{f}_{plastic} = \frac{L}{6\eta EI}\begin{bmatrix} r_i & 0 \\ 0 & r_j \end{bmatrix} \tag{3.3}$$

The variables $r_i$ and $r_j$ either have the valure 0 or 1, depending on if the beam has reached its plastic moment capacity at either ends. Thus, the beam rotational stiffness is either fully elastic and the inverse of equation (3.2), fully plastic and the inverse of equation (3.3), or a combination of both flexibilities, in case only one of the member ends has reached its capacity.

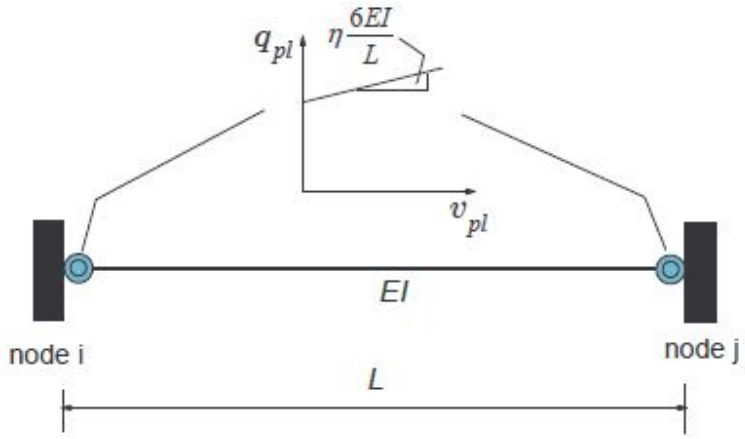


Figure 3.3: One-component model with nonlinear spring stiffness relation (Filippou, 2013).

## 3.2 Improved plastic hinge integration methods

The two-component and one-component models discussed in the previous section have the advantage that they are both fundamentally simple, and therefore easily can be followed up by hand calculations. However, they have significant drawbacks as well. The plastic hinges are for instance concentrated at the end nodes, as if they were singularities. This is obviously not the case in reality, as a larger portion of the member ends are expected to reach plasticity and thus function as hinges. In addition, both models also seperate between the axial and moment response, meaning that a calibration is necessary to achieve their correct interaction (Scott & Fenves, 2006).

To deal with these issues, recent concentrated plasticity elements have fiber modelling at specific lengths at their member ends. Research has been done not only to improve the two-component and one-component model, but also to achieve objectivity for softening response of FB elements. Thus, the fiber modelled member ends are based on the FB formulation presented in section (2.4). As the interior region outside the prescribed plastic hinge lengths are assumed to be linear elastic, the formulation has to be slightly rewritten. The compatibility condition now consists of three different parts, one from each plastic hinge, and one from the interior region. It is given as

$$\boldsymbol{v} = \int_0^{Lpi} \boldsymbol{b}^T(x)\boldsymbol{e}(x)dx + \int_{Lpi}^{L-Lpj} \boldsymbol{b}^T(x)\boldsymbol{e}(x)dx + \int_{L-Lpj}^{L} \boldsymbol{b}^T(x)\boldsymbol{e}(x)dx \tag{3.4}$$

where $Lpi$ and $Lpj$ are the plastic hinge lengths at respectively nodes $i$ and $j$. Due to inelasticity leading to nonlinear analysis, the hinge regions need to be integrated numerically as usual. This gives the expression

$$\boldsymbol{v} = \sum_{i=1}^{N_p} \boldsymbol{b}_i^T \boldsymbol{e}_i \omega_i + \boldsymbol{f}_{int}^{el}\boldsymbol{q} \tag{3.5}$$

where $\boldsymbol{f}_{int}^{el}$ is the flexibility matrix of the interior region of the element, and $\omega_i$ is the length weight of the plastic hinge integration points. As it is linear elastic, it is evaluated by the closed-form integral

$$\boldsymbol{v} = \int_{Lpi}^{L-Lpj} \boldsymbol{b}^T(x)\boldsymbol{f}_s^{el}\boldsymbol{b}(x)dx \tag{3.6}$$

The section flexibility $\boldsymbol{f}_s^{el}$ is simply given as

$$\boldsymbol{f}_s^{el} = \begin{bmatrix} \frac{1}{EA} & 0 \\ 0 & \frac{1}{EI} \end{bmatrix} \tag{3.7}$$

and eventually the element flexibility is expressed by

$$\boldsymbol{f} = \sum_{i=1}^{N_p} \boldsymbol{b}_i^T \boldsymbol{f}_{s,i} \boldsymbol{b}_i \omega_i + \boldsymbol{f}_{int}^{el} \tag{3.8}$$

As previously explained, the new concentrated plasticity element based on FB fiber formulation eliminates the issues experienced with the earlier plastic hinge models. The next focus is therefore solely on representing the strain softening behaviour as accurately as possible. Three criteria that a plastic hinge integration rule has to satisfy is the following (Scott & Fenves, 2006):

1. There should be integration points at the element ends, such that the largest bending moments due to lateral loads are detected.
2. Quadratic polynomials should be integrated exactly to provide the exact solution for linear curvature distributions.
3. The plastic hinge regions at both ends should be integrated by the use of only one integration point.

The integration rules used for the distributed plasticity, Gauss-Legende and Gauss-Lobatto, do not fulfill these criteria. Although both of them satisfy the second one, only Gauss-Lobatto satifies the first, as it has integration points at the element ends. The third criteria is satisfied be neither integration rules, as the number of integration points has to be adjusted depending on the plastic hinge length of the member, which is not a fundamental property of either rules. Next, three commonly known plastic hinge integration rules are presented, which eventually leads to a new method, the modified Gauss-Radau integration method proposed by Scott and Fenves (2006).

### Midpoint and endpoint integration

Two basic plastic hinge integration methods are the midpoint and endpoint methods, which are illustrated in figure (3.4). Both include only one integration point at each plastic hinge. The midpoint method has the intregration points located at the center of its plastic hinge regions, with weights equal to the length of each plastic hinge. Obviously, this method does not satisfy criteria (1), as the integration points are not at the element ends. This will result in an overestimation of the moment capacity of the element in case of lateral loading, as reduced moments and curvatures are detected at the controlling sections. Midpoint integration does also not give an exact integration of quadratic polynomials, criteria (2), and is therefore not able to accurately represent response due to element loads.

The endpoint integration method has its integration points located at the element ends, with weights equal to the plastic hinge lengths. A significant drawback however, is that the endpoint method only is capable of exactly integrating constant functions, which means that a order of accuracy is lost compared to the midpoint method. Thus, the endpoint method satifies criteria (1) and (3), but not (2).

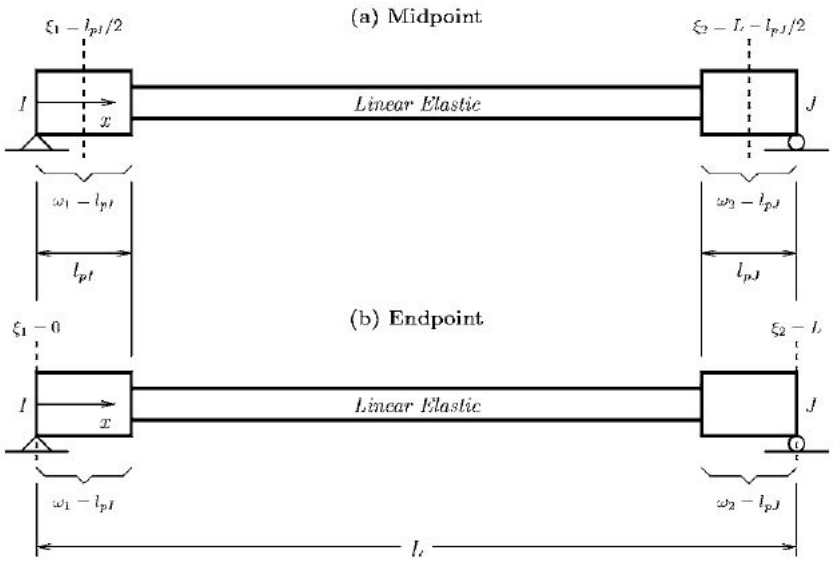


Figure 3.4: Midpoint and endpoint plastic hinge integration methods (Scott & Fenves, 2006).

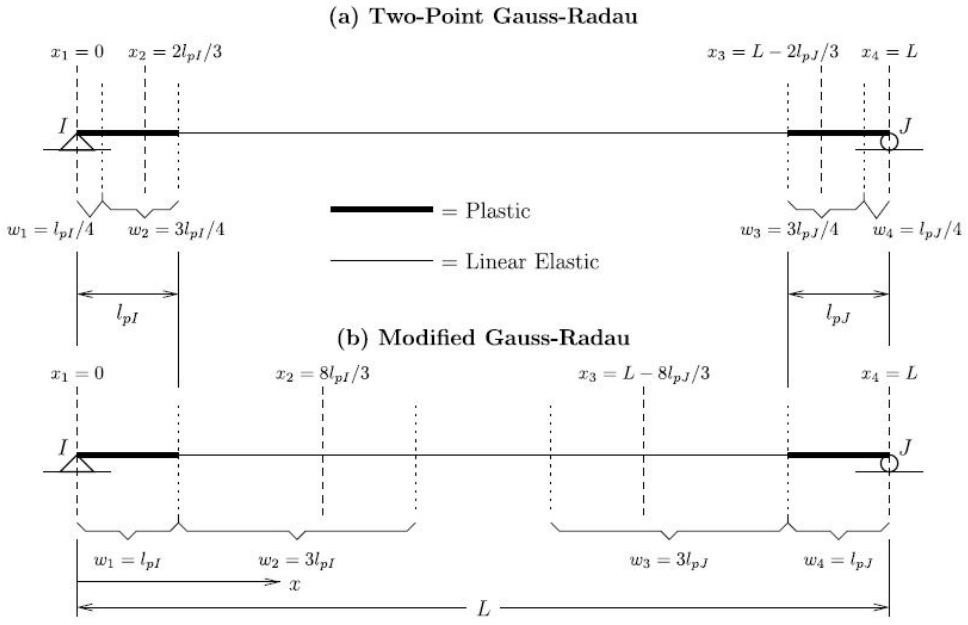


Figure 3.5: Two-point and modified Gauss-Radau plastic hinge integration methods (Scott & Ryan, 2013).

**Two-point Gauss-Radau integration**

The previously discussed plastic hinge integration methods each have one integration pointat each element end, which is not enough to integrate on a high enough order to achieve exact solutions. Therefore the number of integration points have to be increased to at least two. The Gauss-Legendre integration rule does not have points at the element ends, while a two-point Gauss-Lobatto rule is of a lower order, and does not yield exact integration of quadratic polynomials. However, the advantages of both these integration rules can be found in the Gauss-Radau quadrature. It has an integration point at one element end, but not the other, and has an accuracy of $2Np - 2$, which is one order higher than Gauss-Lobatto. Thus, an element using a two-point Gauss-Radau integration rule will instantly satisfy criteria (1) and (2).

The integration scheme of the Gauss-Radau rule for a plastic hinge region is shown in a) in figure (3.5). Integration points are situated at points 0 and $2/3$ on an element with unit length, with corresponding weights equal to $1/4$ and $3/4$. Using a two-point Gauss-Radau rule has two special properties (Scott & Fenves, 2006). The first is that when the sum of the plastic hinge lengths are equal to the member length, the two seperate two-point schemes combine into a four-point integration scheme. Second, when each hinge length are identical and the sum is equal to the member length ($Lpi = Lpj = L/2$), Simpson's $3/8$ integration rule is obtained, which increases the accuracy by one order. Despite its obvious advantages over the one-point integration methods, the two-point Gauss-Radau method is not capable of representing softening behaviour in a satisfactory way. This is because it does not satisfy criteria (3), as the plastic hinge region contain two integration points, making the end controlling section having the weight $Lp/4$ instead of the desired $Lp$.

**Modified two-point Gauss-Radau integration**

To fulfill the criteria stated, Scott and Fenves (2006) proposed a modified two-point Gauss-Radau integration scheme. It is illustrated in b) in figure (3.5), and shows that the plastic hinge regions only contain one integration point each. The second integration point has been extended into the linear elastic interior of the member. This has been done by applying the Gauss-Rada integration rule over the lengths $4Lpi$ and $4Lpj$, instead of the previous $Lpi$ and $Lpj$. As a result, their proposal theoretically satisfies all criteria necessary to represent strain softening behaviour of beam-column elements.

## 3.3 Comparison of concentrated plasticity elements

The cantilever column from section (2.7) has been analyzed using the plastic hinge integration rules discussed. There are two available FB plastic hinge elements in OpenSees. The original command consists of an element with Modified Gauss-Radau integration at its hinges and an linear elastic interior, similar to the one presented in this thesis. However, a recently updated element command allows choosing between either midpoint, endpoint, Gauss-Radau or Modified Gauss-Radau integration. Another significant property of the new command is that the element interior is assumed inelastic, such that inelasticity can spread anywhere on the element, and plastic hinges also can form on the interior due to element loads. This is done by adding two Gauss-Legendre integration points on the element interior, and thus increasing the number of controlling sections to four for the one-point methods, and six for the Gauss-Radau methods. A summary of the integration method's capabilities of representing strain-softening behaviour is shown in table (3.1).

Table 3.1: Strain softening criteria of plastic hinge integration methods.

| Integration method | (1) Integration points at element ends | (2) Exact integration of quadratic polynomials | (3) One integration point in plastic hinge region |
|---|---|---|---|
| Midpoint | No | No | Yes |
| Endpoint | Yes | No | Yes |
| Gauss-Radau | Yes | Yes | No |
| Modified Gauss-Radau | Yes | Yes | Yes |

#### Hardening response

Global hardening behaviour response is depicted in figures(3.6). The Modified Gauss-Radau method with an elastic interior is showing a overly conservative elastic stiffness, which is expected. While the midpoint, Gauss-Radau, and Modified Gauss-Radau method with inelastic interior have identical elastic response, the endpoint method do not. This discrepancy is due to the endpoint integration rule not being capable of exactly integrating linear functions. Even though the midpoint and Gauss-Radau methods give higher post-yield force values, all methods have the same response trend for strain-hardening. Thus, they can all be assumed to model this kind of global structural behaviour in a feasible manner.

On the other hand, an interesting property of the Gauss-Radau method is seen in figure (3.7), which is of the local moment-curvature response. While all the other integration methods yield approximately identical ultimate curvature values, the Gauss-Radau method gives a significantly larger one. This is because the integration weight of the

element end integration point is 1/4 of the plastic hinge length, as oppposed to the other methods having the weight as the whole hinge. Thus, to maintain similar force-displacement response as the other methods, the curvature of the end integration point of the Gauss-Radau method has to become larger.

**Softening response**

The global and local softening behaviour responses are shown respectively in figures (3.8) and (3.9). The localization issue of the Gauss-Radau method due to it having two integration points in the plastic hinge is again easily seen. While the other methods show identical trends, the Gauss-Radau response do not. Also, as expected, the endpoint method differs slightly in the linear elastic range. The overestimation of the post-yield strength of the midpoint method comes from the fact that it does not have integration points at the element ends. As can be seen from the local response, the Gauss-Radau method's ultimate curvature is, similiar to the hardening case, affected by the localization problem with the integration weigths.

The results show that the Modified Gauss-Radau and the endpoint method yield the best estimates of both force-displacement and moment-curvature response. However, the endpoint method must be used with caution, as significant discrepencies may occur because of its low order of integration. This leaves the Modified Gauss-Radau method superior, and is the plastic hinge integration method that should be used to correctly estimate both hardening and softening response of beam-column members. Wether the element interior should be modelled as linear elastic or not, depends on if distributed or concentrated member loads are considered large enough to form plastic hinges. In addition, an elastic interior will require less computational effort than an inelastic one.

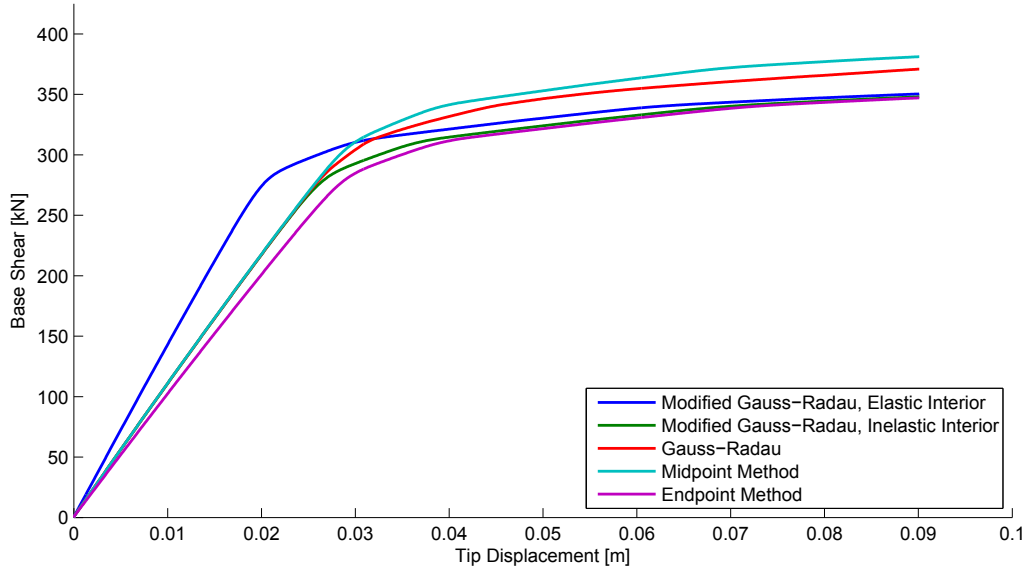


Figure 3.6: Global hardening response of plastic hinge integration methods.

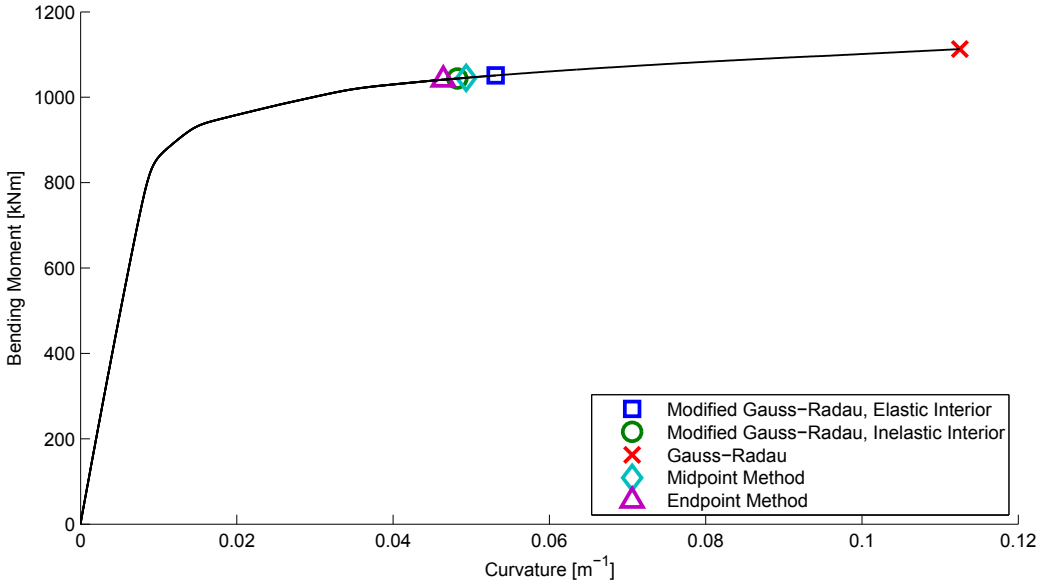


Figure 3.7: Local hardening response of plastic hinge integration methods at 3 % drift.

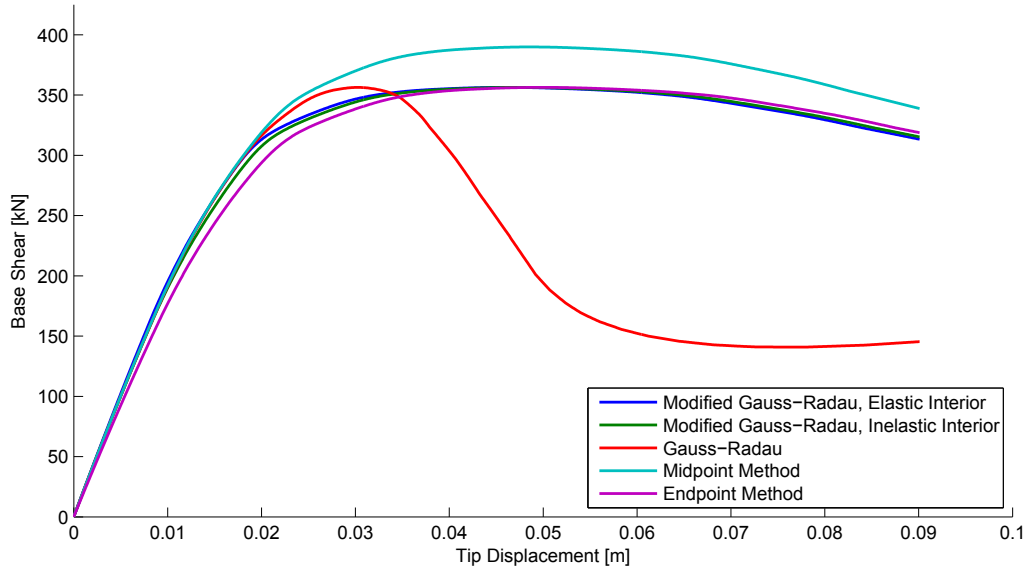


Figure 3.8: Global softening response of plastic hinge integration methods.

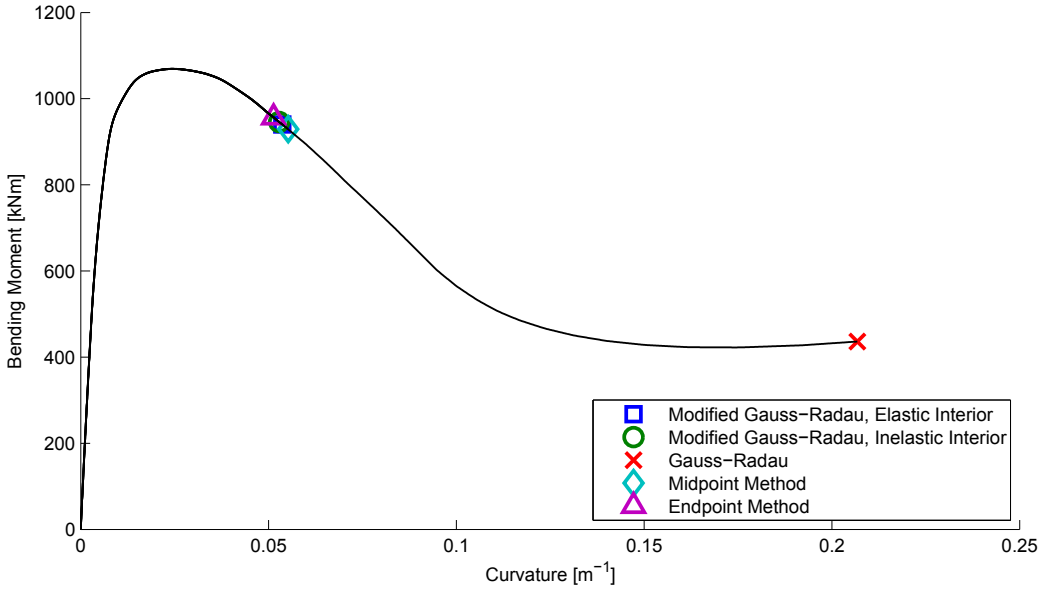


Figure 3.9: Local softening response of plastic hinge integration methods at 3 % drift.

# 4. Application of element models

## 4.1 SeismoStruct

The characteristic properties of the different element formulations were presented in the previous chapters with the use of OpenSees. Based on these commonly accepted results the state-of-art seismic engineering software SeismoStruct has been developed. Unlike OpenSees, SeismoStruct has an user interface, seen in figure (4.1), making it simpler to construct larger models. It contains all the elements discussed earlier, like the DB element, FB element, and the Modifed Gauss-Radau plastic hinge element. The integrated DB element does not have an option of adjusting the number of integration points. It uses a 2-point Gauss-Legendre scheme, which is the same as the one used in OpenSees. The FB element of SeismoStruct can have its integration points adjusted from three to ten controlling sections. The plastic hinge element of SeismoStruct has an elastic interior, with no choice of making it inelastic. This will anyhow not be of any issue as long as the distributed member loads are small.

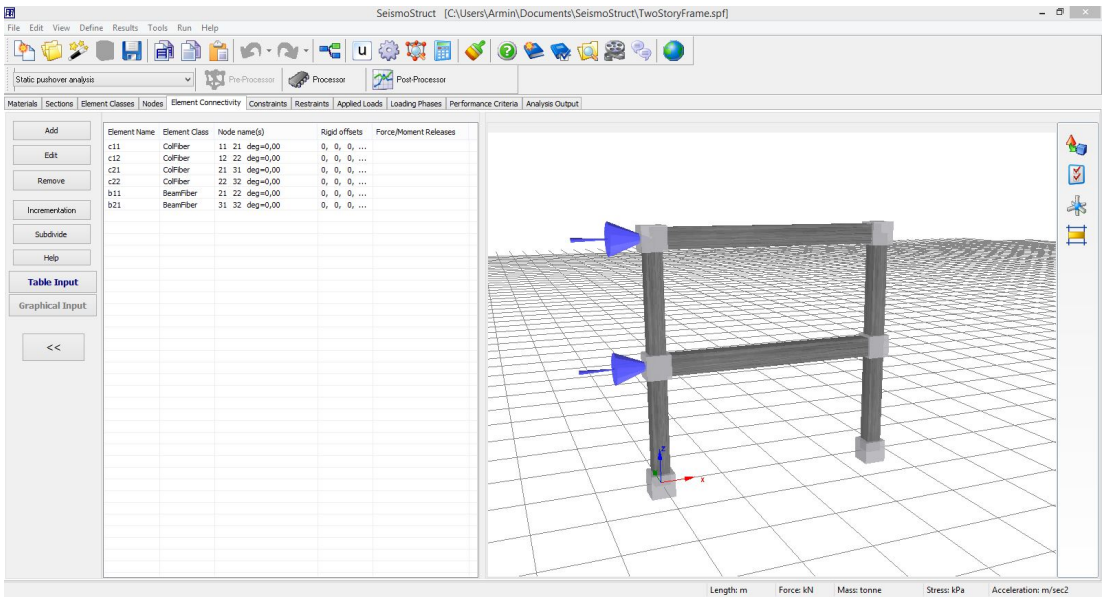


Figure 4.1: SeismoStruct user interface.

## 4.2 One-story reinforced concrete building prototype

The Joint Research Centre of the Europen Commission have performed several seismic experiments on the behaviour of industrial and residential structures. To compare the accuracy of the different element formulations a one-story RC industrial building has been examined. The prototype was made of cast-in-situ beams and columns, consisting of two two-bay frames connected by a slab. A picture of the structure is seen in figure (4.2). To make the structure authentic, it was designed for a dead load equal to 27 $kN/m^3$ including the weight of the slab. The geometry of the prototype is shown in figure (4.3), with the column cross section in figure (4.4). All six columns are $300 \times 300$ $mm$ and identical, having 8 $\phi$ 14 $mm$ longitudinal reinforcement bars throughout their whole length. The transverse reinforcement, which is for both shear forces and confinement, consists of 6 $mm$ bars. In the critical regions, which are 1 $m$ from the bottom and top cross sections, the stirrups were placed with 50 $mm$ spacing. Outside the critical regions, the spacing is150 $mm$. The design of the transverse reinforcement, counting as 4 stirrup legs in both the height and width of the section, yields significant confinement effects. The experiment report does not state any information on the beam $600 \times 300$ $mm$ sections, except that they have such reinforcement that the plastic hinges will form in the columns. The slab between the two frames have a thickness of 150 $mm$.

Prior to the testing of the prototype itself, the materials used for construction were tested. Concrete cube specimen tests gave cylindrical compressive strengths of $f_{cm} = 42.74$ $MPa$ for the columns, and $f_{cm} = 47.2$ $MPa$ for the beams. The longitudinal steel reinforcement had a yielding strength of $f_y = 550$ $MPa$, and a tensile strength of $f_t = 657$ $MPa$.

The cast-in-situ prototype was subjected to a pseudo-dynamic displacement motion. These horizontal displacements were applied with the use of hydraulic jacks, which can be seen are connected to the beams in figure (4.2). In addition, vertical jacks were used to apply additional loads on the slab, such that the columns obtain proper values of axial load. The total vertical loads on the prototype, including slab self weight, were approximately 600 $kN$. Positioning of the vertical jacks are shown in figure (4.5). They have the functionality of swinging around their base hinged connections during the test. This makes the jacks always oriented towards a fixed base point, which means that they do not produce any second order P-delta effects.

The pseudo-dynamic displacement time-history is determined from performing a preliminary dynamic analysis of the prototype. It must be noted that this makes the experiment less authentic, as the damping of the structure is modelled in the analysis, instead of taking effect in the test itself. The seismic ground motion were simulated by an artifical accelerogram, which was generated to yield a response spectrum similar to what given by Eurocode 8 for a subsoil of type 2B. This accelerogram is shown in figure (4.6) for a peak ground acceleration of $0.32g$. The prototype was subjected to four different time-histories based on scaling of the ground motion; $0.05g$, $0.32g$, $0.64g$, and $0.80g$. The time-history of $0.05g$ was applied to calibrate the testing devices, and is therefore included in neither the report or this analysis.

Displacement time-histories for the relevant accelerogram scalings are depicted in figure (4.7). It can clearly be seen that the $0.32g$ ground motion yields an elastic response, as

Figure 4.2: One-story reinforced concrete building (Ferrara & Negro, 2003).

there are no signs of irregularities in the displacement. The 0.64$g$ response gives larger displacement values and some inelasticity, while the 0.80$g$ motion results in large inelasticity. These characteristics were also observed on the prototype. As shown in figure (4.8), the 0.64$g$ time-history resulted in cracking of the columns. Figure (4.9) depicts cover spalling of the concrete after the 0.80g test, in addition to the maximum deflection that occured.

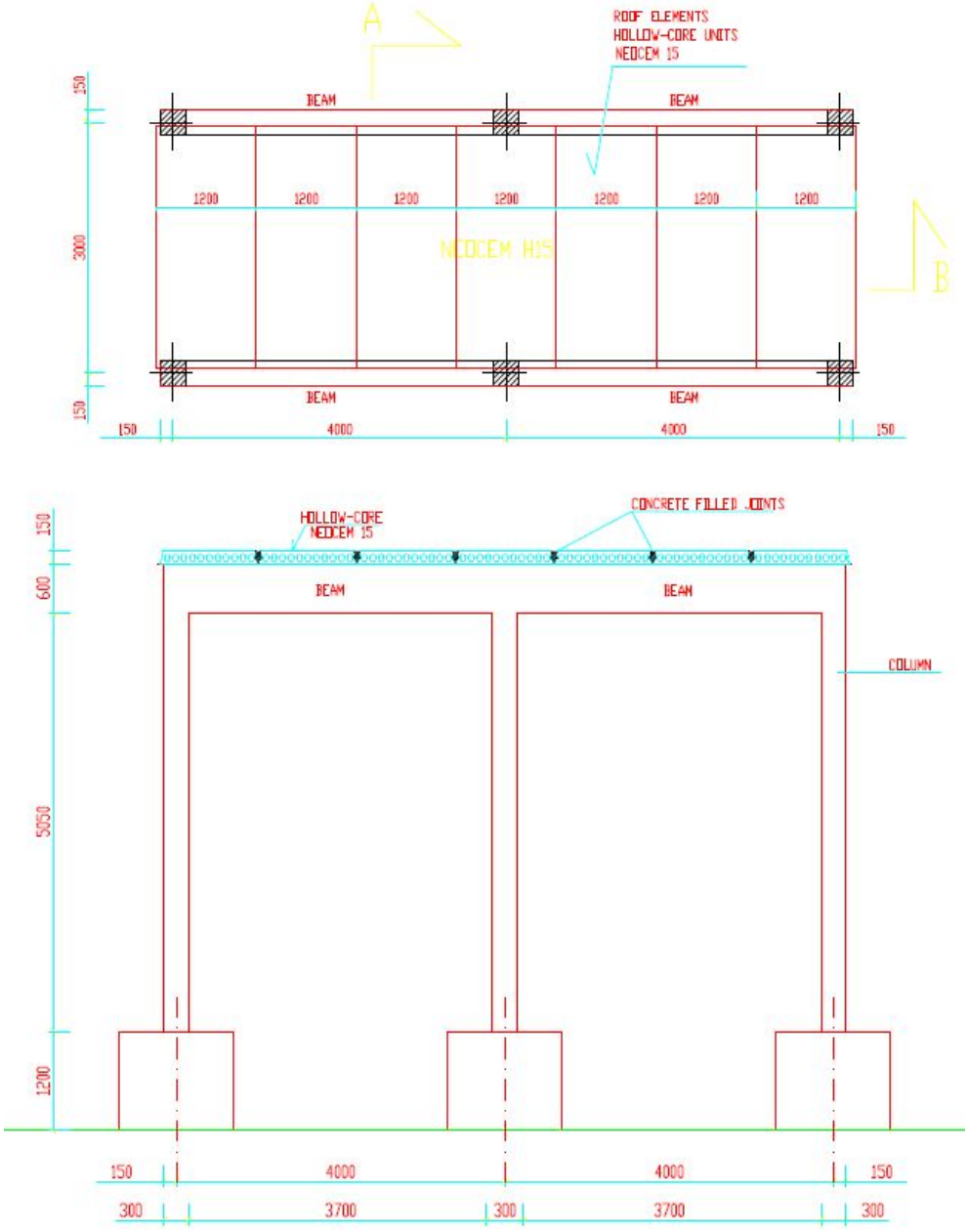


Figure 4.3: Geometry of the prototype (Ferrara & Negro, 2003).

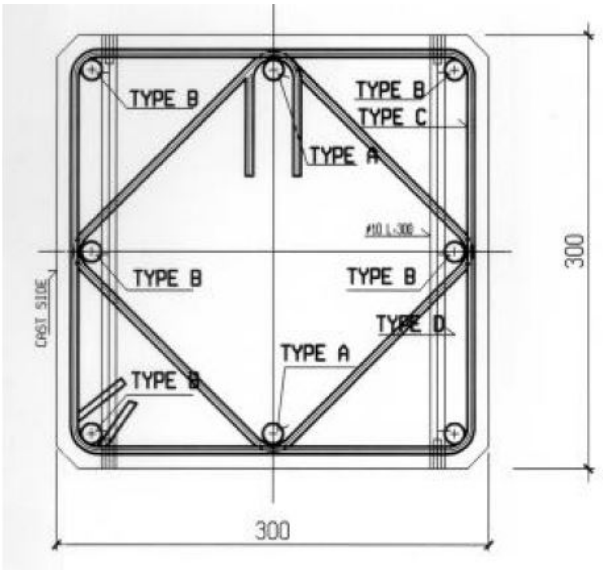


Figure 4.4: Column geometry and reinforcement (Ferrara & Negro, 2003).

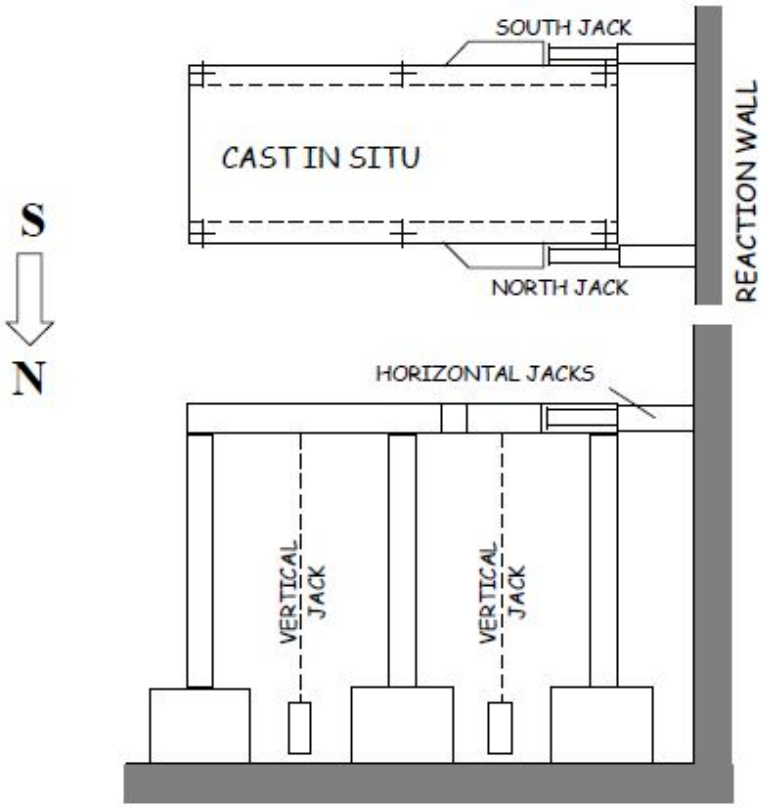


Figure 4.5: Scheme of vertical jacks (Ferrara & Negro, 2003).

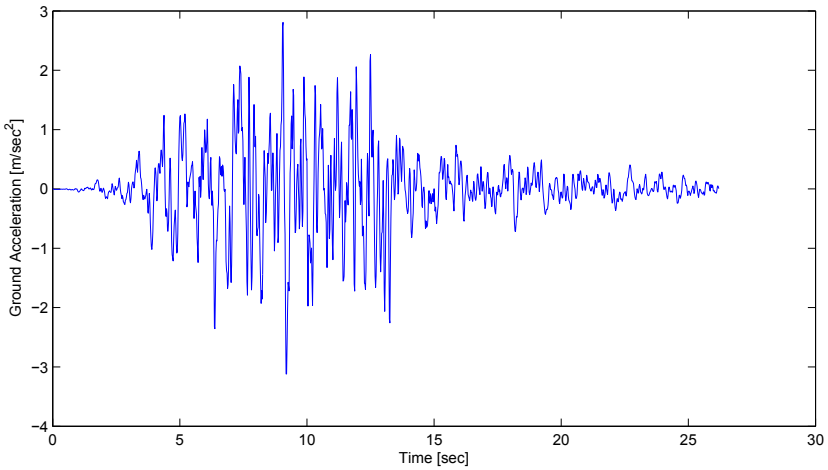


Figure 4.6: Artifical ground accelerogram with PGA 0.32g.

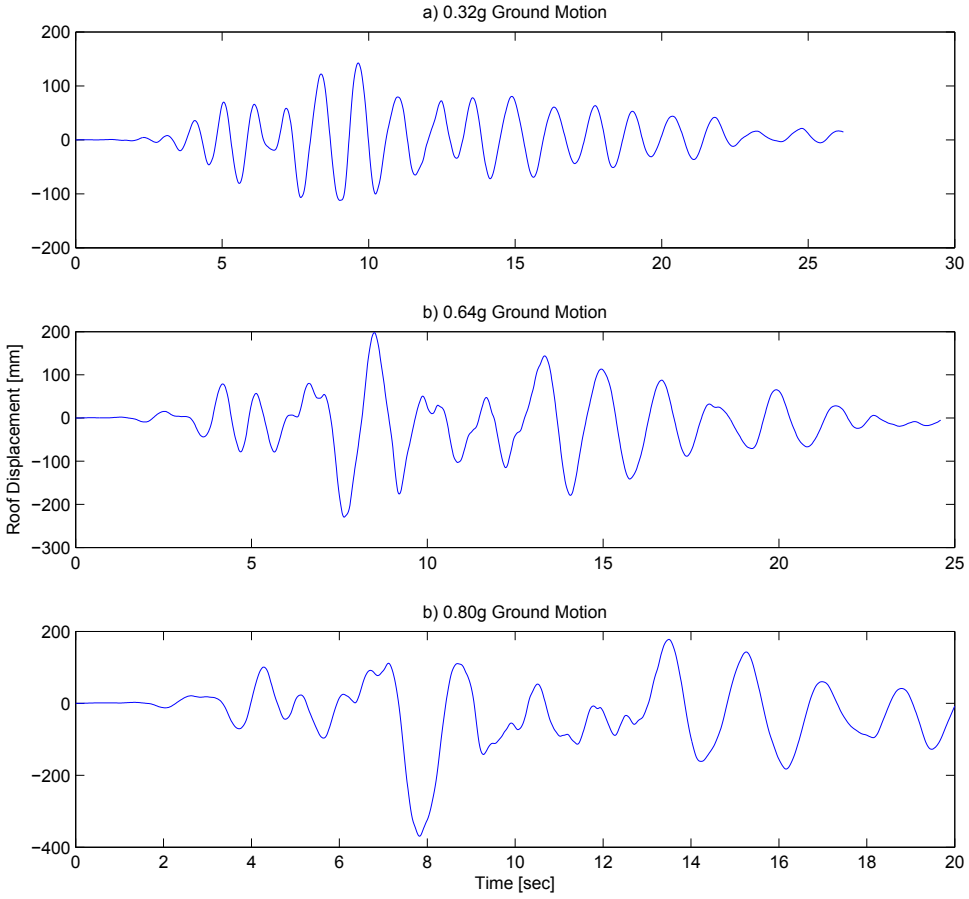


Figure 4.7: Displacement time-histories from dynamic analysis.

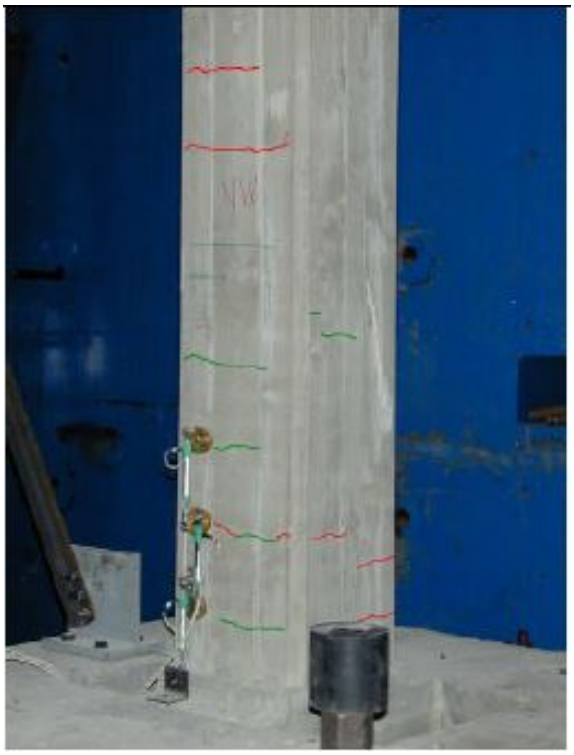

Figure 4.8: Crack patterns on northern frame - western column at the end of 0.64g test (Ferrara & Negro, 2003).

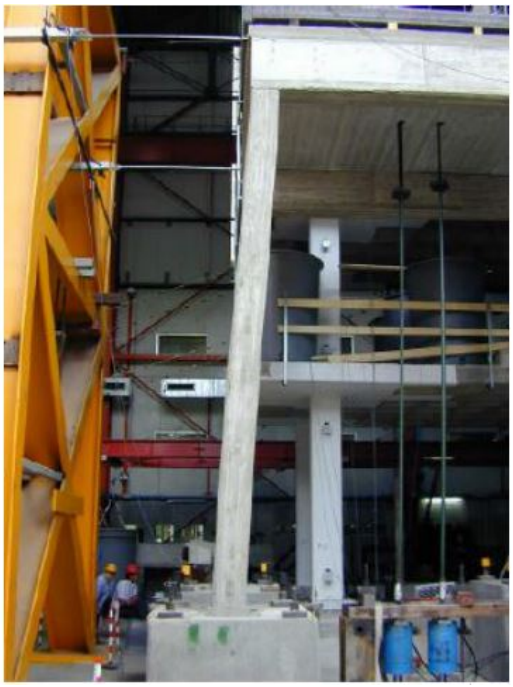

Figure 4.9: Cover spalling and maximum deflection from the 0.80g test (Ferrara & Negro, 2003).

## 4.3 Analysis

### 4.3.1 Modelling

Due to the symmetry of the prototype the static time-history analysis model can be simplified to consist of only one frame. The model used is illustrated in figure (4.10). Analyses have been performed with the use of DB elements, FB elements, and FB plastic hinge elements. Each intensity of the ground motion included in the report is analyzed (i.e., 0.32g, 0.64g, and 0.80g). Based on the findings of the previous chapters, the FB elements are modelled with five integration points along their lengths. The DB elements have their default value of two integration points, with six elements used for each column member. Equation (2.54) is used to calculate the necessary length of the plastic hinge:

$$L_p = 0.08L + 0.022 f_y d_B = 0.08 \times 5.05 + 0.022 \times 550 \times 0.014 = 0.573\ m \qquad (4.1)$$

Thus, the plastic hinge column elements have hinges of 0.573 $m$ at the top and base, while the DB element column have extremity elements of twice the plastic hinge length, which is 1.146 $m$. The FB element columns are modelled with only one element, and do not take any predetermined plastic hinge length into account. Also, since information on the concrete fracture energy is not given, the FB members are not regularized. The column discretization of the different element models are illustrated in figure (4.11). Since the beams are supposed to have an overstrength compared to the columns, no specific hinge lenghts are used. Rather, they are discretized into four elements for the DB formulation, and a default SeismoStruct hinge value of 16.67 % the member length is used for the plastic hinge formulation. It must also be noted that due to the different spacing in transverse reinforcement, the confinement effect differs throughout the column lengths. The plastic hinge lengths at the top and base have a confinement factor of 1.3549, while the interior part has a confinement factor of 1.0701, giving the hinges a significantly more ductile behaviour than the interior. These values have been obtained from SeismoStruct.

The computational times of each time-history analysis are listed in table (4.1). As expected, the DB formulation requires more computational effort than the FB distributed and concentrated plasticity elements. This is due to the increased number of nodes, which is necessary to achieve sufficient accuracy. The average computational time per step is not significantly larger for the DB elements compared to the FB elements. However, this difference is expected to increase as the strucural models increase in size. Textbook matrix multiplication and inversion have running times of $n^3$ for a square $n \times n$ matrix. Basically, this means that as the size of the matrices increase due to increased number of nodes, the computational demand of DB elements increases significantly compared to FB elements. Despite the fact that the running times of the matrix operations can be reduced to $n^{2.373}$ with more efficient algorithms, there is a clear advantage of using FB elements on larger models (Robinson, 2005). The total run times of the different PGA ground motions differ because they do not have a similar amount of time steps. While the $0.32g$ motion has 1310 steps, the $0.64g$ motion has 1230 steps, and the $0.80g$ motion has 1000 steps.

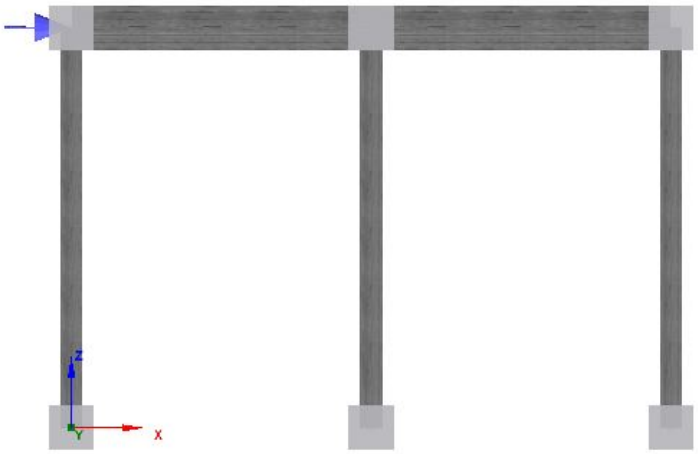

Figure 4.10: SeismoStruct model of prototype frame.

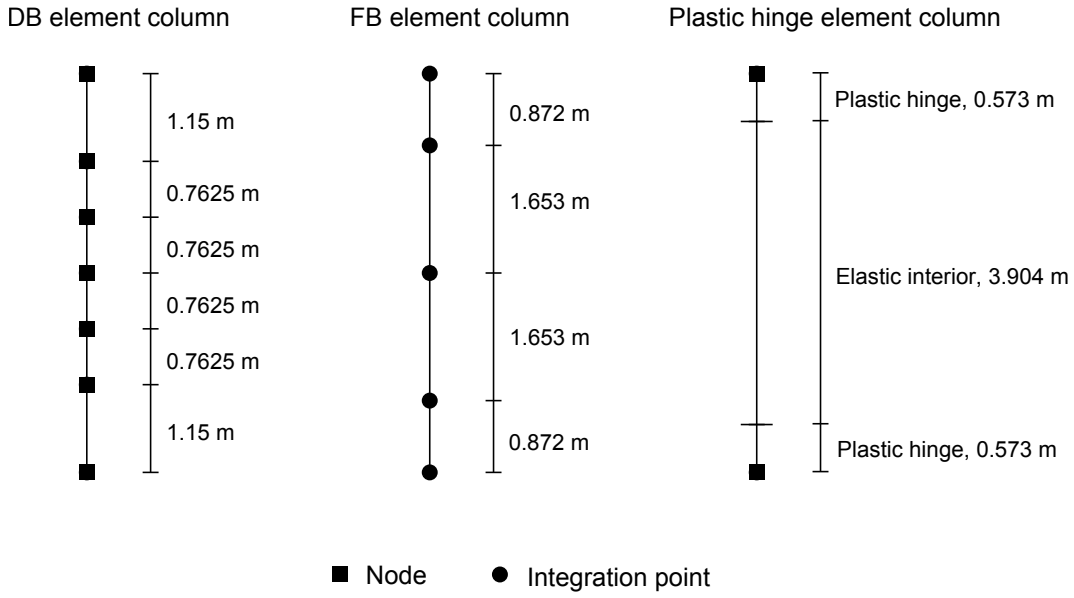


Figure 4.11: Discretization of column members.

Table 4.1: Computational times of analysis.

| PGA | Element formulation | Total time, *sec* | Average time per step, *sec* |
|---|---|---|---|
| 0.32g | DB | 43 | 0.033 |
| | FB | 37 | 0.028 |
| | Plastic hinge | 26 | 0.020 |
| 0.64g | DB | 40 | 0.033 |
| | FB | 35 | 0.029 |
| | Plastic hinge | 24 | 0.020 |
| 0.80g | DB | 32 | 0.032 |
| | FB | 29 | 0.029 |
| | Plastic hinge | 19 | 0.019 |

### 4.3.2 Global response

First, the base shear time-histories from SeismoStruct are compared to the experimental data. These results are depicted in figures (4.12), (4.13), and (4.14), for the $0.32g$, $0.64g$, and $0.80g$ ground motions respectively. All element types show identical response paths as the experiment results for the $0.32g$ motion, despite overestimating the force values slightly at each cycle peak. This overestimation is largest for the DB elements, and smaller for FB and plastic hinge elements. Between the pseudotime of approximately 4 and 8 seconds, all three analysis results show a larger discrepancy in force values. The distributed and concentrated FB elements improve the force prediction for the remaining time steps, while the DB elements do not. A similar trend is seen for the $0.64g$ motion (Fig. 4.13), although the force value discrepancies are substantially larger at the beginning of the time-history.

The analysis of the $0.80g$ ground motion shows a significantly different response (Fig. 4.14), as large levels of inelasticity are obtained in both the SeismoStruct model and the experimental prototype. Like the other ground motion scalings, the numerical analysis is inaccurate in the initial phase of the analysis. After this point, the plastic hinge element model yields the most accurate response compared to the other element formulations.

The peak values of base shear from the time-histories are listed in table (4.2). The observation that the DB element model overestimates the force values compared to the FB and plastic hinge element models is again confirmed by the numbers. While the elements based on the FB formulation have peak base shear errors ranging from -0.8 % to 6.0 %, the DB formulation yield errors between 18.9 % and 26.5 %. Figures (4.15), (4.16), and (4.17) illustrate the force-displacement response from the experiment and analyses. The experimental results are shown in red, while the different element models are in blue. Force-displacement response for the $0.32g$ is shown to be highly linear elastic, with

Table 4.2: Peak base shear values.

| **Peak base shear [kN]** | | | | | Error (%) | | |
|---|---|---|---|---|---|---|---|
| PGA | Experimental | DB | FB | Plastic hinge | DB | FB | Plastic hinge |
| 0.32g | 109.4 | 138.4 | 116.0 | 115.2 | 26.5 | 6.0 | 5.3 |
| 0.64g | 122.0 | 145.1 | 117.3 | 117.4 | 18.9 | -3.9 | -3.8 |
| 0.80g | 118.3 | 146.0 | 117.2 | 117.3 | 23.4 | -0.9 | -0.8 |

the FB and plastic hinge element models having a slightly better representation of the experiemental results than the DB element model. On the stronger ground motions especially, it can be noticed that the elastic stiffness of the analysis models are significantly higher than those of the experimental results. This may explain why the base shear values have been overestimated for the whole time-history of the $0.32g$ earthquake, and at the beginning of the stronger ground motions. However, the response of the $0.64g$ and $0.80g$ time-histories show that the inelastic response range is significantly better predicted, particularly for FB and plastic hinge elements.

### 4.3.3 Local response

Moment-rotation responses at the base of the north-western column, which is basically the western column in the frame model, are depicted in figures (4.18), (4.19), and (4.20) for the three acceleration levels . While the global force-displacement response from the analysis has its displacement values enforced to be similar to the experimental values, the same does not apply for the local response. This gives an increased discrepancy between the analysis and the experiment. The local response for the $0.32g$ ground motion shows fairly accurate hysteretic curves from the analysis, with the FB and plastic hinge element models displaying a better approximation of the experimental results than the DB element model. An important observation is that the DB element model overestimates the bending moment values significantly for all the analyses.

The moment-rotation responses get less accurate as the ground motion intensity increases. The results clearly show that all the analysis models are overly conservative in estimating the peak rotations occuring at the column base. As for the force-displacement response, there can also be seen that the analysis models have a higher elastic stiffness than the experimental prototype. Unfortunately, the experiment report does not provide any information on either elastic moduli or strain values at peak stresses for the concrete, which makes it difficult to determine necessary property values on the section level. The strain value at peak stress were assumed to be 0.002 in the analysis. Nevertheless, especially the FB and plastic hinge elements produce decent results based on the similarity of the response paths.

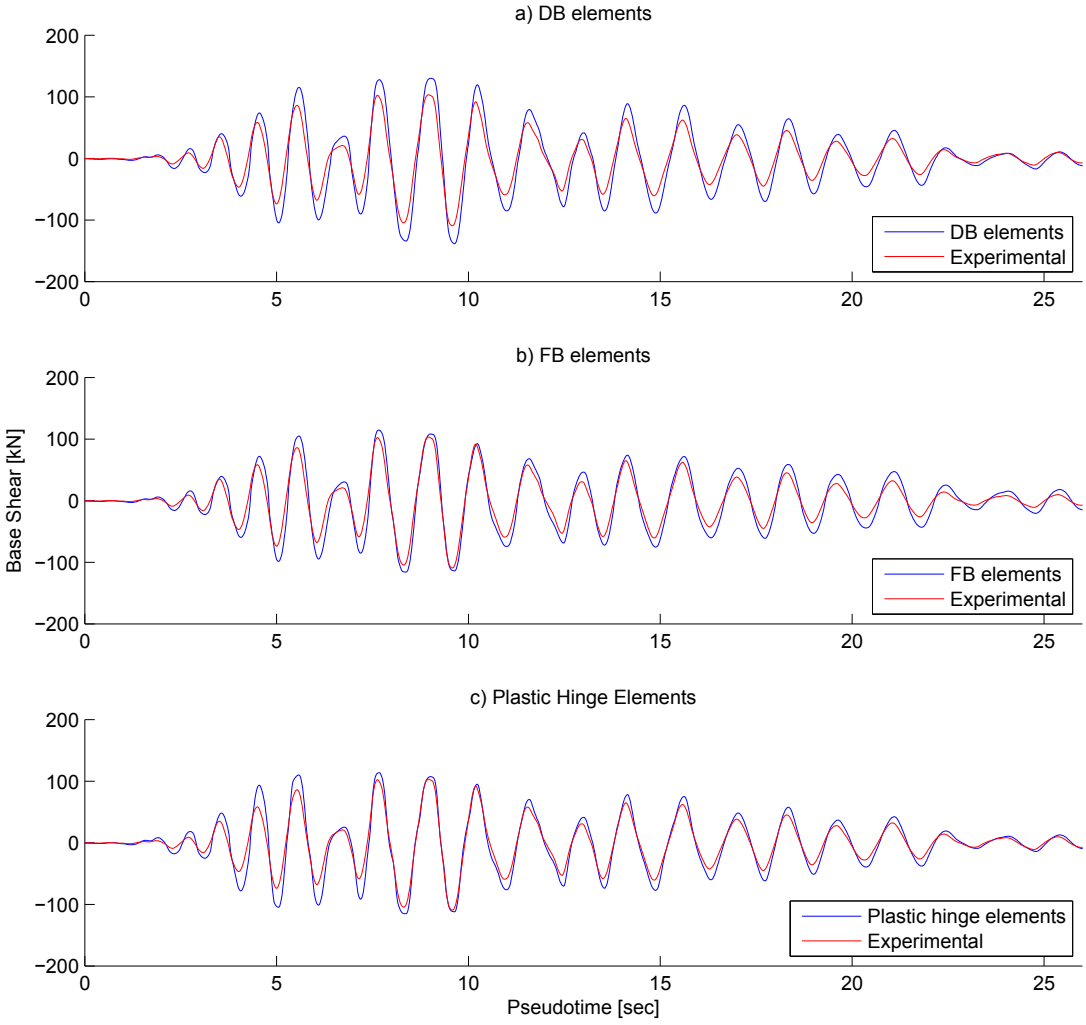


Figure 4.12: Base shears from analysis versus experimental results for 0.32g ground motion.

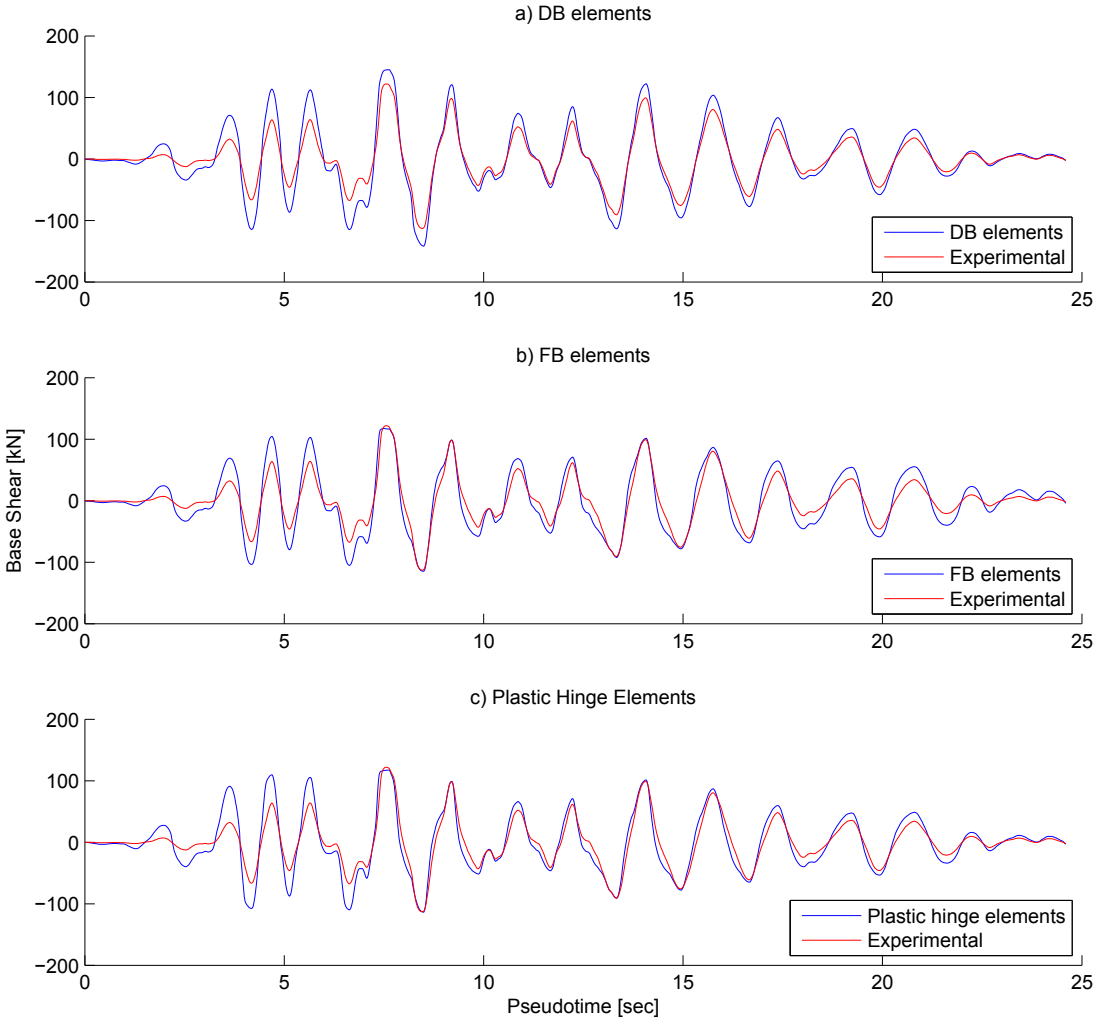


Figure 4.13: Base shears from analysis versus experimental results for 0.64g ground motion.

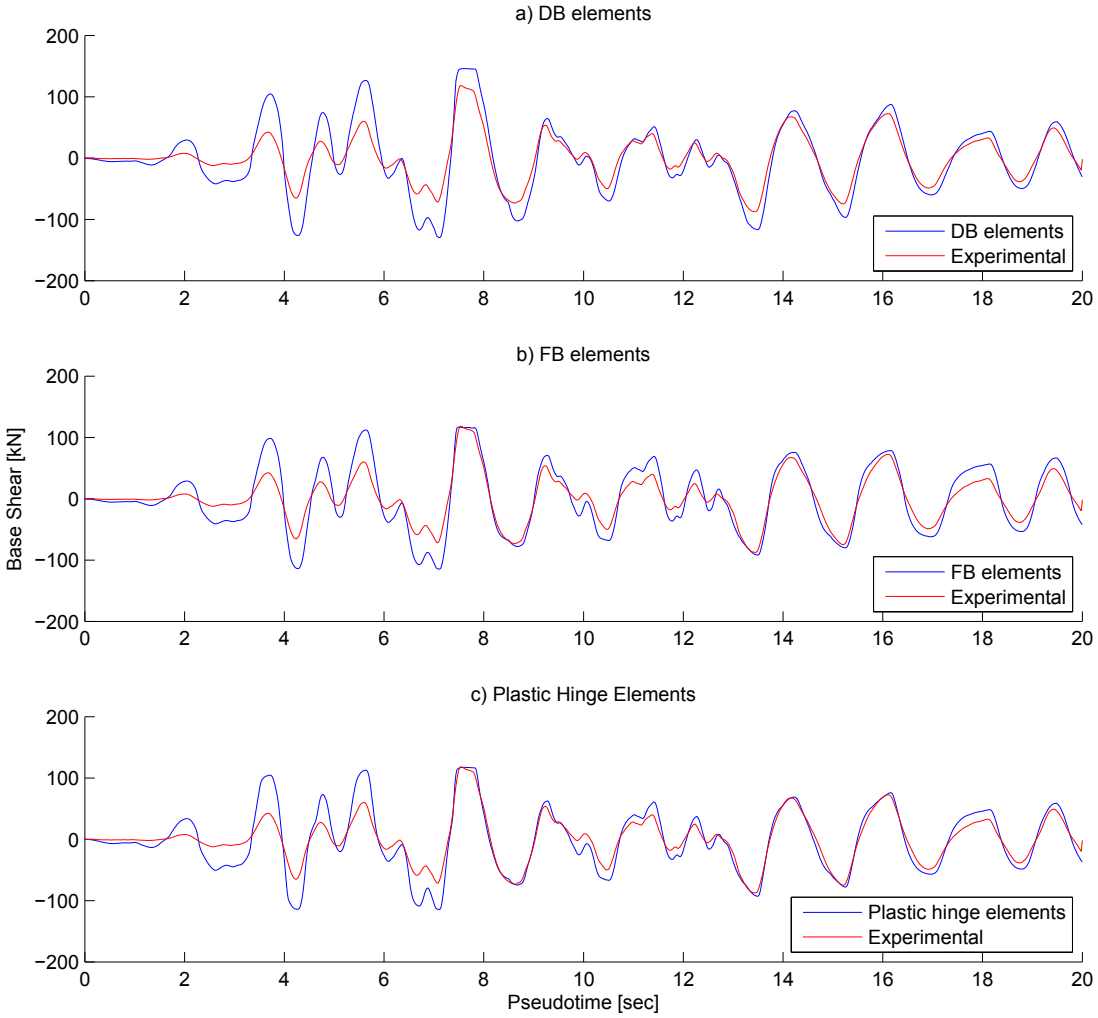


Figure 4.14: Base shears from analysis versus experimental results for 0.80g ground motion.

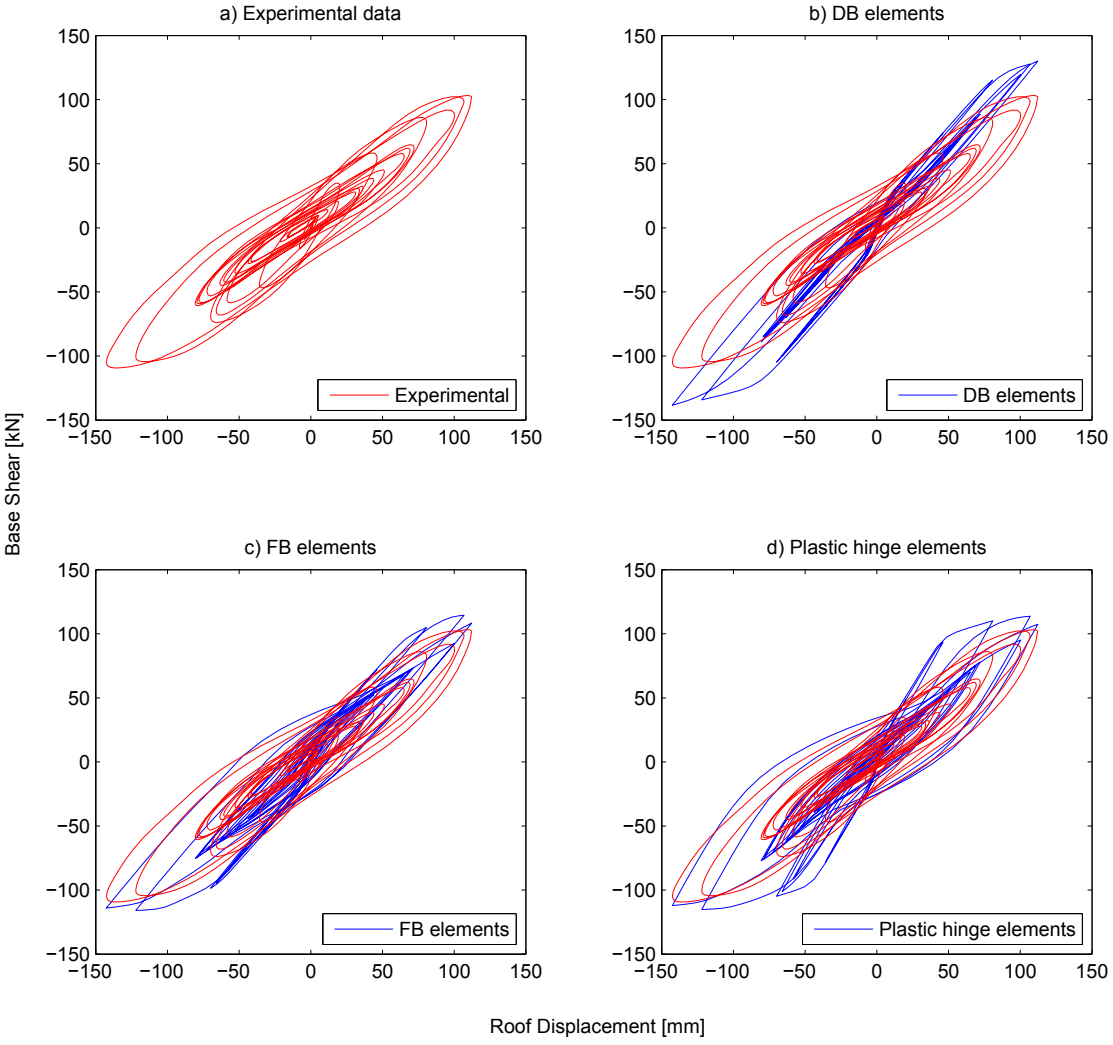


Figure 4.15: Force-displacement response from analysis versus experimental results for 0.32g ground motion.

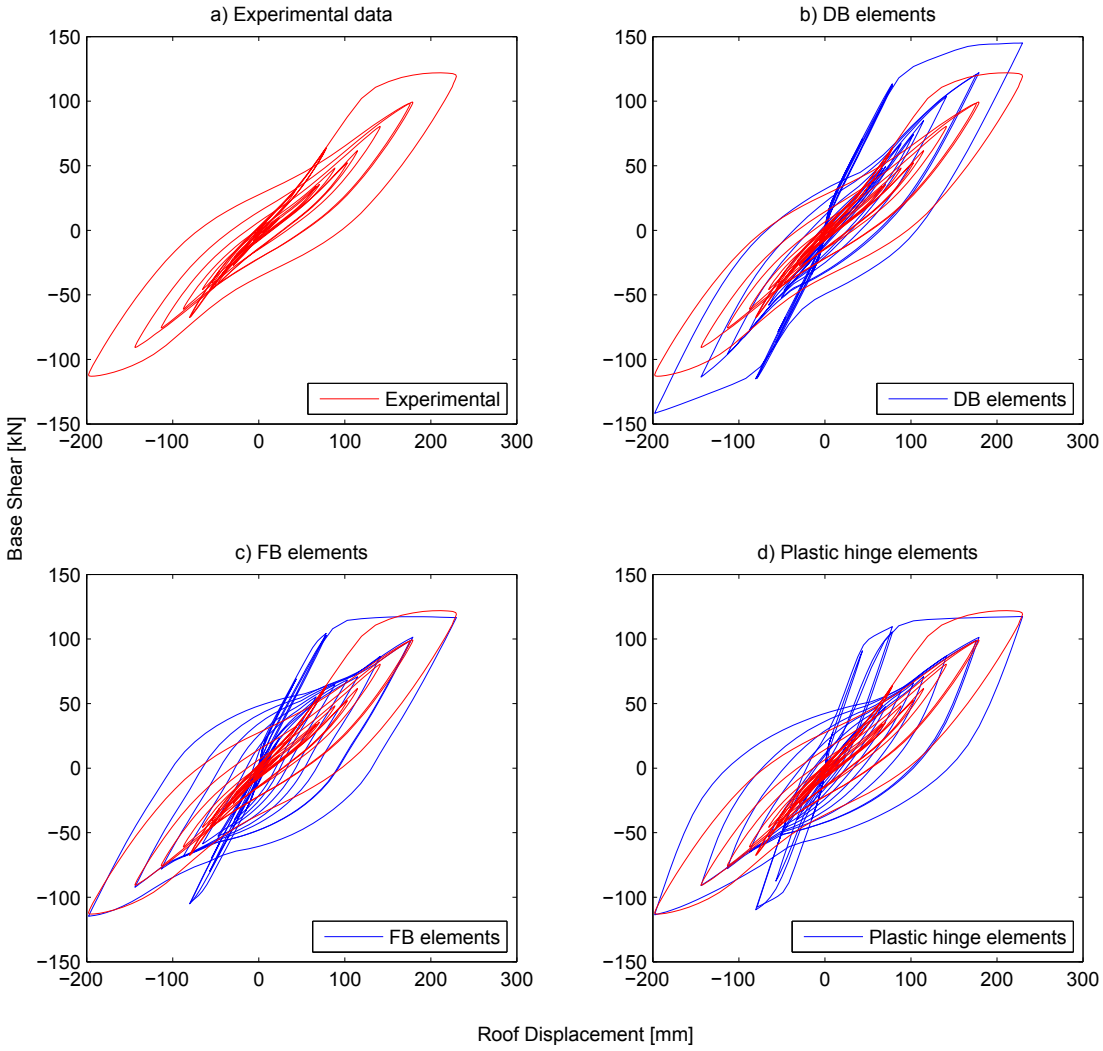


Figure 4.16: Force-displacement response from analysis versus experimental results for 0.64g ground motion.

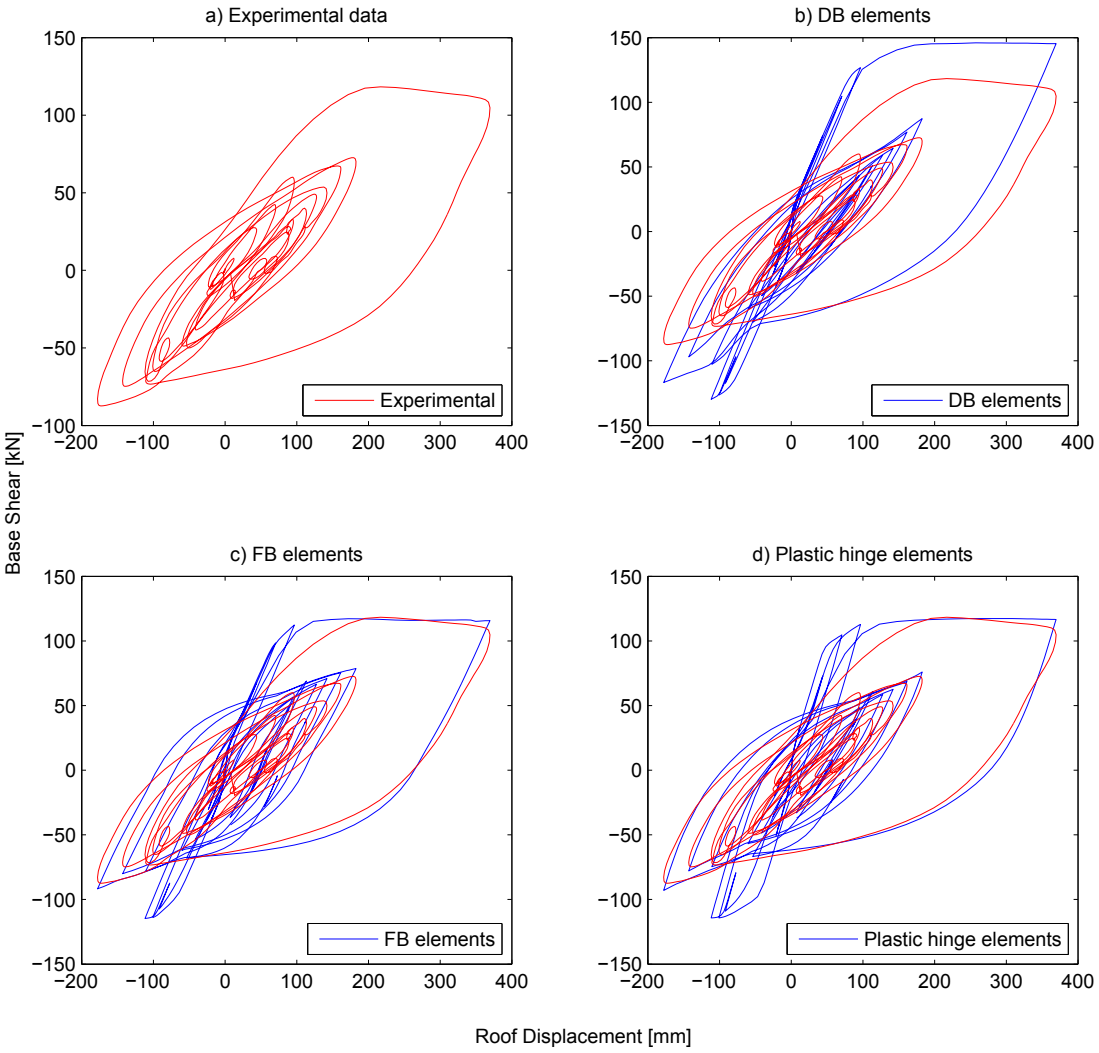


Figure 4.17: Force-displacement response from analysis versus experimental results for 0.80g ground motion.

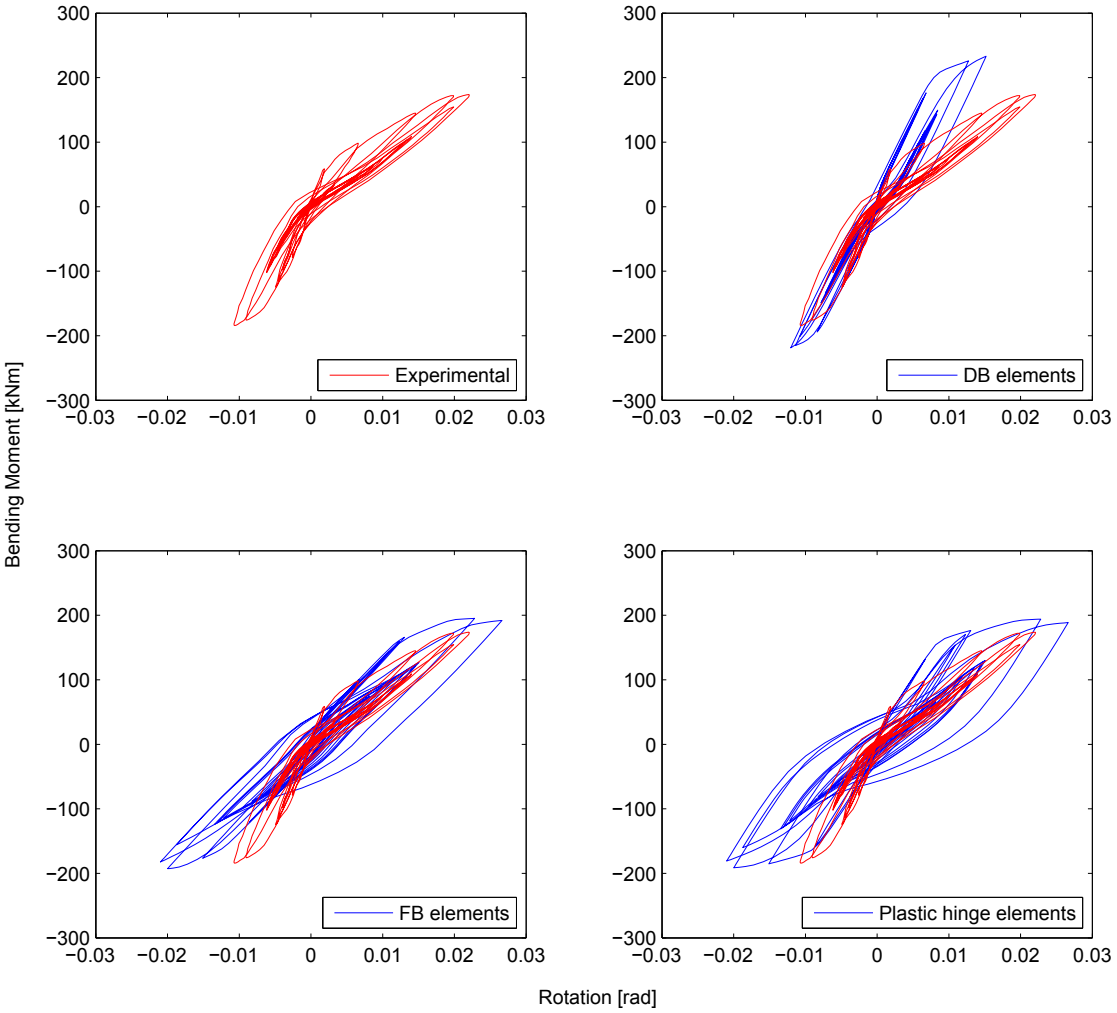


Figure 4.18: Moment-rotation response of north-western column for 0.32g ground motion.

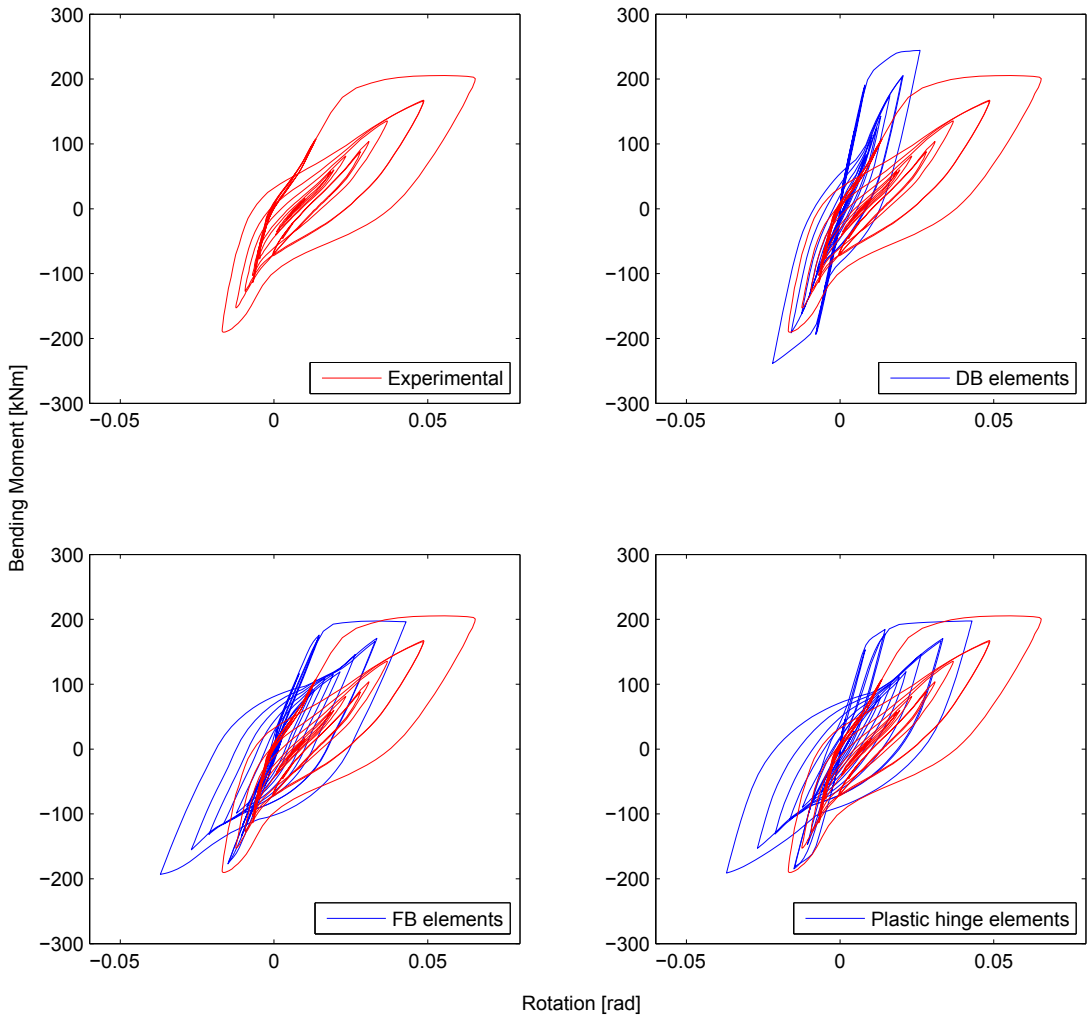


Figure 4.19: Moment-rotation response of north-western column for 0.64g ground motion.

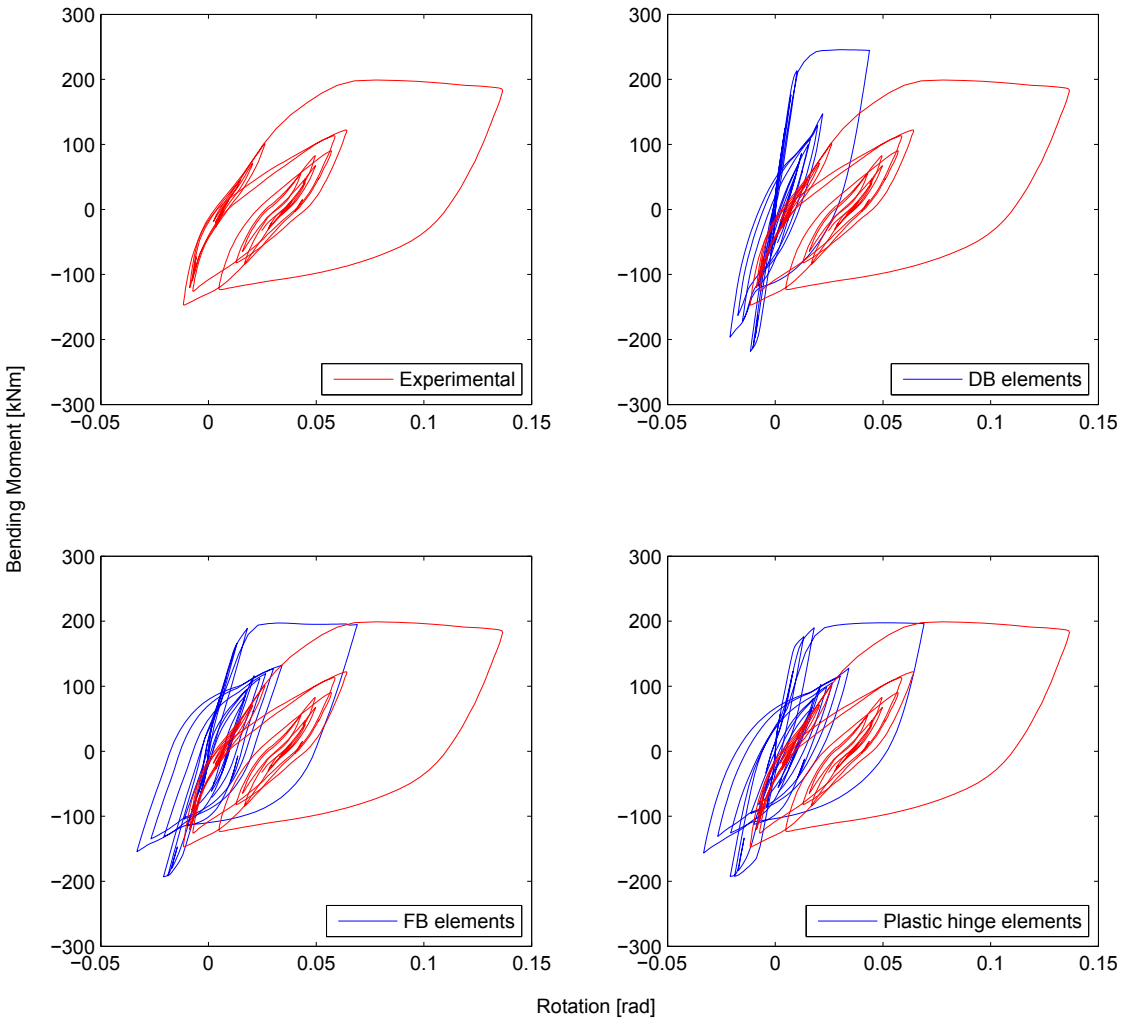


Figure 4.20: Moment-rotation response of north-western column for 0.80g ground motion.

## 4.4 Alternative analysis

An alternative analysis procedure has been performed to investigate if better accuracy is obtained for the response calculations. There is no information in the report stating that the frame specimen was repaired between the testing of the $0.32g$, $0.64g$ and $0.80g$ motions (Ferrera &Negro, 2004). This means that the $0.64g$ and $0.80g$ tests may not have begun at an initial state as the ones assumed in the numerical analysis of section (4.3). Based on the pictures from the laboratory, like figure (4.8), it seems likely that the member stiffnesses have been altered, and thus have different properties than first expected. Because of this, the three ground motions intensities have been combined into one single displacement motion, and thus preserving the material properties from the end of one time-history analysis to the next. This procedure resulted in better accuracy for the global response, but unfortunately no improvement of the local response, which therefore have not been presented.

The base shear time-histories and force-displacement results are depicted in figures (4.21) to (4.24). It can be seen that the force values from the analysis are closer to the experimental results compared to the case in figures (4.13) and (4.14). However, this is not apparent in table (4.3), where the peak base shear values are almost entirely identical to the previous analysis. Obviously the peak values have not been affected, but rather the prediction of the remaining response cycles have been improved; especially for the initial phase of the time-histories. This is further supported by the force-displacement responses, which now tend to have elastic stiffnesses more similar to the experimental results. Again, the FB and plastic hinge elements show superior accuracy compared to the DB elements, which as before still overestimates the force values.

Table 4.3: Peak base shear values from alternative analysis.

| **Peak base shear [kN]** | | | | | Error (%) | | |
|---|---|---|---|---|---|---|---|
| PGA | Experimental | DB | FB | Plastic hinge | DB | FB | Plastic hinge |
| 0.64g | 122.0 | 145.7 | 117.0 | 117.4 | 18.9 | -3.9 | -3.8 |
| 0.80g | 118.3 | 143.5 | 115.7 | 114.8 | 23.4 | -0.9 | -0.8 |

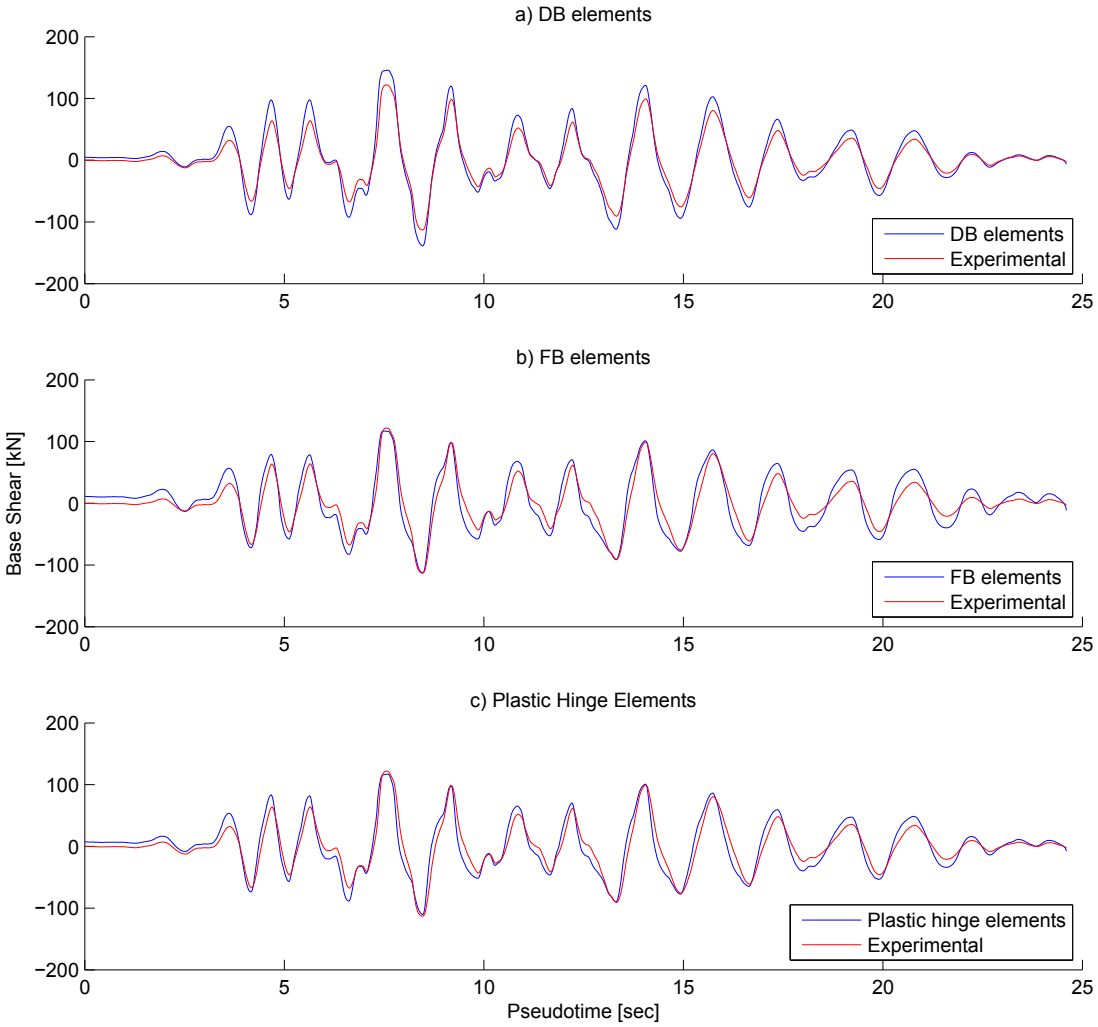


Figure 4.21: Base shears from alternative analysis versus experimental results for 0.64g ground motion.

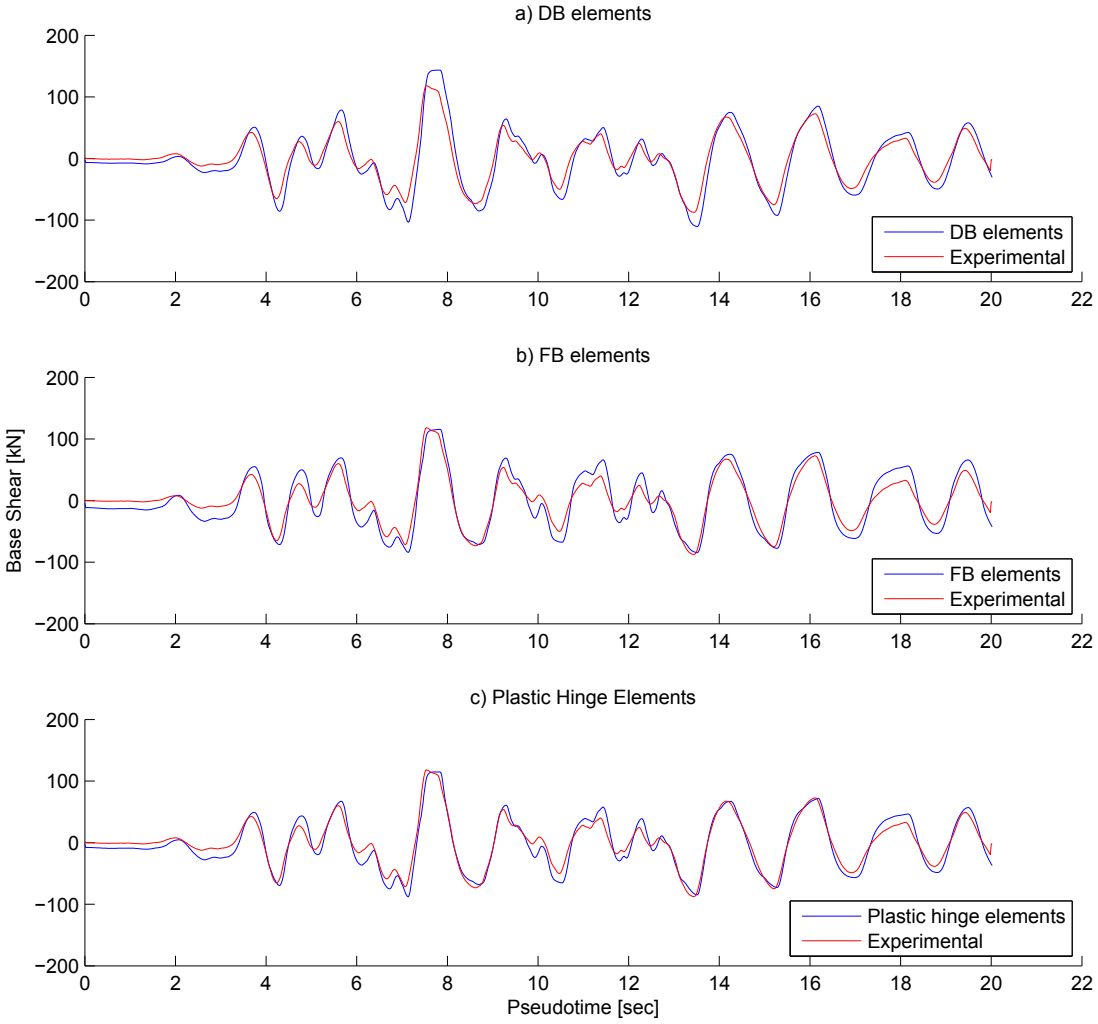


Figure 4.22: Base shears from alternative analysis versus experimental results for 0.80g ground motion.

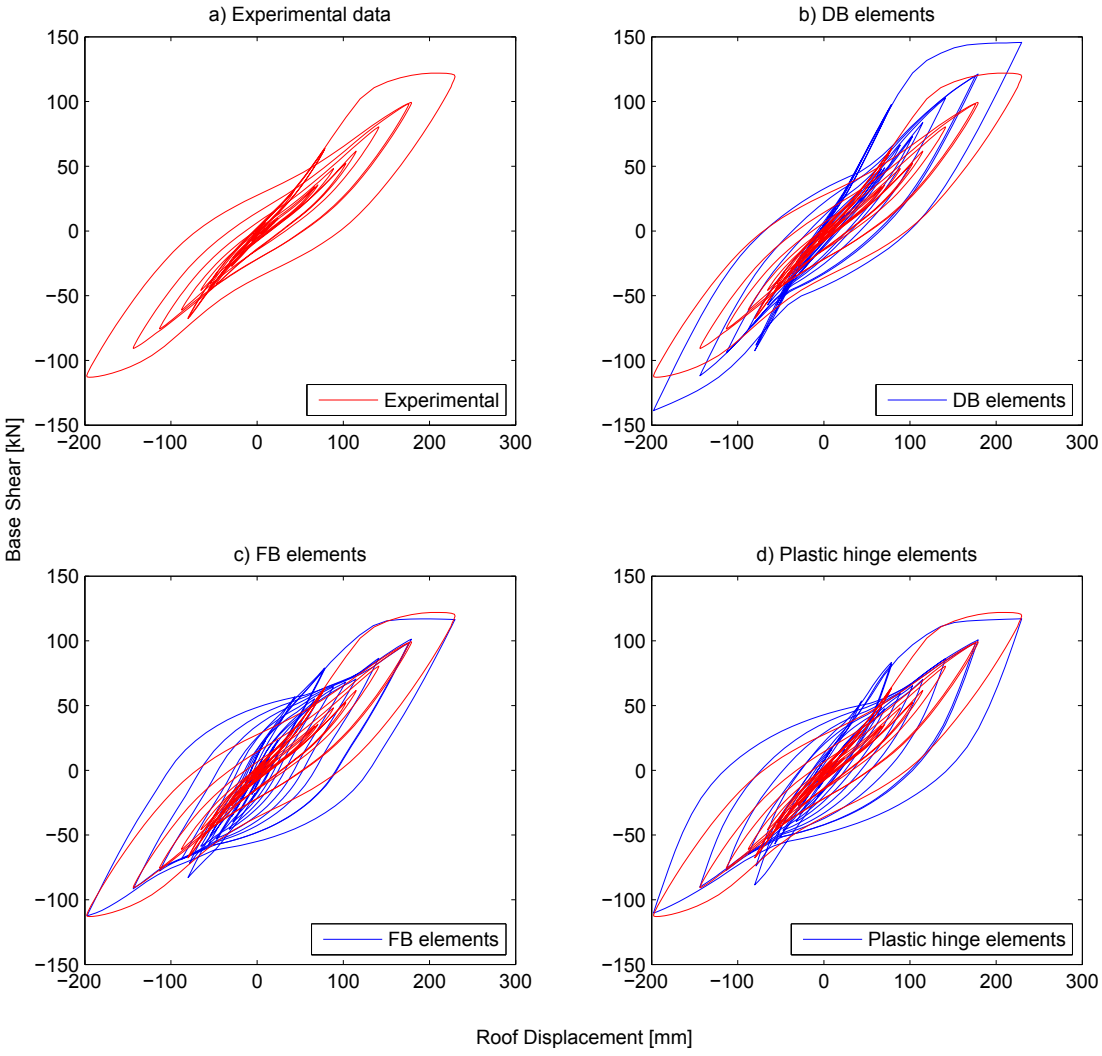


Figure 4.23: Force-displacement response from alternative analysis versus experimental results for 0.64g ground motion.

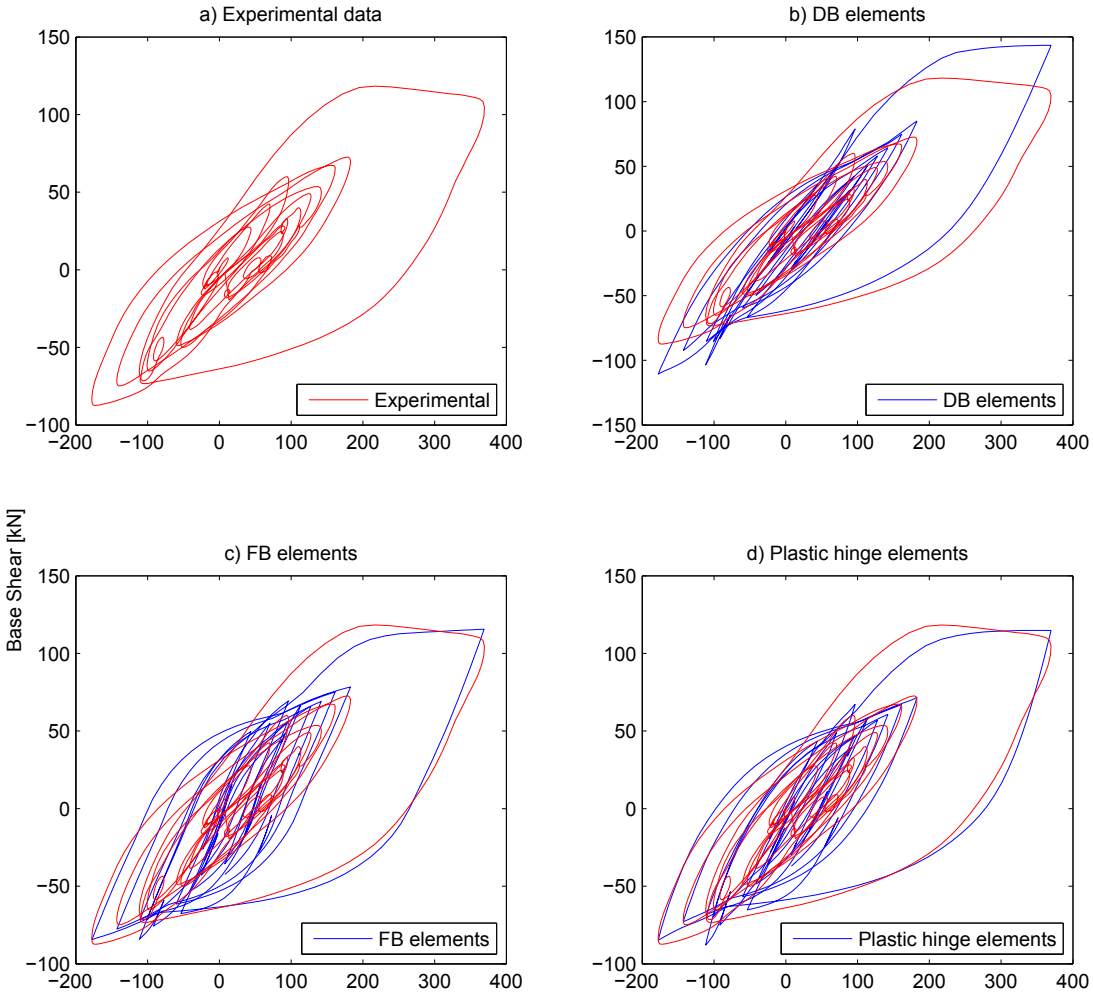


Figure 4.24: Force-displacement response from alternative analysis versus experimental results for 0.80g ground motion.

## 4.5 Conclusions

Based upon the analyses of the three ground motion intensities for each element formulation, the following conclusions are drawn:

The running times of the different analyses, listed in table (4.1), show that the computational demand of structural members with several DB elements is larger than similar members modeled with FB elements. This is expected, as gaining sufficient accuracy with the DB formulation requires several elements for each member, while the FB formulation can do with only one. Thus, the increased number of structural nodes raise the computational effort for each analysis. Since the one-story frame is a rather small model, the difference in average time per analysis step will increase drastically as the size of the structure increases. The fastest known matrix multiplication and inversion algorithm has a running time of $n^{2.373}$ for a $n \times n$ square matrix. Thus, using FB elements instead of DB elements for large finite element models will be very beneficial for computational cost. Plastic hinge elements which have elastic interiors and FB hinge regions, will reduce the computational time of analysis. These kind of elements are however primarily designed for analysis of structures subjected to strong lateral forces. If the peak bending moments occur at member interiors instead of at member ends, the correct inelasticity will not form. Thus, the practicing engineers must determine if dead loads are of critical importance to structures before modeling them with this type of plastic hinge elements. While lateral forces from earthquakes will be dominant for regular frame-based residential buildings, the same may not be the case for structures like ports and quays, which often experience large member loads.

The accuracy of the element formulations can be seen in their comparison with the experimental data from the prototype testing. Base shear time-history plots from the analysis show a good correspondance, although the force values are being slightly larger than experimental results for the $0.32g$ ground motion. Overestimated base shear values is escpecially the case for the DB element model, but this can be expected as the formulation often yields a too stiff solution. The first analysis, where each ground motion was subjected separately, gave too large force values that were expected to occur because of the numerical model having a higher elastic stiffness than the prototype. Yet this was shown to not be the case when the ground motions were subjected consecutively, such that the material stiffness was not brought to its initial state. Generally the response paths of all element formulations show very good results for approximation of global response. However, the approximation of local response for these ground motions are less satisfactory. While all element types yield inaccuracies in their predictions, the FB and plastic hinge models are slightly better than the DB model.

As a concluding remark, the observations from the analyses show that the FB and plastic hinge elements give the most accurate approximations of the pseudo-dynamic response of the one-story frame. Due to the prototype not having any significant strain-softening behaviour, the advantage of the Modified Gauss-Radau integration of the plastic hinge element have not been observed. Also, the accuracy of the DB element model would likely improve by discretizing the members into even more elements; but obviously at the cost of increased running time.

# Bibliography


[1] Addessi, D and Ciampi, V. (2007). "A regularized force-base beam element with a damage-plastic section constitutive law". *International Journal for Numerical Methods in Engineering*, 70 (5).

[2] Alemdar, B. N. and White, D. W. (2005). "Displacement, flexibility, and mixed beam-column finite element formulations for distributed plasticity analysis." *Journal of Structural Engineering*, 131 (12).

[3] Applied Technology Council (ATC), 1997. *NEHRP Guidelines for Seismic Rehabilitation of Buildings, Report No. FEMA-273*, Federal Emergency Agency, Washington, D.C.

[4] Calabrese, A., Almeida, J. P. and Pinho, R. (2010). "Numerical issues in distributed inelasticity model of RC frame elements for seismic analysis." *Journal of Earthquake Engineering*, 14 (S1).

[5] Coleman, J. and Spacone, E. (2001). "Localization issues in force-based frame elements." *Journal of Structural Engineering*, 127 (11).

[6] Fardis, M. N. (2009)." Modelling of buildings for nonlinear analysis." In *Seismic Design, Assesment and Retrofitting of Concrete Buildings* (pp. 379 - 425). University of Patras, Greece. Springer.

[7] Ferrara, L. and Negro, P. (2004). "Seismic behaviour of reinforced concrete structures: Test of the cast-in-situ prototype." European Laboratory for Structural Assessment, Ispra, Italy. EUR 21097 EN.

[8] Filippou, F. C. (2013). Lecture notes from *CE221 Nonlinear Structural Analysis*. University of California, Berkeley.

[9] Hillerborg, A. (1990)."Fractrure mechanics concepts applied to moment capacity and rotational capacity of reinforced concrete beam." *Engineering Fracture Mechanics*, 35 (1).

[10] Jansen, D. C. and Shah, S. P. (1997). "Effect of length on compressive strain softening of concrete." *Journal of Engineering Mechanics*, 123 (1).

[11] Lee, C. L. and Filippou, F. C. (2009). "Efficient beam-column element with variable inelastic end zones." *Journal of Structural Engineering*, 135 (11).

[12] Markeset, G. and Hillerborg, A. (1995). "Softening of concrete in compression - localization and size effects." *Cement and Concrete Research*, 25 (4).

[13] Moehle, J. (2012), Lecture notes from *CE244 Reinforced Concrete Structures*. University of California, Berkeley.

[14] Neuenhofer, A. and Filippou, F. C. (1997). "Evaluation of nonlinear frame finite-element models." *Journal of Structural Engineering*, 123 (7).

[15] OpenSees (2014). *Open System for Earthquake Engineering Simulation*. Retrieved from http://opensees.berkeley.edu/.

[16] Paulay, T. and Priestley, M. J. N. (1992). *(*Seismic Design of Reinforced Concrete and Masonry Building). John Wiley & Sons, New York.

[17] Robinson, S. (2005). "Toward an optimal algorithm for matrix multiplication" *SIAM News*, 38 (9).

[18] Scott, M. H. (2011). "Numerical integration options for force-based beam-column element in OpenSees." Retrieved from http://http://opensees.berkeley.edu/.

[19] Scott, M. H. and Fenves, G. L. (2006). "Plastic hinge integration methods for force-based beam-column elements." *Journal of Structural Engineering*, 132 (2).

[20] Scott, M. H. and Ryan, K. L. (2013). "Moment-rotation behaviour of force-based plastic hinge elements." *Earthquake Spectra*, 29 (2).

[21] Zeris, C. A. and Mahin, S. A. (1988). "Analysis of reinforced concrete beam-columns under uniaxial excitation." *Journal of Structural Engineering*, 114 (4).

# Appendices

# A. OpenSees scripts

## A.1 DB cantilever column

```
## Displacement-based cantilever column ##

set ResponseType Hardening;                # Hardening or Softening
set ResponseType Regular;                 # Regular or Regularized

set dataDir CantileverResults;
file mkdir $dataDir;
set m 1;
set mm [expr $m./1000];

# GEOMETRY
set LCol [expr 3*$m];

foreach nElements {2 3 4 6 8 10} {
wipe;
model BasicBuilder -ndm 2 -ndf 3;

# NODES
if {$ResponseType == "Regular"} {

for {set i 1} {$i <= [expr $nElements+1]} {incr i} {
        set Y [expr ($i-1)*$LCol./$nElements]
        node $i 0 $Y
}

set fys 500;
set db [expr 25*$mm];
set Lp [expr 0.08*$LCol + 0.022*$fys*$db];

} elseif {$ResponseType == "Regularized"} {
set fys 500;
set db [expr 25*$mm];
set Lp [expr 0.08*$LCol + 0.022*$fys*$db];

node 1 0 0;
node 2 0 [expr 2*$Lp];

for {set i 3} {$i <= [expr $nElements+1]} {incr i} {
        set Y [expr $Lp + ($i-2)*($LCol-$Lp)/($nElements-1)]
        node $i 0 $Y
```

```
}
}

print -node

# BOUNDARY CONDITIONS
fix 1 1 1 1;

# SECTIONS
set SectionType InelasticFiber;         # Either Elastic or InelasticFiber
set ColSecTag 1;
set HCol [expr 500*$mm];
set BCol $HCol

if {$SectionType == "Elastic"} {
        set Ec 30e9;
        set Acol [expr $HCol*$BCol];
        set Icol [expr $BCol*pow($HCol,3)/12];
        section Elastic $ColSecTag $Ec $Acol $Icol;

} elseif {$SectionType == "InelasticFiber"} {
        source ConcreteSI.tcl
        source BuildRCrectSection.tcl

        set cover [expr 50*$mm];
        set numBarsTopCol 6;
        set numBarsBotCol 6;
        set numBarsIntCol 8;
        set barAreaTopCol [expr 491*$mm*$mm];
        set barAreaBotCol [expr 491*$mm*$mm];
        set barAreaIntCol [expr 491*$mm*$mm];

        set nfCoreY 20;
        set nfCoreZ 20;
        set nfCoverY 20;
        set nfCoverZ 20;
        BuildRCrectSection $ColSecTag $HCol $BCol $cover $cover $IDconc
$IDconc $IDSteel $numBarsTopCol $barAreaTopCol $numBarsBotCol $barAreaBotCol
$numBarsIntCol $barAreaIntCol  $nfCoreY $nfCoreZ $nfCoverY $nfCoverZ

} else {
        puts "No section has been defined"
        return -1
}


# MASS
set concWeight [expr 25e3*$m*$m];
set g 9.81;
set distMassCol [expr $concWeight*$HCol*$BCol/$g];

# ELEMENT
set IDColTransf 1;
```

```
geomTransf Linear $IDColTransf;         # Linear or PDelta
set nIntegPoints 2;

for {set i 1} {$i <= [expr $nElements]} {incr i} {
        element dispBeamColumn $i $i [expr $i+1] $nIntegPoints $ColSecTag
$IDColTransf -mass $distMassCol
}

# EIGENPERIOD
set pi 3.1416;
set lambda [eigen 1];
set omega [expr pow($lambda,0.5)];
set T [expr 2*$pi/$omega];

# RECORDERS
recorder Node -file $dataDir/DispFree$nElements.out -time -node
[expr $nElements + 1] -dof 1 2 3 disp;
recorder Node -file $dataDir/DisplacementBase.out -time -node 1 -dof 1 2 3 disp;
recorder Element -file $dataDir/ForceColumnBase$nElements.out -time
-ele 1 section 1 force;
recorder Element -file $dataDir/DeformationColumnBase$nElements.out -time
-ele 1 section 1 deformation;

# GRAVITY
set ColWeight [expr $distMassCol*$g];

pattern Plain 1 Linear {
        for {set i 1} {$i <= [expr $nElements]} {incr i} {
                eleLoad -ele $i -type -beamUniform 0 -$ColWeight;
        }

        if {$ResponseType == "Softening"} {
                load 2 0 -6057e3 0;                # 50% of axial yield limit

        } else {
        }
}

set Tol 1.0e-8;
constraints Transformation;
numberer Plain;
system BandGeneral;
test NormDispIncr $Tol 6 ;
algorithm Newton;
set NstepGravity 10;
set DGravity [expr 1./$NstepGravity];
integrator LoadControl $DGravity;
analysis Static;
analyze $NstepGravity;

loadConst -time 0.0

puts "Model built"
```

```
puts "First period is $T sec"

# LATERAL LOAD
set Tolerance 1.0e-8;
set MaxIterations 10;
set MaxDisplacement [expr 0.04*$LCol];
set DisplacementIncrement [expr $MaxDisplacement/1000];
set ControlDOF 1;

constraints Plain;
numberer RCM;
system BandGeneral;
test NormDispIncr $Tolerance $MaxIterations;
algorithm Newton;
integrator DisplacementControl [expr $nElements + 1] $ControlDOF
$DisplacementIncrement;
analysis Static;

set Load 1000;
pattern Plain 2 Linear {
        load [expr $nElements + 1] $Load 0.0 0.0;
}

# ANALYSIS
analyze 1000;         #Steps

}
puts "Analysis performed"
```

## A.2 FB cantilever column

```
## Force-based cantilever column ##

set ResponseType Softening;                # Hardening or Softening

set dataDir CantileverResults;
file mkdir $dataDir;
set m 1;
set mm [expr $m./1000];

# GEOMETRY
set LCol [expr 3*$m];

foreach nIntegPoints {3 4 5 6 7 8} {
wipe;
model BasicBuilder -ndm 2 -ndf 3;

# NODES
node 1 0 0;
node 2 0 $LCol;

# BOUNDARY CONDITIONS
fix 1 1 1 1;

# SECTIONS
set SectionType InelasticFiber;         # Either Elastic or InelasticFiber
set ColSecTag 1;
set HCol [expr 500*$mm];
set BCol $HCol

if {$SectionType == "Elastic"} {
        set Ec 30e9;
        set Acol [expr $HCol*$BCol];
        set Icol [expr $BCol*pow($HCol,3)/12];
        section Elastic $ColSecTag $Ec $Acol $Icol;

} elseif {$SectionType == "InelasticFiber"} {
        source ConcreteSI.tcl
        source BuildRCrectSection.tcl

        set cover [expr 50*$mm];
        set numBarsTopCol 6;
        set numBarsBotCol 6;
        set numBarsIntCol 8;
        set barAreaTopCol [expr 491*$mm*$mm];
        set barAreaBotCol [expr 491*$mm*$mm];
        set barAreaIntCol [expr 491*$mm*$mm];

        set nfCoreY 20;
        set nfCoreZ 20;
        set nfCoverY 20;
```

```
        set nfCoverZ 20;
        BuildRCrectSection $ColSecTag $HCol $BCol $cover $cover $IDconc $IDconc
$IDSteel $numBarsTopCol $barAreaTopCol $numBarsBotCol $barAreaBotCol
$numBarsIntCol $barAreaIntCol  $nfCoreY $nfCoreZ $nfCoverY $nfCoverZ

        } else {
                puts "No section has been defined"
                return -1
        }

# MASS
set concWeight [expr 25e3*$m*$m];
set g 9.81;
set distMassCol [expr $concWeight*$HCol*$BCol/$g];

# ELEMENT
set IDColTransf 1;
geomTransf Linear $IDColTransf;         # Linear or PDelta
element forceBeamColumn 1 1 2 $nIntegPoints $ColSecTag $IDColTransf
-mass $distMassCol

# EIGENPERIOD
set pi 3.1416;
set lambda [eigen 1];
set omega [expr pow($lambda,0.5)];
set T [expr 2*$pi/$omega];

# RECORDERS
recorder Node -file $dataDir/DispFree$nIntegPoints.out -time -node 2
-dof 1 2 3 disp;
recorder Node -file $dataDir/DisplacementBase.out -time -node 1
-dof 1 2 3 disp;
recorder Node -file $dataDir/ReactionBase$nIntegPoints.out -time -node 1
-dof 1 2 3 reaction;

for {set i 1} {$i <= [expr $nIntegPoints]} {incr i} {
        recorder Element -file $dataDir/ForceColumnSec$i.nP$nIntegPoints.out
-time -ele 1 section $i force;
        recorder Element -file $dataDir/DeformationColumnSec$i.nP$nIntegPoints.out
-time -ele 1 section $i deformation;
}

# GRAVITY
set ColWeight [expr $distMassCol*$g];

pattern Plain 1 Linear {
        eleLoad -ele 1 -type -beamUniform 0 -$ColWeight;

        if {$ResponseType == "Softening"} {
                load 2 0 -6057.7e3 0;                # 50% of axial yield limit

        } else {
        }
```

```
}

set Tol 1.0e-8;
constraints Transformation;
numberer Plain;
system BandGeneral;
test NormDispIncr $Tol 6 ;
algorithm Newton;
set NstepGravity 10;
set DGravity [expr 1./$NstepGravity];
integrator LoadControl $DGravity;
analysis Static;
analyze $NstepGravity;

loadConst -time 0.0

puts "Model built"
puts "First period is $T sec"

# LATERAL LOAD
set Tolerance 1.0e-8;
set MaxIterations 10;
set MaxDisplacement [expr 0.03*$LCol];
set DisplacementIncrement [expr $MaxDisplacement/1000];
set ControlDOF 1;

constraints Plain;
numberer RCM;
system BandGeneral;
test NormDispIncr $Tolerance $MaxIterations;
algorithm Newton;
integrator DisplacementControl 2 $ControlDOF $DisplacementIncrement;
analysis Static;

set Load 1000;
pattern Plain 2 Linear {
        load 2 $Load 0.0 0.0;
}

# ANALYSIS
analyze 1000;         #Steps

}
puts "Analysis performed"
```

## A.3 Plastic hinge cantilever column

```
## Force-based plastic hinge cantilever column ##

set InteriorResponse Inelastic;        # Elastic or Inelastic
set IntegrationMethod HingeRadau;        # HingeMidpoint, HingeEndpoint,
HingeRadau, or HingeRadauTwo
set ResponseType Softening;        # Hardening or Softening

set dataDir CantileverResults;
file mkdir $dataDir;
set m 1;
set mm [expr $m./1000];

# GEOMETRY
set LCol [expr 3*$m];

wipe;
model BasicBuilder -ndm 2 -ndf 3;

# NODES
node 1 0 0;
node 2 0 $LCol;

# BOUNDARY CONDITIONS
fix 1 1 1 1;

# SECTIONS
set ColSecTag 1;
set HCol [expr 500*$mm];
set BCol $HCol

source ConcreteSI.tcl
source BuildRCrectSection.tcl

set cover [expr 50*$mm];
set numBarsTopCol 6;
set numBarsBotCol 6;
set numBarsIntCol 8;
set barAreaTopCol [expr 491*$mm*$mm];
set barAreaBotCol [expr 491*$mm*$mm];
set barAreaIntCol [expr 491*$mm*$mm];

set nfCoreY 20;
set nfCoreZ 20;
set nfCoverY 20;
set nfCoverZ 20;
BuildRCrectSection $ColSecTag $HCol $BCol $cover $cover $IDconc
$IDconc $IDSteel $numBarsTopCol $barAreaTopCol $numBarsBotCol $barAreaBotCol
$numBarsIntCol $barAreaIntCol  $nfCoreY $nfCoreZ $nfCoverY $nfCoverZ

# MASS
```

```
set concWeight [expr 25e3*$m*$m];
set g 9.81;
set distMassCol [expr $concWeight*$HCol*$BCol/$g];

# ELEMENT
set IDColTransf 1;
geomTransf Linear $IDColTransf;         # Linear or PDelta

set fys 500;
set db [expr 25*$mm];
set Lp [expr 0.08*$LCol + 0.022*$fys*$db];

if {$InteriorResponse == "Elastic"} {
        set Ecol 36.68e9;
        set Acol [expr $HCol*$BCol];
        set Icol [expr $BCol*pow($HCol,3)/12];
        element beamWithHinges 1 1 2 $ColSecTag $Lp $ColSecTag 0 $Ecol $Acol
        $Icol $IDColTransf -mass $distMassCol

        } elseif {$InteriorResponse == "Inelastic"} {
        element forceBeamColumn 1 1 2 $IDColTransf $IntegrationMethod $ColSecTag
        $Lp $ColSecTag 0 $ColSecTag -mass $distMassCol
}

# EIGENPERIOD
set pi 3.1416;
set lambda [eigen 1];
set omega [expr pow($lambda,0.5)];
set T [expr 2*$pi/$omega];

# RECORDERS
if {$InteriorResponse == "Elastic"} {
        recorder Node -file $dataDir/DispFreeElasticInterior.out -time -node 2
        -dof 1 2 3 disp;
        recorder Node -file $dataDir/ReactionBaseElasticInterior.out -time
        -node 1 -dof 1 2 3 reaction;
        recorder Element -file $dataDir/ForceColumnBaseElasticInterior.out
        -time -ele 1 section 1 force;
        recorder Element -file $dataDir/DeformationColumnBaseElasticInterior.out
         -time -ele 1 section 1 deformation;

        } elseif {$InteriorResponse == "Inelastic"} {
        recorder Node -file $dataDir/DispFree$IntegrationMethod.out -time -node 2
        -dof 1 2 3 disp;
        recorder Node -file $dataDir/ReactionBase$IntegrationMethod.out -time
        -node 1 -dof 1 2 3 reaction;
        recorder Element -file $dataDir/ForceColumnBase$IntegrationMethod.out
        -time -ele 1 section 1 force;
        recorder Element -file $dataDir/DeformationColumnBase$IntegrationMethod.out
        -time -ele 1 section 1 deformation;

}
```

```
# GRAVITY
set ColWeight [expr $distMassCol*$g];

pattern Plain 1 Linear {
        eleLoad -ele 1 -type -beamUniform 0 -$ColWeight;

        if {$ResponseType == "Softening"} {
                load 2 0 -6057.7e3 0;                # 50% of axial yield limit
        } else {
        }
}

set Tol 1.0e-8;
constraints Transformation;
numberer Plain;
system BandGeneral;
test NormDispIncr $Tol 6 ;
algorithm Newton;
set NstepGravity 10;
set DGravity [expr 1./$NstepGravity];
integrator LoadControl $DGravity;
analysis Static;
analyze $NstepGravity;

loadConst -time 0.0

puts "Model built"
puts "First period is $T sec"

# LATERAL LOAD
set Tolerance 1.0e-8;
set MaxIterations 10;
set MaxDisplacement [expr 0.033*$LCol];
set DisplacementIncrement [expr $MaxDisplacement/1000];
set ControlDOF 1;

constraints Plain;
numberer RCM;
system BandGeneral;
test NormDispIncr $Tolerance $MaxIterations;
algorithm Newton;
integrator DisplacementControl 2 $ControlDOF $DisplacementIncrement;
analysis Static;

set Load 1000;
pattern Plain 2 Linear {
        load 2 $Load 0.0 0.0;
}

# ANALYSIS
analyze 1000;         # Steps

puts "Analysis performed"
```

## A.4 Material data

```
## Material data ##

# Units: kg, m, sec

#CONCRETE

# nominal concrete compressive strength
set fc -30e6;                # Concrete Compressive Strength, Pa
set Ec         30e9;                # Concrete Elastic Modulus
set Gc 180;                # Fracture energy, N/mm

# Unconfined concrete
set fc1U  $fc;                # UNCONFINED concrete , maximum stress
set eps1U -0.002;        # strain at maximum strength of unconfined concrete
set Kres 0.2;                # ratio of residual/ultimate to maximum stress
set fc2U [expr $Kres*$fc1U];        # ultimate stress
set eps2U [expr 20*$eps1U];        # strain at ultimate stress

uniaxialMaterial Concrete01 $IDconc $fc1U $eps1U $fc2U $eps2U;

## REINFORCING STEEL

set Fy 500e6;        # Steel yield stress (Pa)
set Es 200e9;        # modulus of steel
set Bs 0.010;        # strain-hardening ratio
set R0 18;        # control the transition from elastic to plastic branches
set cR1 0.925;        # control the transition from elastic to plastic branches
set cR2 0.15;        # control the transition from elastic to plastic branches

set IDSteel 3
uniaxialMaterial Steel02 $IDSteel  $Fy $Es $Bs $R0 $cR1 $cR2
```

## A.5 Fiber section builder

```
proc BuildRCrectSection {id HSec BSec coverH coverB coreID coverID steelID
numBarsTop barAreaTop numBarsBot barAreaBot numBarsIntTot barAreaInt
nfCoreY nfCoreZ nfCoverY nfCoverZ} {

# Fiber rectangular RC section, 1 steel layer top, 1 bot, 1 skin, confined core

#                by: Silvia Mazzoni, 2006
#                        adapted from Michael H. Scott, 2003

set coverY [expr $HSec/2.0];
set coverZ [expr $BSec/2.0];
set coreY [expr $coverY-$coverH];
set coreZ [expr $coverZ-$coverB];
set numBarsInt [expr $numBarsIntTot/2];

# Define the fiber section

section fiberSec $id {

# Define the core patch

patch quadr $coreID $nfCoreZ $nfCoreY -$coreY $coreZ -$coreY -$coreZ $coreY
-$coreZ $coreY $coreZ

# Define the four cover patches

patch quadr $coverID 2 $nfCoverY -$coverY $coverZ -$coreY $coreZ $coreY $coreZ
$coverY $coverZ
patch quadr $coverID 2 $nfCoverY -$coreY -$coreZ -$coverY -$coverZ $coverY
-$coverZ $coreY -$coreZ
patch quadr $coverID $nfCoverZ 2 -$coverY $coverZ -$coverY -$coverZ -$coreY
-$coreZ -$coreY $coreZ
patch quadr $coverID $nfCoverZ 2 $coreY $coreZ $coreY -$coreZ $coverY -$coverZ
$coverY $coverZ

# define reinforcing layers

layer straight $steelID $numBarsInt $barAreaInt  -$coreY $coreZ $coreY $coreZ;
layer straight $steelID $numBarsInt $barAreaInt  -$coreY -$coreZ $coreY -$coreZ;
layer straight $steelID $numBarsTop $barAreaTop $coreY $coreZ $coreY -$coreZ;
layer straight $steelID $numBarsBot $barAreaBot  -$coreY $coreZ  -$coreY -$coreZ;

};        # end of fibersection definition
};                # end of procedure
```

# B. Matlab scripts

## B.1 Regularization of local FB response

```
%% Regularization of local FB response %%

clear all; close all; clc;

L = 3;
fy = 500;
db = 0.025;
wip = 0.5*[1/3 1/6 1/10 0.066667];
Lip = L*wip;
Lp = 0.08*L + 0.022*fy*db;

curvt = load ('DeformationColumnSec1.nP3.out');
momentt = load ('ForceColumnSec1.nP3.out');
curv3 = -curvt(11:end,3);
moment3 = -momentt(11:end,3)/1000;
curvt = load ('DeformationColumnSec1.nP4.out');
momentt = load ('ForceColumnSec1.nP4.out');
curv4 = -curvt(11:end,3);
moment4 = -momentt(11:end,3)/1000;
curvt = load ('DeformationColumnSec1.nP5.out');
momentt = load ('ForceColumnSec1.nP5.out');
curv5 = -curvt(11:end,3);
moment5 = -momentt(11:end,3)/1000;
curvt = load ('DeformationColumnSec1.nP6.out');
momentt = load ('ForceColumnSec1.nP6.out');
curv6 = -curvt(11:end,3);
moment6 = -momentt(11:end,3)/1000;

Myi = 752.62;
Phiy = 0.00455; %From reading of results

for i = 1:length(wip)
    scale(i) = (wip(i)*L^2*(2-wip(i)))/(Lp*(2*L-Lp));
end


for i = 1:length(curv3)
    if curv3(i) > Phiy
        Phii = curv3(i) - Phiy;
        deltai = Phii*Lip(1)*L;
```

```
        Phimodel = deltai/(Lip(1)*(0.5*L-0.5*Lip(1)));
        curvreg3(i) = Phiy + scale(1)*Phimodel;
    else
        curvreg3(i) = curv3(i);
    end
end

for i = 1:length(curv4)
    if curv4(i) > Phiy
        Phii = curv4(i) - Phiy;
        deltai = Phii*Lip(2)*L;
        Phimodel = deltai/(Lip(2)*(0.5*L-0.5*Lip(2)));
        curvreg4(i) = Phiy + scale(2)*Phimodel;
    else
        curvreg4(i) = curv4(i);
    end
end
for i = 1:length(curv5)
    if curv5(i) > Phiy
        Phii = curv5(i) - Phiy;
        deltai = Phii*Lip(3)*L;
        Phimodel = deltai/(Lip(3)*(0.5*L-0.5*Lip(3)));
        curvreg5(i) = Phiy + scale(3)*Phimodel;
    else
        curvreg5(i) = curv5(i);
    end
end
for i = 1:length(curv6)
    if curv6(i) > Phiy
        Phii = curv6(i) - Phiy;
        deltai = Phii*Lip(4)*L;
        Phimodel = deltai/(Lip(4)*(0.5*L-0.5*Lip(4)));
        curvreg6(i) = Phiy + scale(4)*Phimodel;
    else
        curvreg6(i) = curv6(i);
    end
end
```